CRANFIELD UNIVERSITY

School of Applied Science

Thesis

Academic Year 2006-2007

James McColl

On some factors that effect the 'feel' of molecules

Supervisor: Professor Jeremy J Ramsden

Date of registration: 01 November 2004

Table of contents

On some factors that effect the 'feel' of molecules.

Abstract

There is currently a trend towards the increasing use of nanotechnology in food. Emerging technology has the potential to modify the nutritional value and improve the quality of food products. Nevertheless there are difficulties. Perhaps the most problematic area is molecular sensing and in particular mechanical sensing as modification leads to structurally different molecules. The mucosal layers are the first point of contact in the mechanical sensory process. Mucins are the largest component of the mucosa and these high molecular weight glycoproteins can be found across all animal phyla. Their roles are diverse ranging from a non-specific immune response to lubricators. Mucin is investigated and it is proposed to adsorb in a concentration manner in a quasi-composite layer structure. This structure is related to its functional properties and is conserved over a wide temperature range.

Acknowledgements

I would like to thank my supervisor Jeremy Ramsden and Robert Horvath (Postdoc) for help and guidance throughout the project. Sincere thanks to all at Unilever, in particular Gleb Yakubov. I will miss our late evening discussions. There are too many friends and colleagues at Cranfield to mention so I will single out a few. Most important is Amir who always brings biscuits to the coffee meetings (and all the other group members, Yun-Peng, Farah), Chris Shaw and Andrew Stallard for their help over the course of the work with technical issues. Enza, you are one in a million always happy and always helpful. Renauld and Arne, who were always there during those late evenings ready for a beer.

In addition I would like to thank my family who have always given me support and help. To my wife Emma, I thank you and love you dearly. To my children, Chloe and Harrison, be good and I love you. My mum and dad have been an inspiration and I thank them also.

Finally I would like to thank the EPSRC for funding the project.

List of figures

List of tables

1. Introduction

1.1 Overview

The fact that a majority of people now live in cities (and urbanisation will continue to rise) means that an increasing number of nutritional need have to be met by processed foods rather than the farmers market. The transition to processed foods has often been associated with obesity. Here in the UK the number of clinically obese individuals is set to rise to 12 million by 2010 [1]. This increase though is not restricted to the UK and is instead a systematic worldwide phenomenon that will make obesity one of the greatest public health challenges of the 21st century. Concomitant increases in type two diabetes, coronary heart disease and cancers are responsible for spiralling European health care costs with obesity accounting for 2-8% of costs and 10-13% of deaths at present [2].

There are many reasons for the increase in obesity (some of which are socio-economical although this project will not address these [3]). Improving diet is one of the key strategies for reducing obesity (coupled with increased physical activity) that will however be addressed.

The drive towards the consumption of low-fat and low-sugar products is therefore set to rise although the problem here is that many of the products currently available do not mimic well enough their full fat/sugar counterparts. The taste of these low fat/sugar products and also their visual perception can be very well manipulated, however it is mouthfeel that is most difficult to mimic. It is therefore of great importance to understand oral bolus formation, food mixing and mechanoreception in detail when designing novel food products.

1

Mechanical perception is vital for food molecule, noxious substance and foreign material sensing in the oral cavity [4]. Mechanical stimuli (such as pressure or deformation) are sensed via mechanoreceptors. These can be triggered by distortion of the mucus layer and underlying mucosa and possibly via direct action on the underlying epithelial cells. Alternatively stimulation of free nerve endings or C-fibres directly should also effects mechanosensation [5, 6]. The most pertinent example of oral mechanoreception is astringency, a dry, puckering sensation and it has been suggested that the astringent sensation is to a greater extent related to mechanical stimulation. It is a diffuse surface phenomenon, taking many seconds to develop and has been linked to a reduction in saliva lubricating properties [7, 8, 9].

It is imperative that the properties of food perception be maintained as it would be fruitless to design insipid foods or lacklustre beverages even if they were nutritionally well balanced. Patients that receive artificial nutrition such as enteral tube feeding or parenteral nutrition show adverse appetite behaviour and are still hungry (or thirsty) even if their nutritional requirements are met [10]. The smell, taste and overall perception of food in the mouth can impact on the feeling of hunger and appetite [11, 12, 13]. Understanding the mechanisms of food perception is therefore vital for the future development of new (nutritionally beneficial) food products.

1.2 Nanotechnology and food

This section Introduces nanotechnology and then proposes possible future roles within the food industry for the techniques that are available today. The future of food manipulation will be via the use of nanotechnology techniques and is nothing new as cooking can be thought of as nanomanipulation, altering the properties of molecules through heating and mixing. For example sauces and dressings are usually a mixture of an oil and water phase that results in an emulsion. The benefit of using nanotechnology is that it will add an element of control and this section will finish with nanofoods that are commercially available at present.

1.2.1   What is nanotechnology and where is it used now

Nanotechnology is the study and manipulation of processes in biological and non-biological systems at the sub 100 nm length scale. These systems in general have many different chemical, physical and biological properties when compared with those of macroscopic dimensions [14]. For example metal nano-particles exhibit unique optical properties (surface plasmon resonance) and carbon nanotubes have distinctive electrical properties. They can be either metallic or act as semi-conductors. It encompasses many of the well established scientific disciplines such as chemistry, interfacial science, material science and molecular biology (to name a few) and future progress will involve the application and not simply the investigation of these properties. The key areas that utilise nanotechnology at present are the mircoelectronics, aerospace and pharmaceutical industries with the nanofood sector predicted as having great future potential, indeed the market is predicted to grow from $2.6 billion to 20.4 billion in America alone by 2010 [15].

3

1.2.2   Future possibilities – food industry

Nanotechnology will impact on all four main areas of food production,

- Materials – the use of functional particles, emulsions and nano-composites/materials for product design.
- Product – using nanotechnology for controlled delivery and package manufacturing.
- Safety – sensors that detect the properties of the packaged food.
- Processing – food synthesis using nanotechnology.

Some of these applications are of course speculative future predictions such as the use of nanobots that would facilitate the bottom up production of food and are introduced as background knowledge only [16]. Indeed the use of sensors for packaging (smart materials) and food safety are also not included in the scope of this project.

1.2.2.1   Microencapsulation

Microencapsulation is at present utilised by the food industry (albeit at micro and not nano size dimensions) to encapsulate an active component (gas liquid or solid) by a material which isolates it from the immediate environment. These capsules range in size from roughly 1 μm to several millimetres and the component can be released in a controlled manner via several mechanisms such as mechanical rupture of the capsule, temperature degradation, dissolution, ablation and biodegradation. Capsules can also be manufactured to enable diffusion across the cell membrane [17].

Lipid-soluble vitamins such as A, D, E, K and -carotene can be successfully encapsulated at present although water-soluble forms prove more difficult. The adverse effects of tannins and polyphenols on Fe and the ability of this mineral to catalyse the oxidation of other food ingredients (such as fatty acids, vitamins and amino acids) suggest that encapsulation is vital when fortifying foods with Fe to protect both Fe and other ingredients. Western diets (in particular) lack sufficient quantities of -3 polyunsaturated fatty acids, which have been linked to low incidences of coronary heart disease and cancer. Fatty acid fortification of food is therefore necessary (and will become increasingly so as the main dietary source is oily fish, a commodity we are rapidly depleting) and as with Fe these fatty acids are easily oxidised (reducing there nutritional value and modifying the sensory characteristics) and require encapsulation to enhance their activity [18].

Phytochemical encapsulation is of increasing interest as many of these molecules promise potential health benefits, the most pertinent of which being anti-cancer activity [19]. Recently epigallocatechin-gallate (EGCg), a green tea polyphenol has been encapsulated in liposomes [20], a process which could improve the bioavailability of these molecules. This is proposed as a key factor in phytochemical effectiveness as cell culture studies very often conflict with *in vivo* experiments where the availability of the molecule may have been compromised [21]. The interaction of these molecules at interfaces is therefore extremely relevant for there future therapeutic efficacy.

Casein is the highest protein constituent of cows milk (80% by weight) which forms micelles to encapsulate and hence concentrate nutrients for the neonate. These naturally occurring encapsulates (size ranging from 50-500 nm) can be synthesised

and are able to encapsulate the fat soluble vitamin D2 and could be used to fortify low fat milk (or even other beverages) with this essential vitamin [22].

Nanoemulsions are formed via an encapsulation process that involves the formation of small droplets into which active components can be encapsulated and in general this technique prolongs the lifetime of the components. Actives can also be incorporated at the interfacial region or continuous phase of the emulsion [23]. Multiple emulsions as the name suggests are multiple layered structures such as water in oil-in-water (or oil-in-water-in-oil) emulsions. Possibilities for these techniques include the separation of two reactive aqueous phase components or for controlled release although at present these systems are thermodynamically unstable with a tendency to flocculate and coalesce causing the release of any active component [24, 25].

Multilayer emulsions are typically polyelectrolyte encased oil droplets formed using layer-by-layer (LbL) methods which involves the alternate deposition of oppositely charged particles that build up the layers (electrostatic deposition). The potential for these are that the shell (external layer) properties can be modified to target delivery and that particle stability is far superior to that of oil in water emulsions [26, 27].

LbL techniques can also produce nanolaminates comprising of layers (two or more) of chemically or physically bonded films [28]. These laminates could be utilised as food coatings, forming barriers against adverse moisture and gas effects or forming carriers for texture modifying particles, flavour/colour modifiers, nutrient/antioxidant or antibacterial additives.

6

1.2.2.1.1 Biodegradable polymers

Research into the first biodegradable polymer for use in dispersed systems, polylactic acid (PLA) began in 1932 although the high cost and its poor resistance to hydrolytic breakdown made it unsuitable for medical and agricultural applications [29]. Bacterial fermentation production of PLA in the 1980's reduced the cost and renewed interest in PLA, which later saw it combined with polyethylene glycol (PEG) to improve intestinal delivery as PLA alone is degraded very quickly by the lower gastrointestinal tract [30].

1.2.2.2 Nanocomposite, nanofibres and nanotubes

It is proposed that the incorporation of clay (approximately 5% by weight) into polysaccharide films [31, 32, 33] increases their tensile strength and reduces the water repulsive properties of the film. Chitosan is another interesting molecule, itself a cationic polysaccharide, isolated from shellfish and derived via the deacetylation of chitin is non toxic and presently used in applications such as wound healing and as a food preservative. Industrial uses are diverse ranging from waste water treatment to the cosmetics industry [34, 35].

Nanofibres are of little interest at present for the food industry as most of the fibres produced at present are of synthetic origin, hence they are not biocompatible. Future fibres produced using biocompatible materials should increase nanofibre use within the food industry. As with nanofibres there is little or no use of nanotubes as there are many associated difficulties pertaining to processing procedures and safety/ethical issues i.e. inhalation [36]. More promising is the use of globular proteins such as -lactalbumin from milk which self assembles into nanotube structures. Here

7

proteolysis causes the self assembly into nanotubes when calcium is added [37, 38, 39, 40].

1.2.3   Nanofood today

At present nano food products are not available for purchase in Europe although they can be found globally with microencapsulation already being used to manufacture several products. Indeed there are no regulations that governs nanofoods in the United States whereas Europe have regulatory controls albeit that at present these have not been implemented. It may therefore be that European manufacturers are fearful of public perception and not regulatory bodies at present. Some global examples include chocolate flavour chewing gum which has in the past been problematic to produce as cocoa added to gum adversely effects its properties. Encapsulating the cocoa for release upon mechanical rupture provides a chewing gum packed with chocolate flavour. Vitamin C is encapsulated in cooking oil, Omega-3 in orange juice and bread produced for the Australian market contains encapsulated Omega-3 (tip-top) [41].

An increase in nanomanipulation of food molecules (encapsulation etc) will result in a concomitant increase in novel particles at biological surfaces. A greater knowledge of biological interfaces (and in particular their response mechanisms) are imperative for understanding the future impact that these novel compounds will have on individuals.

1.3 Biological surfaces

The first point of contact for food products (either manipulated or not) are the body surfaces. This section introduces the relevant body surfaces of interest and the nervous system that transmits the mechanosensation.

8

1.3.1 The skin

Skin is the largest organ of the human body and accounts for approximately 16% of total body weight. There are two layers, the dermis and epidermis that are separated by the basal lamina. In addition skin also contains hair follicles, sweat glands and oil producing sebaceous glands. The main functions of the skin are barrier formation, environmental communication and minimising water loss. Additional less characterised roles include vitamin D formation and temperature regulation [42].

1.3.1.1 Epidermis

The outer epidermis is several layers thick, consists mainly of keratinocytes and has stem cells at the basal layer that proliferate to produce new cells. Keratinocytes differentiate as they age forming the stratified layers of the skin which are eventually exfoliated into the environment as corneocytes from the *Stratum corneum*. Other cell types found in the epidermis are pigment-producing melanocytes, neuronal Merkel cells and immune system cells that include antigen presenting Langerhans cells and T-lymphocytes.

1.3.1.2 Stem cells

Stem cells are undifferentiated cells that can proliferate to produce additional undifferentiated cells. An undifferentiated cell has the ability to become more than one of the 220 cell types there are in the human body. Totipotent stem cells are able to become any cell type, for example eggs released from the ovary are totipotent whereas multipotent stem cells produce many different cell types that are generally organ specific and unipotent stem cells are able to produce only one cell type such as the keratinocyte stem cell of the skin [43].

For skin the inter-follicular stem cells of the epidermis proliferate to renew the stratified epithelia above them. Stem cells are also located in glabrous epidermis and at the hair follicle. During wound healing, hair follicles, sebaceous glands and inter-follicular epidermis can all be reconstituted by multipotent stem cells found at the hair follicle. The bulge region of the hair follicle is therefore thought to be the major multipotent stem cell pool site [44].

1.3.1.3   Basal lamina

This is a membrane no thicker than 60-120 nm that separates the epidermis and dermis. The basal lamina is made up of extracellular matrix (ECM) components such as laminin and fibronectin that are produced by the surrounding cells. Its main function is as a base on which cells can adhere and where necessary migrate along. Epidermal basal cells bind to laminin through integrin receptors on one side of the membrane whilst a collagen rich layer facing the dermis binds the connective tissue [45].

1.3.1.4   Dermis

The dermis is constructed of connective tissue that has a significant ECM. This serves to protect, support and bind the epidermis to the underlying muscle. Fibroblasts are the main cellular constituent of the dermis and produce most of the collagen and elastin that make up the bulk of the ECM. Collagen is an insoluble protein fibre that gives strength to the tissue whilst elastin as the name suggests is a fibre with flexible elastic properties. Adipocytes or fat cells are present here with their role being energy storage and insulation, whilst blood vessels and lymphatic vessels vascularise the dermis but do not cross the basal lamina. In addition the nervous system innervates both the dermis and the epidermis [46].

The interface between the dermis and epidermis is often depicted as a flat horizontal layer of epithelia although in reality this is untrue. The basement membrane instead undulates like a wave increasing the shear strength of the skin [45].

1.3.1.5 Hair follicle, sebaceous and sweat glands

Hair covers almost all of the body and is a very important sensory structure. The hair follicles are invaginations of the epidermis into which the hair sits. Each follicle is supplied by a sebaceous gland that secretes sebum (oil) onto the skin. The erector pilli muscle attached to the hair shaft can be instructed to erect the hair under nervous control and when erect sebum is also released into the follicle. A neural net at the base of the hair follicle transmits both sensory signals received from the hair and signals from the central nervous system (CNS). Sweat glands are used for temperature control, located in the dermis and release water (and salts) onto the surface of the skin [47].

1.3.2 Mucosa and their innervations (nerves)

The term mucosa pertains to the body cavity epithelial coated mucous membrane linings that develop from mostly endodemal origin tissue with the best known examples being the respiratory system, gastrointestinal tract and urogenitary tract. The structure is epithelial tissue similar in many ways to that of the skin with the main difference being the presence of the lamina propria, a thin layer of loose connective tissue [48].

11

1.3.2.1   Oral mucosa

The oral mucosa is the stratified squamous epithelia of the mouth of which there are three types.

- Masticatory mucosa which is keratinized (in a similar manner to that of the skin) and found at the rear of the tongue (dorsum), the anterior roof of the mouth (hard palate) and at the gums (gingival).

- Lining mucosa which is not keratinized and makes up most of the rest of the oral cavity lining including that lining the cheeks (buccal mucosa).

- Specialized mucosa pertaining to the taste bud papillae.

Lower cavity mucus secretion occurs via the submandibular gland and the mandibular gland whilst the paratoid and accessory paratoid gland (via the paratoid duct) secrete mucus at the palate [49].

1.3.2.2 Gastro Intestinal tract mucosa

The gastric mucosa pertains to the lining of the stomach with a morphology that consists of a single layer of columnar epithelium cells. Dispersed within the epithelial lining are goblet cells and gastric glands [50]. The intestinal mucosa or lower gastrointestinal tract comprises of the small intestine (duodenum, jejunum, ileum), large intestine (cecum, colon, rectum) and anus. The structure of the layer is similar to that of the gastric mucosa although here there is an additional thin layer of muscle (muscularis externa) that is involved in peristalsis [51].

1.3.2.3 Additional mucosa

There are other mucosa that will not be directly relevant to this project (at present) such as the endometrial mucosa, a specialised mucosal lining that lines the inside of the blood vessels, the olfactory mucosa that line the inside of the nose and the mucosa of the eye.

1.3.3 Nervous system

For all organisms, including those that are unicellular the ability to sense and react to the environment is essential. Higher animals such as humans use a nervous system consisting of the CNS and the peripheral nervous system (PNS).

Most neurons of the nervous system share the same basic structure consisting of a cell body (soma) that contains the nucleus (where almost all proteins are produced), dendrites that protrude from the soma and form connections with other neurons and an axon (a very long dendritic outgrowth from the soma) containing terminal axons at the point furthest from it. There are two types of mammalian neurons. 1. Multipolar inter-neurons that have many dendrites each of which receives synaptic information from other neurons. The interneurons are primarily located in the CNS and the axon carries information to other neurons via the terminal branches. 2. Mammalian motor neurons though have less dendrites and an axon that extends to effector cells, they are myelinated and are predominantly of PNS origin.

Schwann cells insulate the axon by wrapping a portion of their membrane around it that during development (and repair) squeezes out the water. Myelination is important as it increases the velocity of the action potential [52]. Axons conduct changes in electrical potential across the cell membrane (action potentials). Neurons have a

resting potential of around -60mV that rises to as much as +50mV at the peak of an action potential. The action potential is an opening of cell membrane channels that allow positive ions to flow into the cell. The potential is transmitted along the axon to induce action in another cell via a synapse. These can be either a chemical synapse that involves the release of neurotransmitters from the synaptic cleft at the end of the axon or an electrical synapse that acts through gap junctions on the adjacent cell [53].

1.3.3.1   Specialised neuron receptors (mechanoreceptors)

Specialised neurons are responsible for registering mechanical stimulation or distortion. Large Pacinian corpuscle receptors belong to the rapidly adapting receptor family, acting like a switch to the onset of pressure and to higher vibration signals. They are mainly found in deep subcutaneous tissue and near joints. These respond to large changes and vibrations and as such are of little interest when studying the mucosa [54].

Meissners corpuscles are numerous at the mucosa, are stimulated by pressure (touch response) and are located at the tips of the dermal papillae. Also found at the mucosa are Ruffini endings, thin flattened and encapsulated nerve endings that respond to stretching of the skin [55]. These also respond to heat whereas the bulboid corpuscle responds to cold. The Merkel discs are the most sensitive of the mechanoreceptors to low frequencies (5 to 15 Hz) and are slowly adapting, essentially they continually sense pressure differences [56].

1.4 Research objectives and methodology

Research objectives

- Develop advanced theoretical understanding of body surface response to external stimuli.
- Develop model systems for measuring response in situ using novel instrumentation.

External stimuli response may be viewed as hierarchical whereby the molecules detected may first interact with the mucus layers and then the underlying/attached cells before finally triggering a nervous system signal. This work therefore follows a structured approach, investigating first the characteristics of the major component (mucin) of the mucosal layers. Temperature and solute effects are investigated and then mucins interaction with biologically relevant active compounds are further characterised. Cell morphological responses to actives are then investigated. We limit the scope of this study to the adsorption/desorption, nanostructure and nanoscale mechanical sensing at the mucosal interfaces. Nervous system signalling and mental perception of feel is not investigated here.

15

2. Background and literature review

The objective of this research is to further understand the trans-mucosal delivery and sensory attributes of the mucosal layer. The research is essential as the growth of nanotechnology will inevitably lead to an increase in its application to food products. How will these be perceived? Will the integrity of the layer be compromised by manufactured products? Is it possible to traverse the mucosal layers, easily and without adverse effects for applications such as drug delivery? These are some of the questions that will require a profound knowledge of the mucosal layers. They also protect the underlying epithelia from mechanical damage by lubricating the surface and structural properties of the layer should also provide key insights into the structure-function relationship. A priori knowledge of protein adsorption at solid/liquid interfaces is essential due to the interfacial nature of the mucosa. Indeed the addition of other molecules (e.g. food molecules) at the surface adds additional complexity to the problem. This chapter will present the current situation, the challenges faced by the field and how this work will take the field further.

2.1 Proteins, polyelectrolytes and polyampholytes

Polypeptides (proteins), glycoproteins and deoxyribonucleic acid (DNA) are a few examples of biologically relevant polyelectrolytes. Polyelectrolytes are polymers with electrolyte groups, some of which are used in mucoadhesive systems (such as food and personal hygiene products) as modifiers of rheological or structural properties. The electrolyte group charges the polymer chain and the molecule retains both the properties of the salt (charge) and of the polymer (flexibility) [57].

This chapter will first review proteins, the best studied molecules and continue onto a

16

brief overview of polyelectrolytes followed a review of polyampholytes. The emphasis will be on adsorption. Also the effects of salt as these are inextricably linked with mucosa and temperature as the function of these interfaces span wide temperature ranges and salt concentrations.

2.1.1   Protein structure

The inherent conformation of a protein is determined by its amino acid sequence and the conformations of proteins generally fall into two catagories, globular (closed proteins) and fibrous (unfolded). The globular proteins are numerous and by far the most common and well studied category and tend to have their apolar side chains located at the interior of the protein whilst polar residues are found at the exterior. Fibrous proteins however are elongated and flexible, typically with characteristic subdomains which arrange as globules analogous to beads on a string [58, 59]. This natively unfolded conformation is the most relevant for this project as this mucin is believed to fall into this category. The conformation also affects the adsorption characteristics of proteins such that the fibrous proteins (when compared to globular) should undergo major inter-globular rearrangement when binding the surface [57, 60].

2.1.2   Protein adsorption

Protein adsorption at solid liquid interfaces is an essential process for most (if not all) biological systems. Signalling processes, for example in plants, bacteria and eukaryotic organisms, very often require the binding of one or more molecules to a substrate whilst protein attachment to implants is the first step in implant-induced thrombosis [61]. Their adsorption behaviour is complex and the vast array and

17

diversity of proteins makes the field byzantine and overall poorly understood [62, 63, 64].

The adsorption of simple uncharged homopolymers is driven by changes in enthalpy (the internal energy of a system) and restricted by conformational entropy (the ability of a system to respond to change). Protein adsorption per se is more complex, as many enthalpy and entropy factors are involved. Enthalpy forces include van der Waals and electrostatics between the surface and the protein occur at distances of a few angstroms. Whilst entropic factors such as counter ion release and protein molecule conformational changes during adsorption add to the complexity of protein adsorption [65].

The surface free energy is an important characteristic of the surface properties and relates to the distribution of inter-molecular bonds formed when the surface is created. An interpretation of the surface energy (or wettability) of a surface can be obtained by contact angle measurements. Here a water droplet is placed on the surface and the contact angle at one edge of the droplet is measured. A low contact angle indicates that the droplet is sitting high on the surface and that the surface is hydrophobic and a high contact angle implies that the droplet spreads and that the surface is hydrophilic. Surface charges are also important characteristics.

When the protein first adsorbs, the binding energy between the proteins anchoring point and the surface will be small. Typically proteins will readily adsorb to surfaces. Further relaxation of the molecule after adsorption affects the overall energy state. These relaxation processes generally have longer timescales than those of adsorption and include surface diffusion and post adsorption conformational changes. For an

18

adsorbing protein, which undergoes large conformational changes, non-electrostatic forces are dominant whereas the opposite is true for proteins which change very little [66, 63]. Once on the surface proteins may diffuse and it is also possible that some molecules could desorb. This however is highly unlikely as most proteins adsorb irreversibly. Finally the molecule may continue to spread, forming further bonds with the surface [67].

Even spheroidal proteins can show bulk concentration dependent post adsorption transitions [68] providing clues for assessing conformation. These e ects are more marked (and have been quite thoroughly investigated) for the adsorption of brous proteins from a liquid suspension at a solid surface [69, 70, 71]. This is in contrast to proteins such as lysozyme, RNase, cytochrome c and subtilisin which undergo very little post adsorption transitions. For example lysozyme adsorbs as a monolayer, with an adsorbed layer thickness of approximately 3 nm on silica (determined using ellipsometry). This suggests very little change in conformation upon adsorption as the molecular dimensions of lysozyme in the bulk is typically 3 x 3 x 4.5 nm) [72].

Adsorption becomes increasingly complicated when more than one type of protein compete for adsorption. For example, let us imagine a protein that diffuses very quickly and has a low affinity for the surface and a protein which diffuses slower but has a high surface affinity (very often this is the larger protein). The faster diffusing protein will initially occupy the surface. The arrival sometime later of the second protein displaces the first as it has a higher affinity for the surface. This is known as the Vroman effect [73].

19

The adsorption behaviour of even larger and more complex biomolecules such as mucin has been much less comprehensively investigated. Malmsten *et al* have performed some initial investigations and on two mucins, porcine gastric mucin (PGM) and rat gastric mucin (RGM). These adsorbed onto surfaces in very thin layers of between 50-80 nm which is much smaller than the molecules radius of gyration, measured at ~ 200 nm [74]. Other molecules which behave in a similar manner are proteoglycans, made up of a protein core with covalently bound, carboxylated and sulphated glycosaminoglycans. Proteoheparan for example forms adsorbed layers which are much thinner than would be expected for such a large protein [75, 76].

For this work it was hypothesised that mucin would show bulk concentration dependent adsorption as their daisy chain conformation in solution is analogous with fibrous proteins such as fibronectin. In addition the layer thickness should be thinner than that which would be expected from the molecular weight of the mucin.

2.1.2.1   Protein adsorption kinetics

The study of protein kinetics is one of the most effective methods for extracting further the parameters which characterise the protein. The advances in label free sensing equipment [77] have led to a better understanding of the more widely studied proteins (albumin and fibrinogen) at solid liquid interfaces [63, 66]. Many proteins such as albumin, fibrinogen, -albumin and globulin adsorb onto a solid/liquid interfaces in a monolayer conformation [66]. On the other hand some fibrous proteins are known to form multi-layers upon adsorption [75].

20

2.1.3 Modelling adsorption kinetics

The complex nature of proteins makes modelling difficult and to date there is no single universal protein adsorption model. It helps if the proteins are thought of as a colloidal particle. Several models can then be applied such as Langmuir and random sequential adsorption (RSA), although one must always consider the limitations of each before using. Whilst a brief overview of adsorption models is discussed here this work makes use of the RSA model and as such the majority of this section will be devoted to RSA. Adsorption models are reviewed extensively in Schaaf, Voegel and Senger [78].

2.1.3.1 Adlayer formation

It is first necessary to understand the manner in which an adsorbed layer (adlayer) is formed at the interface as molecules adsorb from the bulk solution onto the surface.
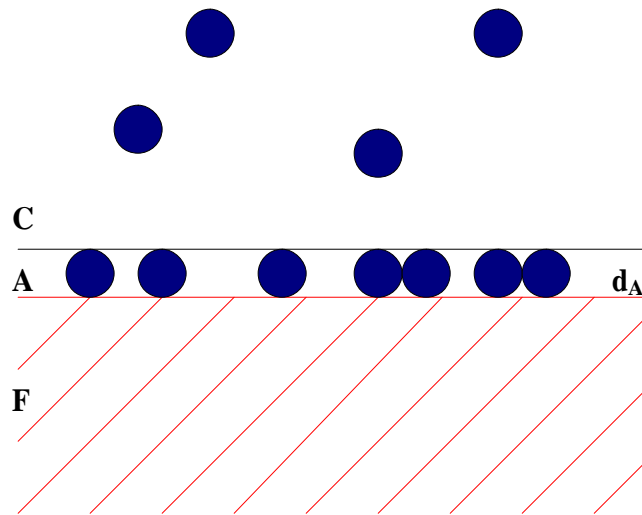
Figure 2.1: Schematic drawing showing idealised adsorbed protein layer, where the cover layer (C) contains molecules in solution at concentration C_b, the layer formed (A) and thickness (d_A) and the substrate F onto which the particles adsorb. Adapted from Ramsden (1995) [68].

The molecules adsorb at the substrate (F) from the bulk solution (C) as an adlayer (A) whose thickness is defined as d_A (Fig. 2. 1). When investigating protein adsorption the most important factor is   (mean mass of molecules at the interface) which is related to the surface coverage   by $= m /a$ where m is the mass and a the area of the molecule [77].

2.1.3.2   Diffusion limited adsorption

For this simple model, diffusion is the limiting factor and particles adsorb irreversibly with a probability of one [79]. There are two limitations for this model. First, the surface characteristics during adsorption are neglected. Second, diffusion is only limiting during early adsorption as more molecules arrive at the surface with time and will impede adsorption. The probability will no longer be one.

2.1.3.3   Langmuir model

Here all of the surface that is not already covered can be used for adsorption with function   ( ) = 1-   with   being the surface area available and   surface coverage [80].

2.1.3.4   Random sequential adsorption (RSA)

The random sequential adsorption model presumes that particles arrive one after another at a solid substrate in such a manner that they do not overlap. The substrate is assumed to be smooth and the particles rigid and homogeneous. When coming into contact with the substrate, particles will only attach if there is space, therefore if any section of the adsorption site is occupied by another molecule, the particle will return to the bulk solution [68, 81, 82, 83, 84].

As the molecules adsorb onto the surface their geometrical shape will impact on the available surface for further adsorption. After a time adsorption will stop as the surface becomes jammed. This is the jamming limit ($_J$) (e.g. a sphere has $_J \sim 0.547$). The available area is at first close to one but as the molecules start to adsorb and the surface becomes more occupied the corrections become increasingly prominent [85].

23

At a certain point the surface cannot accommodate further adsorption, despite there being space, and the jamming limit is reached [86]. The limitations of the RSA model are that only monolayers can be considered and it is a simplified model of what is actually occurring at the surface it cannot for example account for surface mobility.

It is anticipated that the RSA model will be relevant for mucin due to the large size of this molecule. The mass adsorbed, molecule area and jamming limit are powerful parameters that can be extracted and used for evaluating protein characteristics such as adsorption rate coefficients at the solid/liquid interface [68, 87].

2.1.3.5   Modelling adsorption characteristic using RSA

First one must determine the most appropriate model (Langmuir or RSA), which can be determined by plotting d /dt vs . For the Langmiur model a straight line fit is possible but it is not possible for the RSA model (Fig. 2. 2)
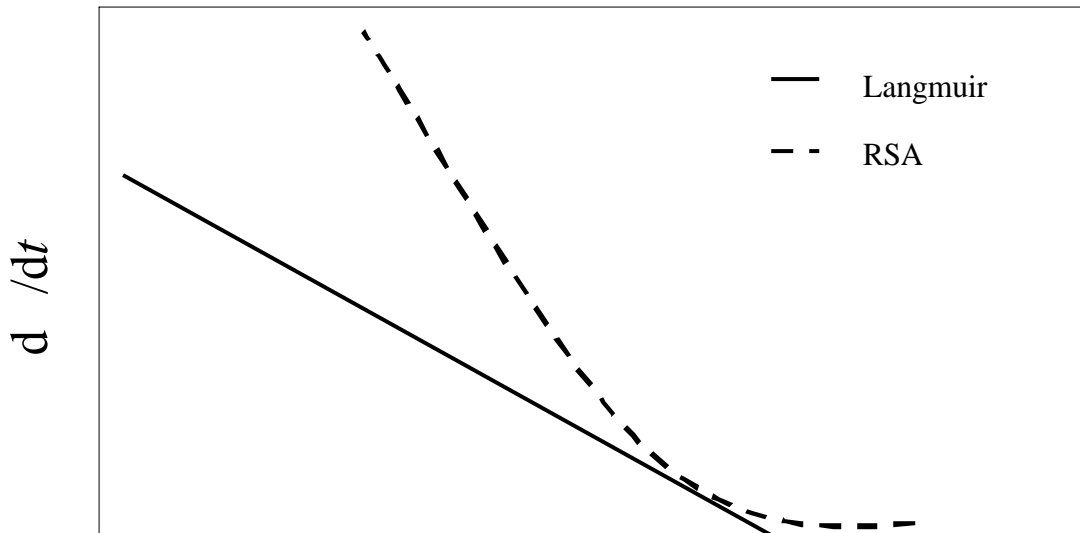
Figure 2.2: Representative schematic plots of d /dt vs   plots of protein adsorption for the Langmuir and RSA models where   is the mean mass of molecules at the interface and d /dt the derivative of   as a function of time (t).

Fitting the d /dt vs   slope with RSA (Appendix A, equation A. 9) provides the adsorption rate and molecule size (adsorbed) using

$$\frac{dM}{dt} = k_a c * \varphi(M, a)$$

(1)

where k_a is the adsorption rate coe   cient, $c*$ is the e   ective concentration in the vicinity of the adsorbent surface (we shall assume that $c* \sim cb$),   is the available area function and a is the area occupied per molecule. The statement dM/dt versus M is related to M by

$$M = \frac{\theta_J m}{a}$$

(2)

where m is the mass per molecule, and $_J$ is the jamming limit [88].

2.1.4   Proteins – temperature effects

Increasing the temperature above a critical temperature alters the tertiary (and occasionally secondary) structure of proteins causing denaturation, a good example of which can be observed when one cooks an egg. Here the albumin proteins of the white are denatured resulting in aggregation and a visible colour change. This type of denaturation is irreversible but many proteins can be reversibly denatured, returning to their native conformation once the temperature is lowered [89].

One can think of thermal denaturation of proteins as an unfolding of the protein as tertiary bonds are broken and the structure expands upon heating. This is the classic interpretation of thermal denaturation. There are however examples of proteins that exhibit inverse temperature dependence. Examples of which include insulin [90], amylases [91], elastin [92, 93, 94], lysozyme and ribonuclease A [95].

It is important to investigate temperature dependence as many poikilothermic organisms exist at varying temperature ranges. It is already well established that the enzymes (themselves proteins) of microbial extremophiles have subtly different amino acid sequences from those of their relatives living at normal temperatures. In other words, nature has solved the problem of altering enzymes to work at different

26

temperatures. However, an enzyme adapted to high temperature functions badly at low temperatures, just as the ordinary versions of the enzyme function badly at high temperatures. The enzymes (and other proteins) of poikilothermic organisms require a more sophisticated adaptation that allows them to function over a broad range of temperatures. Mucins are present across all animal phyla and must function at many temperatures. Teleosts for example live in the subzero temperatures of the Antarctic Ocean, and at another extreme desert ants such as *Cataglyphis bicolor* forage at temperatures that can exceed $60\,^{\circ}C$ [96]. Indeed temperature dependence is also relevant for humans as body temperature will vary e.g. marathon runners body temperature will increase to $\sim 40\,^{\circ}C$ [97, 98] whereas the body temperature will lower during major heart surgery (cardioplegia) [99].

Conformational relaxation is proposed as an inverse temperature dependence mechanism for some enzymes. Here rapid relaxation occurs at the active site during catalysis and as the enzyme binds the substrate the active site is no longer in equilibrium with the rest of the molecule. This induces strain, altering the surface energy on which the reaction takes place. Successive relaxation steps for the enzyme (once bound) involve the making and breaking of many weak bonds albeit at a slower rate than the catalysis reaction [100, 101]. The enzyme reaction rate should therefore exhibit inverse reaction rate (Arrhenius) behaviour as the conformational relaxation of the molecule is accelerated by an increase in temperature therefore leaving less time for the strained molecule to increase the reaction rate.

Thermal denaturation of fibrinogen [102] and -lactoglobin [103, 104] leads to an increase in adsorbed mass. This is most likely due to the increase in degrees of

27

orientation and the exposure of sites that can bind the substrate. For this project it is to be expected that mucin will behave in a similar manner.

2.1.5   Proteins - the Hofmeister series

The presence of salts in the bodily fluids has a profound effect on many proteins. Adding salts in vitro alters the solubility of proteins in solution. For low concentrations of salt the solubility can be increased (salting in) as oppositely charged counter ions surround the protein. They screen it and reduce electrostatic activity with the solvent which leads to increased solubility (Debye-Huckel theory) [105]. High salt concentrations will reduce the solubility and precipitate the protein. The large quantity of salt ions interact with the solvent reducing its ability to solvate the protein and hence it is precipitated.

As biological processes take place in the presence of salts the Hofmeister series is highly relevant for understanding further the behaviour of proteins. This series is concerned not only with the salting in and salting out effects but also the effect of ions on water structure. Aggregation and adsorption of are important factors in biological systems e.g. the immune response where complexes are formed during blood clotting and are affected by salt concentration and type.   The Hofmeister series is characterised as having the following effects.

- Active at moderate to high salt concentrations of 0.01-1M,
- Sodium chloride (NaCl) is effectively the cross-over point and has only a small effect on behaviour,
- Effects are additive over all salts,
- Anions dominate (change solubility more than cation for a given change in radius).

28

Structure makers, termed kosmotropes, interact strongly with water molecules and stabilise protein whereas chaotropes are structure breakers, interacting weakly with water and destabilising biomolecules (Fig. 2. 3). Generally, kosmotropes stabilise the native conformation and for enzymes the result is enhance activity, presumably because the native conformation is the active state. There are however exceptions, such as NADP-glyceraldehyde-3-phosphate which increases its activity in the presence of chaotropic salts. Haemoglobin also has reduced oxygen affinity in the presence of monovalent anions. The authors suggest that the solute affects the tensed (T) and relaxed (R) equilibrium of the haemoglobin subunits [106].

KOSMOTROPE									CHAOTROPE	
Anions	F^-	PO_4^{3-}		SO_4^{2-}	CH_3COO^-	Cl^-	Br^-	I^-	CNS^-	
Cations	$(CH_3)_4N^+$	$(CH_3)_2NH_2^+$	NH_4^+	K^+		Na^+	Cs^+	Li^+	Mg^{2+}	Ca^{2+}	Ba^{2+}

Table 2.1: Ions categorised according to the classic Hofmeister series interpretation.

The mechanism of the Hofmeister series has yet to be clarified. The challenge which faces the series is that the correlation of experimental results with a single Hofmeister parameter is not possible. This is due to the nature of the components involved. All proteins differ in conformation and subtle environmental changes are usually all that is required to induce large-scale molecule changes. Therefore each biomolecule has to be studied individually [107, 108].

Recently Dér *et al* have shown that for the natively open proteins one expects inverse Hofmeister behaviour whereby kosmotropes should destabilise structure and chaotropes should stabilise [109]. If this is indeed the case one would expect for these

mucin investigations that chaotropes should stabilise the native conformation and that adsorption may be increased. Although it may be the case that post adsorption conformational changes (if these occur for this molecule) could be inhibited and the absorbed amount may be decrease. Kosmotropes should destabilise mucin and this may lead to a partially denatured, unravelled molecule which in theory should adsorb much more readily.

2.1.6   Polyelectrolytes

Dependent upon their dissociation constant, polyelectrolytes can be either weak or strong. Those which dissociate well in solutions of intermediate pH are called strong whereas as those that only partially dissociate are called weak. Changing the solution pH or ionic strength will alter the net charge of polyelectrolytes in solution. The physical properties of polyelectrolytes are directly related to their degree of charging. During adsorption at a surface, counter-ions may be released into the solution [110].

2.1.7   Polyampholytes

Polyampholytes are polyelectrolytes which contain both cationic and anionic charges. Due to the competition between charges the physical behaviour of these molecules are more complicated than those of single charge polyelectrolytes. Gelatin (denatured collagen), bovine serum albumin (native conformation protein) and synthetically produced co-polymers are all examples of polyampholytes. If polyampholytes are weak then altering the solution pH will alter the charge of the polyampholyte and at pH values far from the isoelectric point (pH at which protein carries no net charge) the polyampholytes behave as polyelectrolytes [111].

30

2.1.7.1 Polyampholyte behaviour in solution

In the 1950's five basic properties were suggested for dilute polyampholytic solutions that have been confirmed by many further studies

- The conductivity, coils size and viscosity of polyampholytes are at a minimum when at the isoelectric pH.
- Polyampholytes only dissolve at pH values far from, and precipitate at values close to the isoelectric point.
- Viscosity and size increase with the addition of salt.
- Viscosity and size decrease at pH values far from the isoelectric point.
- Viscosity and size in water have a minimum that relates to co-polymer composition.

Due to the random nature of charges along the polyampholyte backbone most natural polyampholytes are asymmetric. These have a structure in solution which is random, similar to that of a denatured protein and the conformation is that of a daisy chain (beads on a string) (Fig. 2. 3).
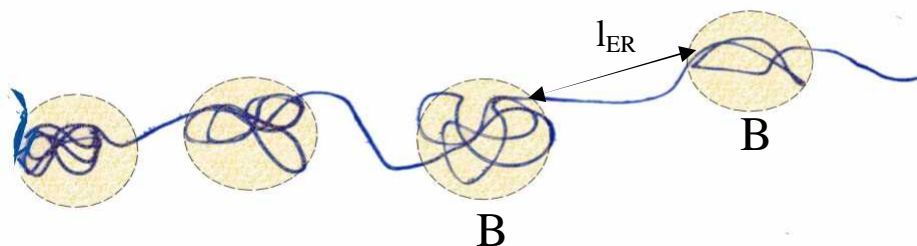
Figure 2.3:. Daisy chain configuration of an asymmetric polyampholyte. Beads (B) are separated, through electrostatic repulsion by length (lER).

Here the beads (B) are repelled via electrostatic repulsion at a length of l_{ER} [112]. This is the structure, in solution, of the mucin used in this project [113].

Polyampholytes in solution are catagorised as [114]

- Dilute – very low concentration, chains infrequently contact each other.
- Semi-dilute – increasing concentration, chains will periodically become entangled.
- Entangled – very high concentrations, chains will frequently entangle.

2.1.7.2   Polyampholyte adsorption

Initially the desire by the photographic industry to understand gelatin adsorption stimulated interest in polyampholytes at interfaces. Gelatin, a polypeptide co-polymer can be either cationic or anionic (dependent upon pH) and maximum adsorption occurs close to the isoelectric point. In experiments using mica as the substrate (negative charge) the gelatin adsorbed well even if the molecule also had a net

negative charge. Therefore the gelatine binds using its positive groups that bind ionically with the negative surface charges [110].

2.1.7.2.1 Polarization-induced attraction model

The polyampholyte chain monomers (of opposite charge) will be pulled in opposite directions, elongating the chain. The polarization-induced attraction model suggests that the asymmetric polyampholyte chains become polarized and adsorb as elongated chains within the electric field of a charged substrate [115, 116]. The electric field [E (z)] with a number of charges per area decay from the surface ( ) can be represented as

$$E(z) = \left(\frac{4\pi e \sigma}{\varepsilon} \right) \left(\frac{\lambda}{\lambda + z} \right)$$

(3)

when = (2 l_B) Debye length, l_B the Bjerrum length, z the height of the electric field, e the elementary charge of the solvent and the dielectric constant of the solvent. For the polarization-induced attraction model there are three regimes. The first is the pole regime (z <) where the chain size increases linearly with as it is held in the extended conformation in the electric field (Fig. 2. 4).

33
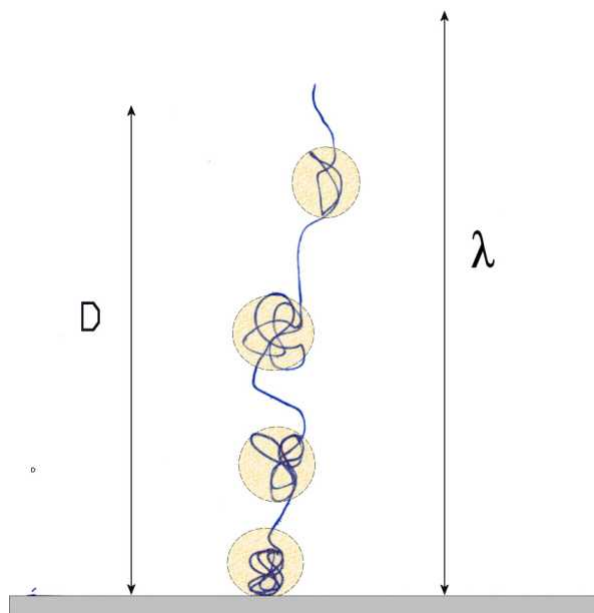
Figure 2.4: Pole regime of asymmetric polyampholyte adsorption. The charges decrease from the surface at length   and D the chain size, extended from the surface by the electric field. Adapted from Dobrynin [111].

where D is the chain size perpendicular to surface. As the surface coverage (2) increases,   decreases (as an increasing number of surface charges are utilised by the protein) until the chain size at the surface is equal to that of . At surface densities above 2 the molecules adsorb in a fence configuration where the chain is restricted to lambda (Fig. 2. 5).
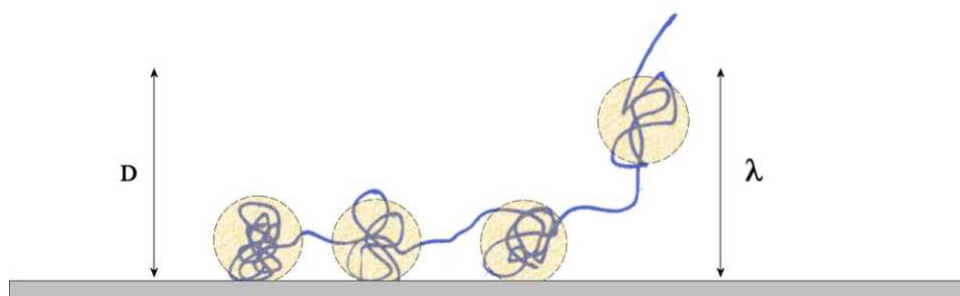
Figure 2.5: Fence regime of asymmetric polyampholyte adsorption. The decrease in free surface charges as the polyampholyte attaches further decreases . Adapted from [111].

A further increase of surface area coverage (3) results in the formation of pancake structures. Here all opposite charges (compared with those of the surface) are constrained within whilst surface equivalent charges are suspended as loops in the covering media outside of (Fig. 2. 6).
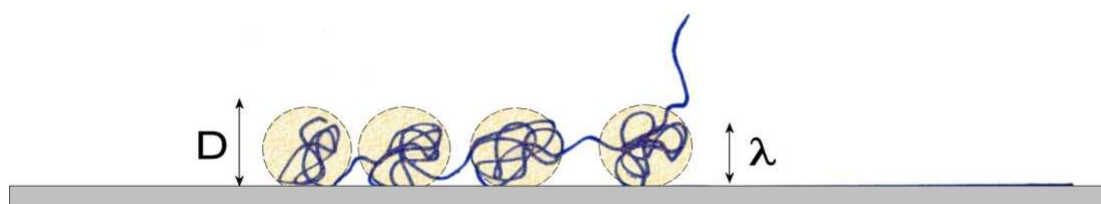
Figure 2.6: Pancake regime of asymmetric polyampholyte adsorption. is reduced further as the free surface charges are occupied further. All molecule charges which oppose the surface are within whilst all surface equivalent charges are above. Adapted from Dobrynin [111].

35

2.1.7.2.2 Multilayer adsorption

The polyampholytes adsorb as multilayers forming stretched chains and pseudobrush structures (Fig. 2. 7) [114].
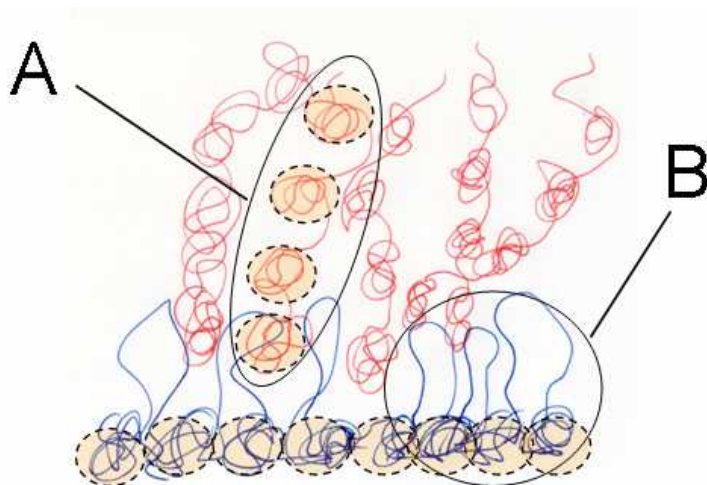
Figure 2.7: Multilayer adsorption regime of asymmetric polyampholyte. A denotes stretched chains and B pseudobrush structures.

The mucin used for this project should therefore adsorb in this conformation.

2.1.8 Polyampholyte salt effects

Katchalsky and Miller (1954) found that increasing the acidic properties of the copolymer increased the dissociation of bases from the polyampholyte at a given pH. Dissociation is reduced when salt is added as the electrostatic interactions are screened [117]. The viscosity decreases as the number of charged groups increases, reducing the size of the polyampholyte [118].

Increasing the salt concentration initially leads to a decrease in viscosity, most probably due to electrostatic screening which extends the chains. Adding further salt

36

reverses this. Increasing the viscosity and swelling the chains as the local charge attractions are screened, in turn condensing the polyampholyte [119].

2.2   Mucin

This section introduces mucin, a heavily glycosylated glycoprotein, which is the largest constituent of the mucus layer. Humans secrete a mucosal layer the majority of their body surfaces, such as the oral cavity, gastrointestinal tract, respiratory airways and surface of the eye [120]. The major component of the mucosa is mucin (Fig. 2. 8), a high molecular weight glycoprotein that is found across all animal phyla. For humans there have been 19 mucin genes [121] characterised thus far. Many mucin genes are tissue-specific and the glycosylation configuration within a tissue can also vary between individuals suggesting a recognition role for these molecules. They are able to identify non-host (hostile) microbes and also 'self' such as during fertilisation and when communicating with the outermost epithelial cell layer of the body surface [122].

Branched sugar side chains
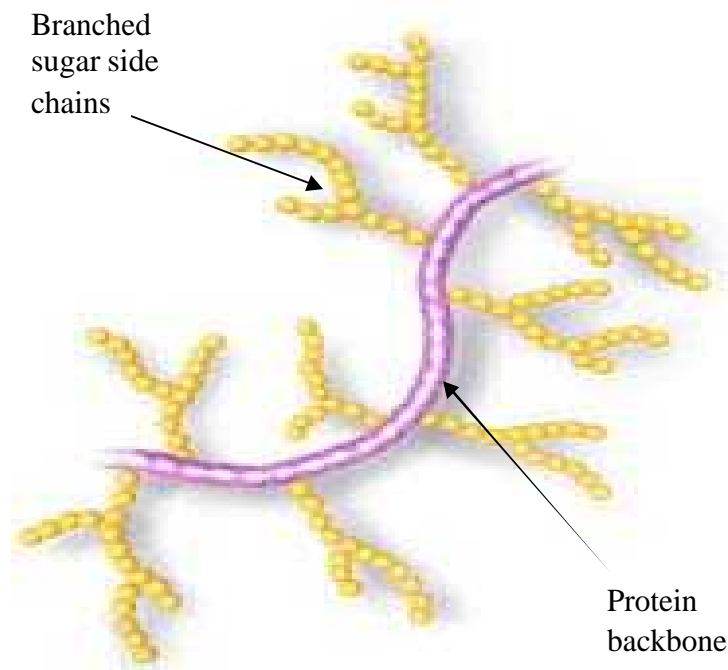
Protein backbone

Figure 2.8: Schematic diagram of mucin molecule which consists of a central protein core with branched glycosylated side chains. Adapted from reference [120].

2.2.1   Mucin structure

The structure consists of a protein backbone that is heavily glycosylated (approximately 50-80% by weight of the molecule is made up of sugar moieties). Mammalian mucins in general contain fucose, galactose, N-acetylglucosamine, N-acetylgalactosamine and sialic acid with a relatively small quantity of mannose also present. Figure 2. 9 shows a schematic representation of the mucin sugar chains, the majority of which are linked via O-glycosylation to one of the numerous serine or threonine amino acids through the N-acetylgalactosamine (GaN) sugar. There are a small number of N-glycans that are linked via asparagine residues and some C-mannosyl residues linked through the tryptophan amino acid [120].

38
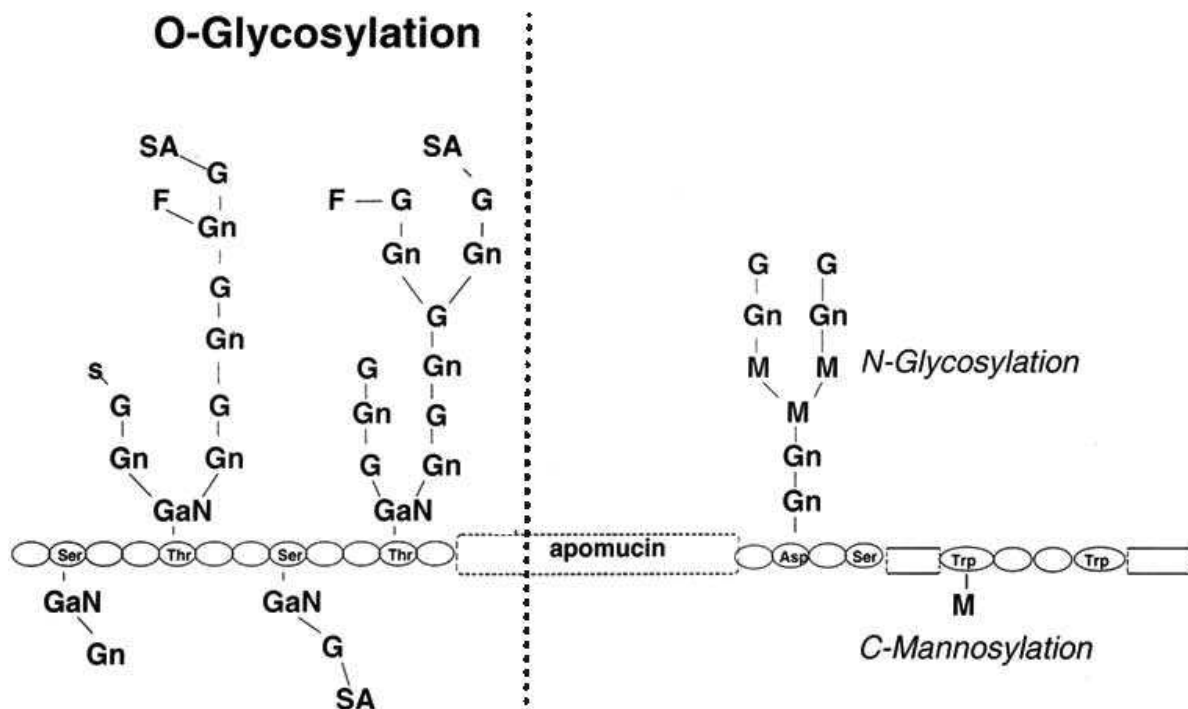
Figure 2.9: Scheme depicting mucin carbohydrate chains. Adapted from reference [120].

Mucin has diverse roles ranging from lubrication [122, 123, 124] (e.g. as a component of the fluid between the eyelid and cornea, saliva, gastro-intestinal tract, lungs and airways) through to an immune system role whereby invading bacteria are engulfed and neutralized by the mucus layer. The outstanding lubricating properties of mucin have been linked to its ability to adsorb to surfaces of practically any chemical nature, forming a layer that retains water. This creates a repulsive force that greatly reduces friction between surfaces [125, 126]. Mucins are therefore key components of saliva and the ability of saliva to adsorb onto surfaces is due to mucin's film forming properties [127, 128]. Consequently when mucin based saliva substitutes are tested they lubricate and reduce wear better than their saliva counterparts [129, 130].

Regulation of both membrane bound and secreted mucins also have a role during tumor development, [131] such as the reduction of cell adhesion due to corrupted expression, releases cells into circulation thus facilitating metastasis [132, 133].

2.3   Catechins

The focus of this project is to characterise the mucosal layers and investigate the mechanical, structural and therefore sensory impact on the properties of the layer. Astringency is believed to form part of an astringent perception. It is a mechanical response and one group of molecules that cause an astringent sensation are plant polyphenols [5, 6, 7, 8, 9, 134, 135] which complex with salivary proteins leading to aggregation [136]. Catechins are a group of polyphenolic flavonoids, secondary plant metabolites. It is widely believed that salivary proteins act as a primary defence against harmful, mainly high molecular weight tannins polypenolic flavanoids, (e.g. tannins) forming insoluble complexes that inhibit their functionality, e.g. absorption from the intestinal canal or interaction with other biological compounds [137].

2.3.1 Catechins, health benefits and types

Epidemiological studies show that the risk of contracting many diseases such as cancer, heart disease, diabetes is reduced when eating a diet containing high quantities of fruits and vegetables. Although many of the mechanisms and components have yet to be clarified it is thought that phyto-chemicals are the active components [139]. One group of phytochemicals are the catechins, which include gallocatechin (GC), epigallocatechin (EC), epigallocatechin (EGC), epicatechin gallate (ECG), epicatechin (EC) and epigallocatechin gallate (EGCg). A very high quantity of these are found in green tea *Camellia sinensis* with EGCg being the most biologically active and abundant source in green tea (Fig. 2.10) [140, 141, 142].

40
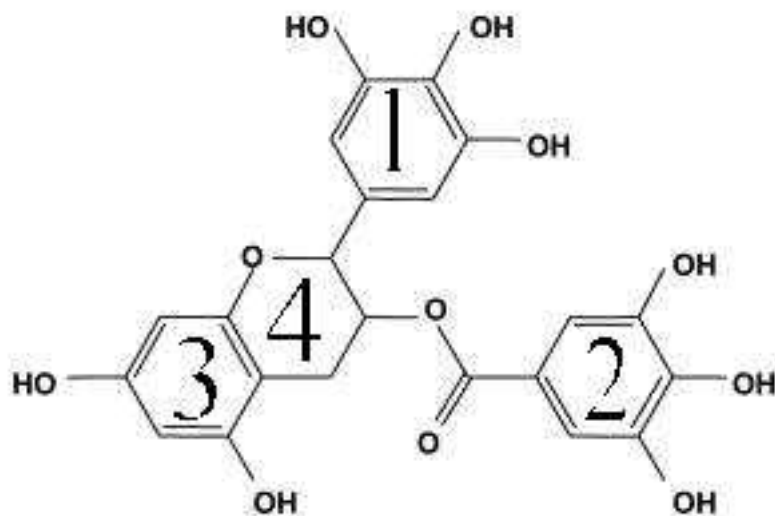
Figure 2.10: Diagram of EGCg structure. Molecular weight 458.37 and chemical formula $C_{22}H_{18}O_{11}$. Adapted from reference [141].

2.3.2 EGCg effects on astringent perception

It is suggested that the major components of saliva responsible for aggregation are proline rich proteins (PRP) and histatins [143, 144], with the molecular basis of polyphenol-PRP-like aggregation being well understood [137, 145]. The pyrrolidine rings of the prolyl groups act as potential binding sites that stack face-to-face with the galloyl rings of the phenolic substrate with other interactions (such as hydrogen bonding) further stabilizing the complex [146, 147]. Recent investigation of binding to a synthetic proline rich peptide (GLN-GLY-ARG-PRO-PRO-GLN-GLY) found that majority of interactions occurred at the ARG-PRO-PRO site with the Arg side chain positioned close to ring 1, PRO4 positioned over ring 2 and PRO5 positioned over ring 3 (Fig. 11). Prolines were almost always involved in stacking [145].

41

2.4   Biolubrication

Lubrication reduces friction between body surfaces and contributes to the sensory perception of foreign material (e.g. food in the mouth and dust in the eye). Furthermore, for eukaryotes, movement is a survival pre-requisite and, when there is movement, lubrication is vital for wear reduction and effective function. Examples are diverse and numerous ranging from mammals that lubricate their joints and coat, for example their respiratory airways, gastro-intestinal and ocular surfaces with mucosa to cephalopods that utilise a mucus-coated foot on which they move [120]. Biolubrication is also crucial for many human processes involving movement, such as oral processing which greatly impacts on mastication and mouthfeel [148].

2.4.1 Friction

Leonardo da Vinci (1452-1519) first quantitatively investigated friction 200 years before Newton introduced the notion of force and proposed that friction is independent of the surface area and that doubling the load would double the friction. Guillaume Amonton (1663-1705) revived da Vinci's work and added that the friction is related to the roughness which the surfaces must overcome. Leornhard Euler (1707-1783) first introduced static and kinetic friction and Charles August Coulomb (1736-1806) later published and added to the knowledge stating that friction is related to the force between two surfaces and the properties of the surfaces themselves [149].

Static friction applies to objects in contact that are not moving relative to one another whilst kinetic friction occurs when two moving objects rub together [150]. Stribeck (1902) introduced the velocity dependence of friction in the presence of liquid whereby at high velocities an elastohydrodynamic (EHL) fluid film regime forms which prevents the surfaces from coming into contact. Conversely boundary

lubrication or nanofriction (a lubricating film of less than 100 nm) is characterised at low speeds and is the separation of solids at the molecular level whereas the mixed regime occurs when the roughness of the surface is comparable with the film thickness at those velocities between the EHL and boundary regimes [151].

2.4.2   Biolubrication molecular mechanisms

The three well known molecular mechanism components by which lubrication in biological systems can be described are presented here.

2.4.2.1 Ion ball bearing

Using force apparatus, Klein *et al*. first proposed the ion ball bearing model highlighting the role of interstitial fluid. Friction forces for aqueous solutions maintain a bulk water shear fluidity status when subjected to a shear force, implying that molecules in solution slide over one another, acting as molecular ball bearings [152].

2.4.2.2 Brush-brush interaction and counter ion depletion

The addition of neutral polymers to a solution greatly reduces the friction of sliding surfaces separated by solution [153, 154, 155], whilst the use of charged polymers has an even larger effect. Charged polyelectrolyte brushes are in a swollen state at low ionic strength and opposing brushes repel one another creating a repulsive force preventing surfaces from coming into close contact (where attractive van der Waals force would snap them together). This prevents dry friction between soft solid or semi-solid surfaces such as tongue-on-palate or tongue-on-teeth.

2.4.2.3 Cartilage matrix exclusion theory

Water is by far the major component of the cartilage matrix making up between 70-90% of the some matrix (by weight) made up of water. Collagen (10-20%) and proteoglycans (2-10%) make up the rest with interstitial water between the collagen fibrils providing the cartilage with its highly effective lubricating properties. The density of the proteoglycans are key for lubrication as many proteoglycans are bound close together in the matrix creating a repulsive force (as the negative charges are constrained together in a small area) that is neutralised by positive ions in the external fluid. The increase in ion concentration within the tissue (compared with that of the exterior) leads to a swelling pressure and, as the joint is moved, the interstitial fluid is removed. This exclusion of the water increases the density of charges and in turn increase the repulsion [156].

It is anticipated that mucin will form a layer which contributes to lubrication, most likely through the mechanisms above.

2.5 Cells and cell spreading

The mucosal layers form barriers that protect the underlying cell layer. These epithelial layers, linked with the mucosal layers play an active sensory role. Cells fall into two categories, prokaryotes and eukaryotes. Both contain DNA, have a membrane and may have a cell wall that separates them from the external environment and contain cytoplasm. Bacteria are prokaryotes which carry their DNA in the cytoplasm with strains such as *Staphylococcus, Corynebacterium, Brevibacterium and Acinetobacter* living on the skin and *Propionibacteria* residing in the hair follicle. The most noticeable difference for eukaryotes is the presence of a nucleus that contains the DNA [45].

44

2.5.1 Cell adhesion

The cells of multicellular organisms bind to the extracellular matrix (ECM) and each other. The ECM consists of macromolecules secreted by cells, such as collagen, proteoglycans and glycoproteins (e.g. fibronectin and laminin) that interact with the cell through receptors at the cell surface. The glycoproteins give an ordered structure to the extracellular matrix and the adhesion molecules on the surface of the cell bind to these. There are a number of receptors involved in cell adhesion

- Integrin receptors which are attached to cytoplasmic filaments and span the cell membrane, attaching to arginine-glycine-aspartate (RGD) domains on extracellular proteoglycans [157].
- Cell adhesion receptors belonging to the immunoglobulin superfamily (IgSF) have an immunoglobulin domain and are mainly immune system cell type specific.
- Selectins are transmembrane glycoproteins involved in cell adhesion.
- Cadherins are calcium dependent cell-cell adhesion molecules.

2.5.2 Cell morphology

The suspended cell morphology (for many cell types) in solution is that of a sphere. When attaching to a substrate cells bind and spread as they become established which affects viability [158].

2.5.3 Cell-cell signalling and cell signalling pathways

Cell to cell signalling involves the release of a signalling molecule from one cell which binds to a specific receptor on another cell. This can be paracrine, endocrine of autocrine and in addition cells can also communicate via gap junctions. Binding of the signalling molecule results in a receptor conformational change which initiates secondary signalling cascades that travel through the cell's internal machinery [159].

3. Experimental techniques

This chapter focuses on the primary experimental technique used throughout this work, optical waveguide lightmode spectroscopy (OWLS). An overview of the technique and the physical principles underlying the technology are presented as are the experimental procedures used. The details of cleaning procedures are provided, which were devised and adapted from previous work. Finally the cell culture and imaging protocols are presented.

3.1 Label-free optical sensing

Whilst techniques involving radioactive and fluorescent labelling have provided insight and many clues as to the nature of various cellular processes the fact remains that they require a modification to the molecule of interest. This will inevitably affect the function of the molecule [77]. Therefore non-invasive label-free optical sensing and other novel techniques play an important role in future investigations of cellular and subcellular systems.

3.1.1 Optical waveguide lightmode spectroscopy (OWLS)

The OWLS technique is extremely powerful for measuring thin films at the solid/liquid interface and has mainly been used to study the adsorption of protein layers [160, 161, 162]. This technique is also very well suited for cell-based experiments which investigate cell binding and cell spreading parameters [163, 164]. Cell spreading can also be measured using light microscopy [165], although the results are harder to quantify. Quartz crystal microbalance (QCM) investigations [166, 167, 168] also give information on attachment kinetics, however with very little information on spreading.

47

Hug *et al* (2000) have taken the possibility of OWLS as a whole cell sensor by looking at cell adhesion and morphology changes of fibroblasts. The strong skin irritant benzalkonium chloride produced a concentration-dependant cell response measured by the OWLS. Colchicine however reduced the OWLS signal, which would be expected as colchicine disrupts cytoplasmic microtubules that play a vital role in both in cell structure and movement [169].

3.1.1.1   OWLS principle

OWLS technique confines the light within a thin, high refractive index material whereby the upper and lower interfaces confine the light which propagates via total internal reflection (Appendix A.1 and Fig. 3.1). A grating coupler couples the light into the high refractive index material [170].
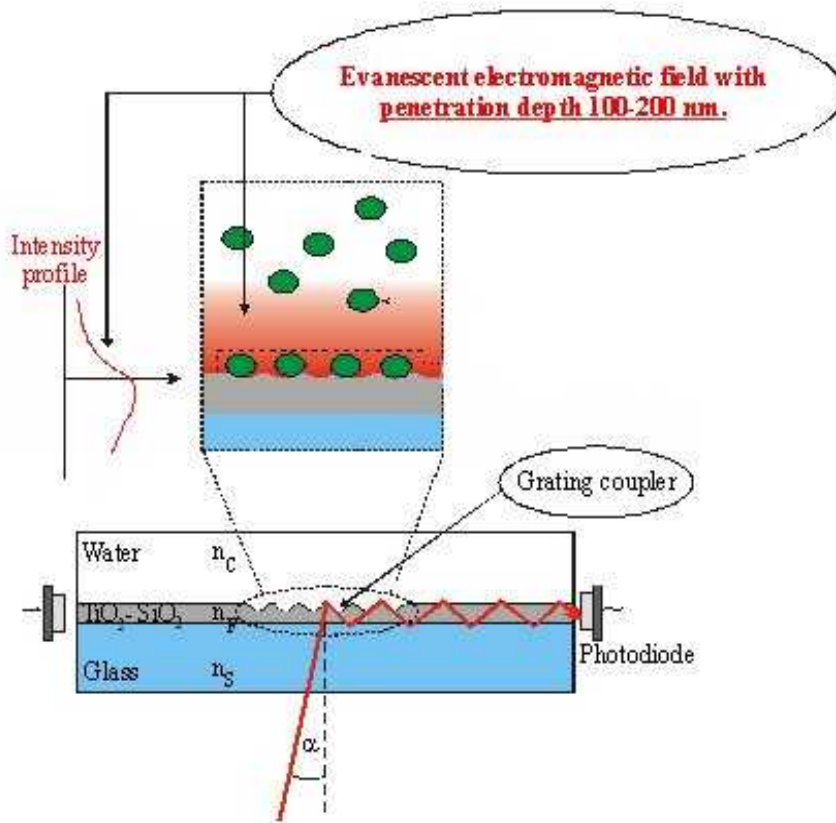
Figure 3.1. Optical waveguide lightmode spectroscopy. The waveguide is roated on a goniometer between -6 to +6 degrees. At a critical angle ( ) light is coupled into the waveguide and propagates to the photodiode. As it propagates it travels via total internal reflection within the $T_iS_iO_2$ layer and the electromagnetic evanescent field (penetrates 100-200 nm above the surface) is the sensing area. Molecules adsorbed at the surface of the waveguide will interfere with the evanescent field causing a shift in the measured propogation constant.

To determine the characteristics of the waveguide (S, F and C: Fig. 15) the effective refractive index (propagation constant; N) is calculated [171].

$$N = n \sin(\alpha) + \frac{k\lambda}{\Lambda}$$

(4)

where n is the refractive index (of air),   the angle of the incoupled light, k the diffraction order,   the wavelength of the light and   the period of the diffraction grating. A three layer model is used to calculate the waveguide parameters. Adsorption of material onto the surface will form an adlayer (A, Fig. 2. 1) with the parameters characterised using the four layer mode equation [77, 172]. The refractive index of the adlayer, n_A is calculated and the thickness, d_A (Appendix A. 2) from which the adsorbed mass can be determined using [173, 174]

$$M = d_A \frac{n_A - n_C}{dn/dc}$$

(5)

Two experimental waveguide systems were used, the OWLS 110 (Microvacuum, Budapest, Hungary) setup pictured in Figure 3. 2. This was used for the majority of experiments with the custom built setup used (built by postdoc R. Horvath see [175, 176] for setup details) for the cell experiments. The custom built setup enabled the extraction of raw data and the calculation of additional parameters [177].

50
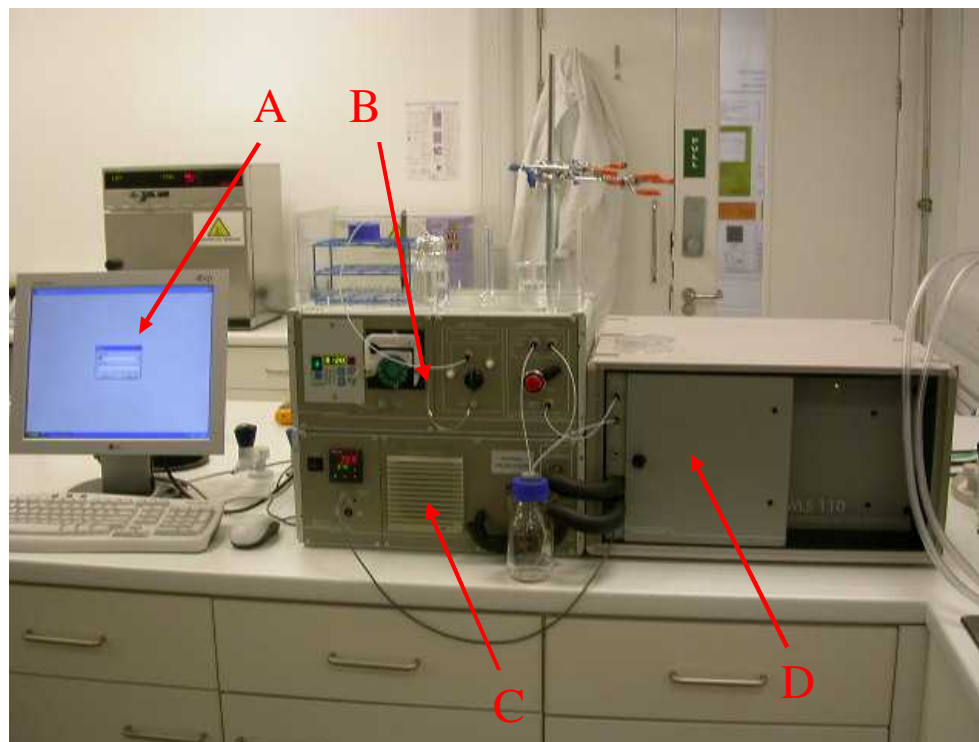
<u>Figure 3.2: Experimental setup of OWLS 110 system (Microvacuum, Budapest, Hungary).A, control panel, B, injection system, C, temperature control unit, D, goniometer set up with mounted cuvette.</u>

A schematic representation of the flow through cuvette system (Fig. 3. 3) shows the experimental setup in a little more detail. The waveguides are first cleaned, inserted into a holder and the cuvette secured on top of the waveguide (sealed using an 'O' ring).

In   Out

O ring

C

Waveguide

F

S

PD

Polarised Light

C – Cuvette (measuring area)
F   - High R I film
S   - Substrate
PD – Photodiode
\ - Grating coupler
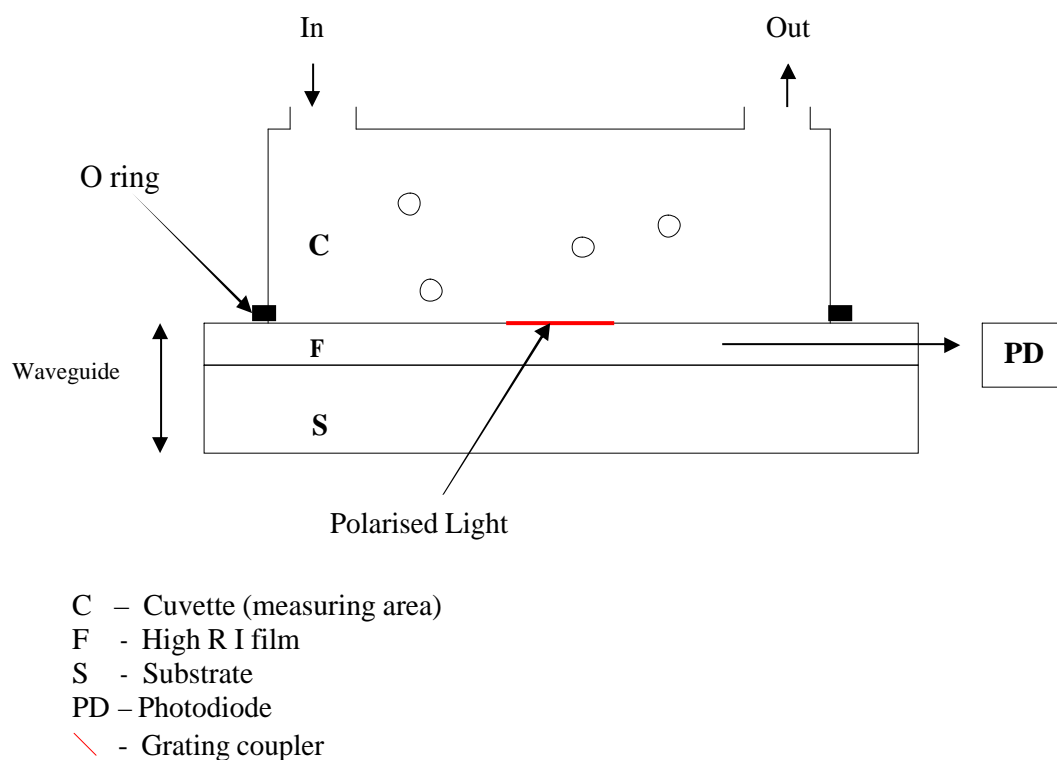
Figure 3.3: Schematic depiction of OWLS setup.

To determine the mass of species at the surface is it important to have the refractive index increment of the molecules (dn/dc). A J357 refractometer (Rudolph research analytical, Hackettstown, USA) was used to measure the refractive index of all solutions used for OWLS investigations (Fig. 3. 4). The refractometer has a sapphire prism onto which a 632.816 nm wavelength laser is focused. The refractive index of the solution is determined by the amount of light that is reflected back onto the photodiodes.

52

Figure 3.4: Rudolph J357 refractometer.

3.2 Experimental procedures (OWLS)

Five separate experiments were conducted using OWLS to define

1. Adsorption/desorption characteristics of mucin layers on $S_iT_iO_2$ waveguide surfaces

2. Temperature dependence of mucin adsorption on waveguide surfaces

3. Salt effects on adsorption characteristics

4. The effect of catechins on

    a. Adsorption of mucin and EGCg mixed solutions onto waveguide surfaces

    b. Impact of EGCg on a previously adsorbed mucin layer

    c. Impact of mucin and EGCg mixed solutions on a previously adsorbed layer

5. Cell response to adsorbed mucin and mucin + EGCg layers.

3.2.1   Mucin adsorption/desorption

Initially the adsorption/desorption characteristics of mucin were investigated using OWLS. Waveguides were pre-equilibrated overnight in ultrapure water at 25°C and were assembled with the cuvette. The e ective refractive indices N of the transverse magnetic $T_{M}0$ and transverse electric $T_{E}0$ modes were repeatedly and continuously determined while, successively, (i) water owed through the cuvette, then (ii) mucin solutions in water at di erent concentrations spanning ve orders of magnitude, from 0.0001 to 10 weight % w/w (spanning the actual concentrations encountered in living organisms), and nally (iii) ultrapure water again for measuring the desorption kinetics. During the entire sequence of owing water, mucin and water again, the e ective refractive indices (propagation constants) of the zeroth order transverse electric and transverse magnetic lightmodes were measured. The wall shear rate (Appendix B. 1) of the fluids passing through the cuvette was 31 s^{-1} and the temperature was maintained at 25.0^{o}C.

The $N_{TM}(t)$ and $N_{TE}(t)$ values for the adsorption/desorption sequences were inserted into the two mode equations characterizing propagation of the guided light in a four-layer structure with isotropic layers: support, waveguiding lm, protein adlayer, and cover [70]. The two unknowns obtained were the thickness and refractive index of the protein adlayer. These in turn were combined to yield the mass of protein adsorbed at the waveguide surface [173].

The refractive index increment (dn/dc) [174] of mucin dissolved in water required for the calculation was determined using the refractometer by measuring the refractive

index at different concentrations. The determined value was 0.138 cm^3/g (Appendix B. 2). The practical outputs of the kinetic adsorption/desorption experiments were plots of adsorbed mass of mucin versus time.

3.2.2 Temperature dependence of mucin adsorption

The experimental procedure is similar to that of mucin adsorption/desorption except that the entire system (microcuvette, water and mucin solution) was maintained at 25.0, 37.0 and 60.0 ^0C whilst (i) water, (ii) 0.1% w/w mucin solution in water, and (iii) pure water again was owed through the cuvette. The dn/dc for 37 ^oC (0.141 cm^3/g) and 60 ^oC (0.138 cm^3/g) were both determined (Appendix B. 2).

3.2.3 Hofmeister series effects on mucin adsorption/desorption characteristics

Waveguides were pre-equilibrated in 0.2M sodium chloride (NaCl), sodium iodide (NaI) and sodium fluoride (NaF) (Sigma Aldrich, Dorset, U.K.) dissolved in ultrapure water overnight. The salt solution was passed over the waveguide followed by 0.1% w/w mucin dissolved in the salt solution and then rinsed with fresh salt solution. This procedure was carried out for all salts. The dn/dc for NaCl was 0.146 cm^3/g, NaF was 0.128 cm^3/g and NaI 0. 136cm^3/g, for details see Appendix B. 2.

3.2.4 Mucin + catechin adsorption/desorption

EGCg of various concentrations, 0.01, 0.1, 0.5 and 1% w/w was added directly to mucin (0.1% w/w in water) and mixed. Three systems were investigated. First the adsorption/desorption characteristics onto uncoated waveguides were determined for

55

mucin mixed with EGCg. Secondly a mucin layer was adsorbed onto the waveguide surface and investigating the effect of EGCg, and last mucin mixed with EGCg was investigated on the adsorbed layer. The dn/dc was calculated as $0.186\,\text{cm}^3/\text{g}$ (Appendix B. 2).

3.2.5　Cell response to mucin and mucin + EGCg layers

For these experiments the waveguides were coated with either 0.1% w/w poly-L-lysine in water, 0.1% w/w mucin in water or 0.1% w/w mucin + 0.1% w/w EGCg in water. The mucin stock solution was made up and pre-equilibrated overnight with EGCg added to the mucin stock solution and mixed 20 minutes before use. Solutions were applied for 20 minutes, washed twice (first using water, then McCoy growth medium, [MGM], Invitrogen, U.K. See Appendix C. 1 for details) and incubated for 40 minutes ($37\,^\circ\text{C}$, 5% CO_2 environment) in MGM. Following the baseline measurement (0.1M Hepes buffered MGM) an aliquot of 4×10^4 McCoy fibroblast cells (ECCAC #CB3009. HPA, Wiltshire, UK) in 100 μl buffered MGM were added directly to the cuvette of the custom built OWLS system using a micropipette whilst the TM incoupling peak was continually monitored and saved. 100 μl of buffered MGM was first removed from the cuvette and then the cell suspension added. Cells were counted using an optical microscope in conjunction with a haemocytometer, with the number of cells and surface coverage (60-70%) confirmed using phase contrast microscopy inspection of the waveguide after the experiment.

3.3   Substrate cleaning

The sensitivity of the OWLS instrument ($1ng/cm^2$) [77] makes cleaning the most important factor for obtaining reproducible and hence reliable results. The waveguides were used several times to reduce costs and were cleaned after each experiment. Factors determining the cleaning methods used are dependent upon the experimental substances investigated and individual experimental parameters. Proteins, for example, can be removed fairly easily using a weak acid solution whereas some polyelectrolytes that adhere more aggressively require more robust detergent and cleaning parameters. For this work several cleaning protocols were used.

3.3.1 Proteins

For proteins, cleaning waveguides under sonication in Roche solution for 10 minutes, rinsing with ultrapure water and then treating with O_2 plasma (20 mW for 2 mins) was sufficient to remove all residues from the surface. The glycoproteins (mucin) attach more rigorously to the waveguide and Roche solution alone is not sufficient to remove them. Sonication in sodium dodecl sulphate (SDS; 0.2M) for 10 minutes at 50 ^{o}C, rinsing in ultrapure water, sonication in Roche solution (10 minutes), rinsing in ultrapure water and treating with O_2 plasma (20 mW for 2 mins) removes all mucin at lower concentrations (see Appendix C. 2 for details of protocols).

3.3.2 Mucin

Higher concentrations of mucin and mixtures of active compounds (e.g. polyphenols) and glycoproteins adsorb on the waveguides and cannot be removed by Roche solution or SDS/Roche treatment. A protocol using chromesulphuric acid (Fisher

Scientific, U.K.) whereby waveguides are immersed for 3 minutes and then extensively rinsed under alternate sonication and flowing water for 30 minutes before being O_2 plasma treated (20 mW for 2 mins) removes all adsorbed molecules (see Appendix C. 2).

3.4 Cell culture

The cells used for this project were McCoy fibroblast cells (ECCAC #CB3009. HPA, Wiltshire, UK). These were chosen as these cells spread well which makes them a good model system for investigating cell shape change. All cells of the body and those grown *in vitro* metabolise and multiply (mitosis) constantly renewing themselves and the tissues they are part of. Therefore they require energy and, *in vitro*, the cells are supplied with medium containing mainly sugars, salts and small amino acids. In addition they also require hormones that signal morphological changes and gene transcription for mitosis. For this foetal bovine serum (FBS; Invitrogen, U.K.) is added to the medium.

Cells were cultured at 37 ^{o}C in a 5% CO_2 environment with growth media relevant to their requirements (see Appendix C. 1) in cell culture flasks. Cells were detached using 0.05% trypsin/EDTA and collected using centrifugation (1000 rpm for 5 minutes). Cells were counted using a haemocytometer in conjunction with an optical microscope.

Cells are stored in liquid nitrogen. This process involves substituting some of the medium with dimethyl sulfoxide (DMSO; Sigma Aldrich, U.K.) and slowly freezing the cells first in either a -80 ^{O}C freezer or in dry ice. Once frozen the cells are kept in liquid nitrogen and can be thawed (rapidly) at a later date.

3.5 Cell staining

OWLS is extremely powerful for investigating the kinetics of adsorption and desorption of material very close to the surface, however a drawback is the lack of images. To obtain a bigger picture (and also confirmatory evidence) of cell spreading on mucin and mucin + EGCg substrates the cells were stained and imaged. The cytoplasm was visualised using a 1 μg/ml streptavidin-Alexa Fluor555 fluorescent conjugate (Molecular Probes, U.K.) diluted in PBS that binds endogenous mitochondrial biotin. Sytox green nuclear stain (500 μM Molecular Probes, U.K.) diluted in DMSO (Sigma) counterstained the DNA and slides were mounted using a glycerol-based mountant (Dako Ltd, Cambridgeshire, UK).

3.6 Confocal microscopy

This technique first patented by Minsky in 1957 [178] and uses a laser to produce high resolution images and, unlike conventional fluorescence microscopy it does not illuminate the entire sample. A schematic is presented in Figure 3. 4.
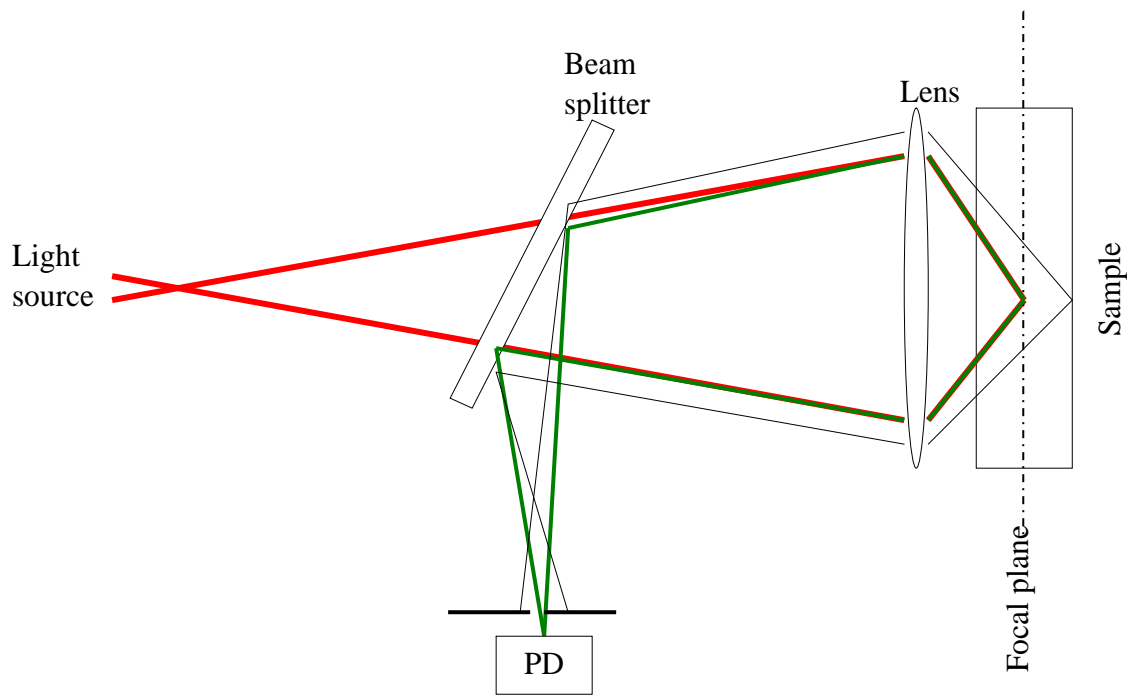
Figure 3.5: Schematic representation of confocal microscopy. The laser light is focused onto the sample via the lens. Emitted light is directed toward the detector via the beam splitter and a pinhole. The pinhole ensures that no light outside the focal plane is detected.

Laser scanning confocal microscopy (LSCM) provides images of thick samples built up by scanning at several focal planes (Fig. 3. 5).
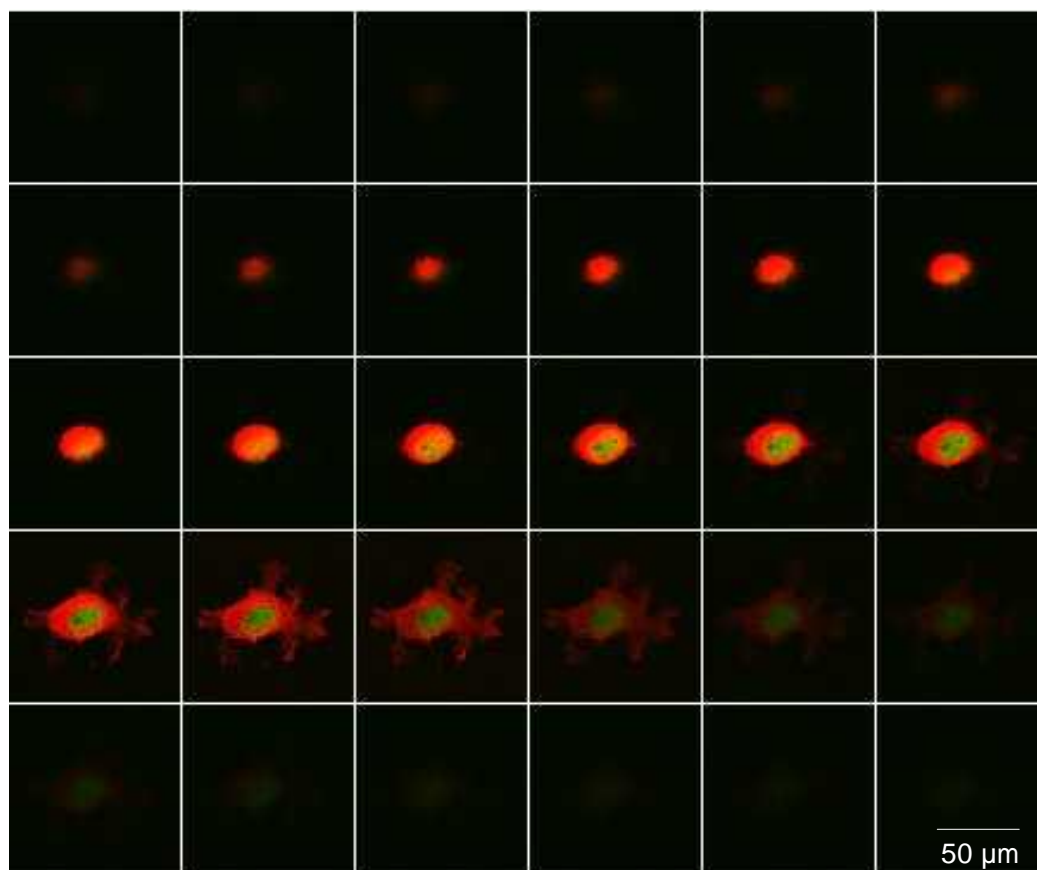
Figure 3.6: Image showing slice through McCoy fibroblast on poly-L-lysine substrate after 30 minutes. The cytoplasm stained using a streptavidin-Alexa Fluor555 and the nuclear fractions stained using Sytox green. Images are taken every 0.5 μm. The scanning starts top right and finishes bottom left. The scale bar is applicable for all individual squares.

Confocal microscopy is now used widely for studying biological systems, a few recent examples are cell adhesion to ceramic scaffolds [179], tracking herpes simplex virus type 1 DNA polymerase catalytic subunit (pUL30) location to the nucleus [180] and for diagnosing skin tumors [181].

Cells were imaged using a Zeiss Laser Scanning Confocal microscope (LSM 510 Meta, Zeiss, Hertfordshire, UK) with a minimum better to state what you used if you canx 40 objective. The Sytox green nuclear stain was excited using an Argon (488 nm) laser with emission detected via a 505-550 nm band-pass filter and the Alexa Fluor555A excited using a helium neon (HeNe, 543 nm) laser source with detection through a 560 nm long-pass filter.

4.0   Structure of adsorbed mucin film

The function of mucin is usually intimately related to its presence at solid/liquid interfaces, hence the careful and detailed study of adsorption (and desorption) behaviour is an essential pre-requisite to achieving a deeper understanding of the mechanisms underlying their highly e ective functional behaviour. Mucins persist in both homeo and poikilothermic organisms which exist across a wide range of temperatures and for this reason we have investigated the effect of temperature on the characteristics of the adsorbed mucin layer. Salts, present within a biological system, should also affect the behaviour of the mucin and as such are also investigated. Finally there were unexpected results which arose throughout the course of this work (entropic depletion and anisotropy) and these are also discussed.

4.1   Adsorption – mass at saturation

The OWLS technique is used to measure the adsorption/desorption characteristics of a wide range of mucin concentrations at a fixed temperature (25 ^{o}C). Together with complementary atomic force microscopy[1] (AFM) and microrheology data[2] (carried out by the sponsor) we suggest a composite structure, which is not a monolayer and instead a two-layer like structure where the uppermost layer may not be complete.

---

[1] Atomic force microscopy was used to visualise mucin molecules at the solid/liquid interface. Work carried out at Unilever Colworth by Dr Gleb Yakubov (Appendix D. 1 and D. 3).

[2] Microrheology data supplied to determine mucin viscosity. Work carried out at Unilever Colworth by Dr Gleb Yakubov (Appendix D. 2).

Whilst the adsorption and desorption of inorganic and synthetic organic nanoparticles at the solid/liquid (i.e. buried) interface is relatively straightforward and well understood [182, 183], spheroidal globular proteins can show bulk concentration dependent post adsorption transitions [68], and these e ects are more marked (and have been quite thoroughly investigated) for the adsorption of brous proteins from a liquid suspension at a solid surface [69, 70, 71]. The adsorption behaviour of even larger and more complex biomolecules such as mucin has been much less comprehensively investigated. Here we investigate the adsorption (and in the following section desorption) characteristics of mucin.

Figure 4. 1 shows a typical plot of adsorption and desorption for aqueous mucin. Adsorption was typically continued until a de nite plateau was reached, at which for all practical purposes the amount of adsorbed mucin was no longer increasing.
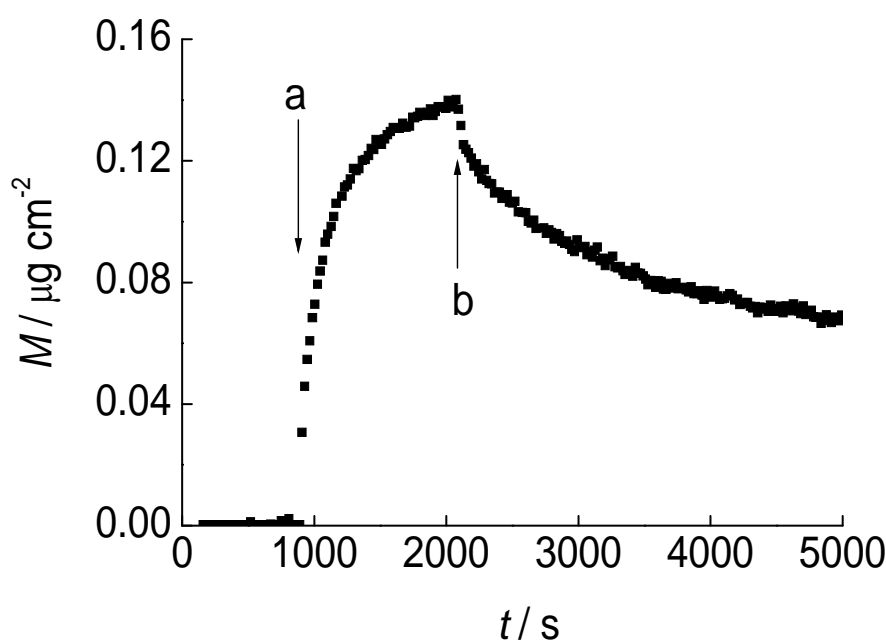
Figure 4.1: Representative plot of the amount of mucin, calculated from the OWLS data, adsorbed on $Si_{0.6}Ti_{0.4}O_2$ from a 0.1% w/w bulk solution against time. The arrows

a and b correspond to the start of mucin ow and the start of pure water ow (desorption phase).

The adsorbed amounts M_{sat} at these plateaux are plotted against the bulk mucin concentration (Fig. 4. 2). The most reasonable interpretation of the behaviour of M_{sat} is that at very low concentrations the protein is adsorbed in the extremely extended conformation typical for isolated molecules for entropic reasons [184]. In the intermediate bulk concentration regime (0.01–1%) interactions between neighbouring adsorbed molecules prevent the formation of the highly extended conformation and a fairly dense protein monolayer is formed. This behaviour has previously been shown to occur for brous pro teins such as bronectin [69, 70, 71]. The puzzle with mucin is that at the higher bulk concentrations (above approximately 2%) the deposited amount starts increasing again.
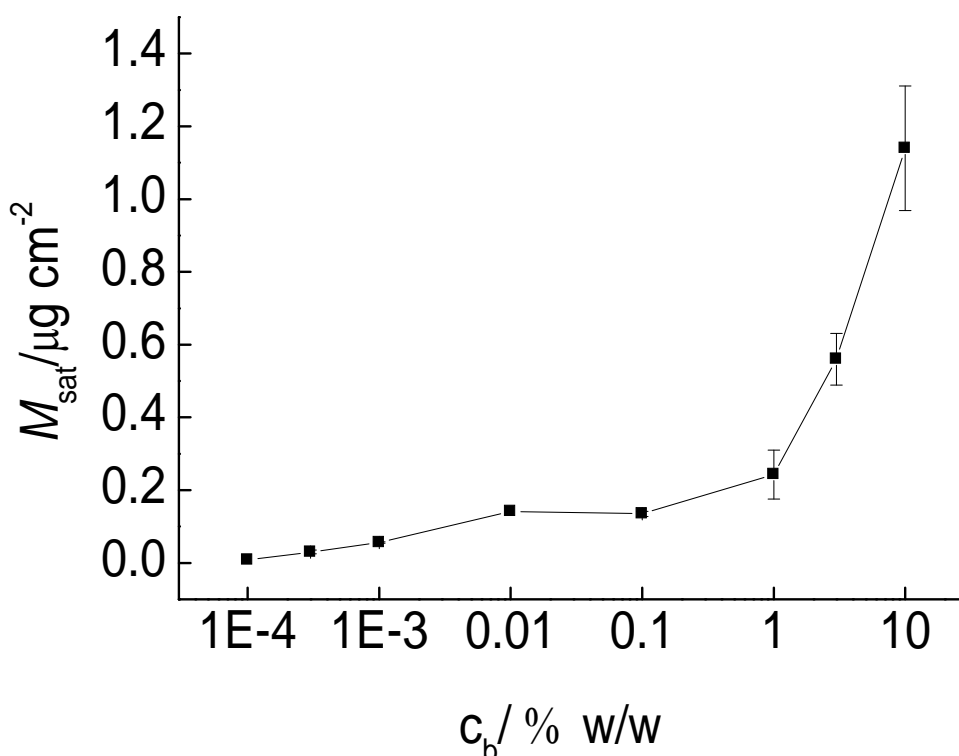
Figure 4.2: Saturation adsorption of mucin dissolved in water on $Si_{0.6}Ti_{0.4}O_2$ plotted against the bulk concentration of mucin. Error bars denote s.d. for M_{sat}.

A clue to this increase is given by the atomic force microscopy image (Appendix D. 1), which clearly shows the existence of a second layer at the higher concentrations. This feature is absent in the images of deposits created at low concentrations. Hence we infer that at high concentrations mucin molecules start depositing on top of the monolayer to form a second layer.

Further insight into this behaviour comes from bulk viscosity measurements (Appendix D. 2). The viscosity of mucin solutions plotted as a function of bulk concentration and clearly the viscosity with bulk concentration falls into two zones characterized by the exponents, $c^{1/2}$ and $c^{3/2}$ (corresponding to the well known semi-dilute and entangled regimes [114]), with the boundary between the regimes at about 2.4% w/w (44 µmol/L). The variation of the amounts of mucin adsorbed at saturation also shows a transition at about the same concentration: above about 1% M_{sat} is steeply increasing with bulk concentration, whereas below it is practically invariant, except at very low concentrations (below 0.001%) where it becomes very low. From these results we infer that entanglement facilitates the adsorption of the second layer, a feature that is definitely absent from the adsorption behaviour of brous proteins like bronectin.

66

4.1.1 Adsorption kinetics: low concentrations

Mass calculated for mucin spanning concentrations 0.0001 to 0.1 % are presented in Figure. 4. 3.
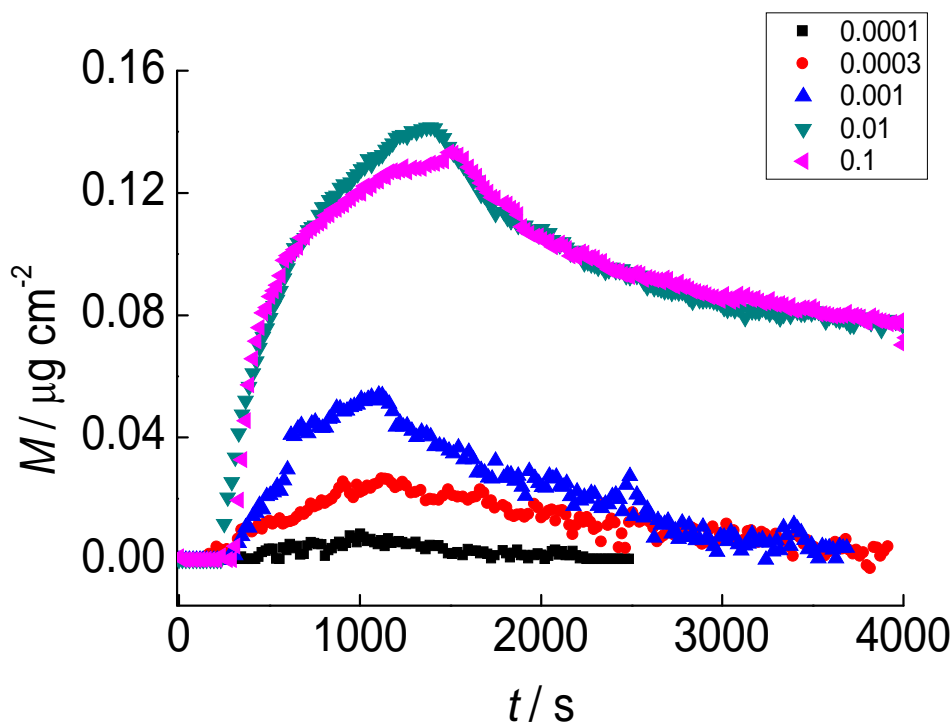
Figure 4. 3: Representative plot of the amount of mucin, calculated from the OWLS data, adsorbed on $Si_{0.6}Ti_{0.4}O_2$ from 0.0001, 0.0003, 0.001, 0.01 and 0.1% w/w bulk solution against time.

It is clear that mucin adsorbs in a concentration dependent manner up to 0.1% w/w. Above which it seems to become stable (reflected by the similar 0.01 and 0.1% plots). Indeed we have already inferred that these concentrations are characteristic of mucin regimes. Plots of dM/dt vs M could be very well tted (Fig. 4.4) by a random sequential adsorption process for all concentrations [88].
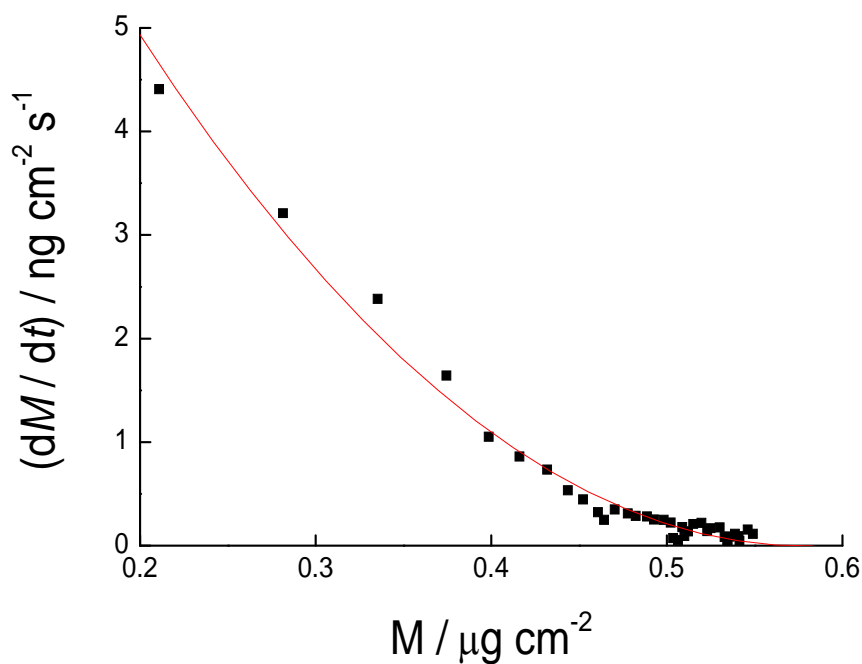
Figure 4.4: Time derivative of absorbed mass plotted against adsorbed mass 0.1% w/w.

The tting parameters were (a/m $_J$) and $k_a c^*$. The fitted parameters, or the practically

useful quantities derived from them, are gathered in Table 4. 1.

Table 4.1: Adsorption parameters for low concentration mucin.

c_b / % w/w	a / nm^2	k_a / mHz cm s^{-1}
0.0001	735.6 ± 0.04	0.11 ± 0.08
0.0003	723.4 ± 0.04	0.13 ± 0.07
0.001	577.1 ± 0.03	0.18 ± 0.07
0.01	262.3 ± 0.02	1.12 ± 0.02
0.1	267.0 ± 0.02	1.20 ± 0.04

It is clear that as the concentration increases the adsorbed molecule reduces in size

which could be attributed to an extended conformation at lower concentrations. As the

concentration increases the molecules would not be able to extend and hence they

occupy less area. These parameters confirm the conclusions for the M_{sat} data. In

68

addition the decrease in size as bulk concentration increases also suggests that post adsorption conformational changes occur [185].

4.1.2. Adsorption kinetics: High concentrations

An unforeseen issue that arose from this work is that for high concentrations of mucin (above 1% w/w) the adsorption curve shifts down resulting in negative mass (Fig. 4.5).
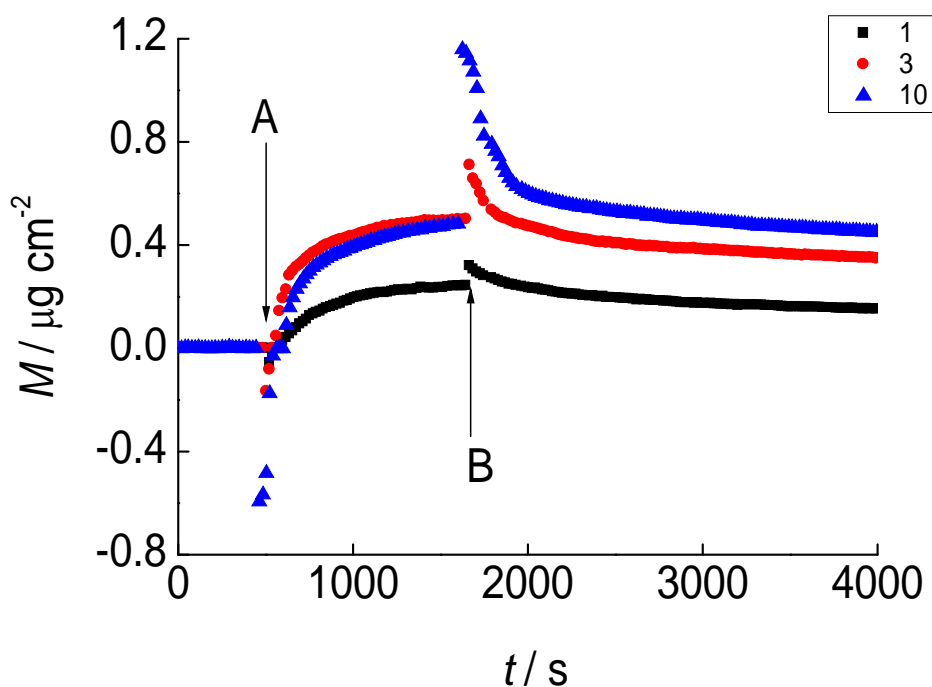
Figure 4.5: Representative plot of the amount of mucin, calculated from the OWLS data, adsorbed on $Si_{0.6}Ti_{0.4}O_2$ from a 1, 3 and 10% w/w bulk solution against time. The arrows a and b correspond to the start of mucin ow and the start of pure water ow (desorption phase).

The N_{TE} (and N_{TM}) curves do not shift (Fig. 4.6) indicating that the problem occurs when the refractive index of the cover solution is entered when calculating the mass.
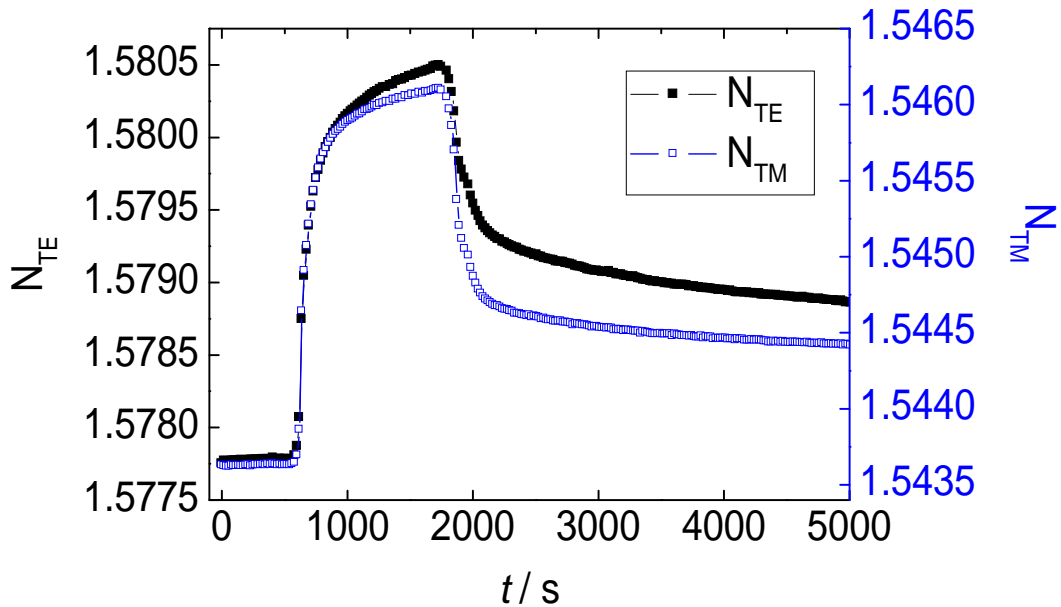
Figure 4.6: Raw data N_{TE} and N_{TM} plots for 10% w/w mucin adsorbed on $Si_{0.6}Ti_{0.4}O_2$ against time.

The shift begins when the refractive index of the solution increases by more than approximately 0.0002. Suggesting a discrepancy between the bulk refractive index, which one measures using the refractometer, and that at the interface. To determine the refractive index 'seen' by the OWLS we can use [174]

$$n_C = n_C \text{ buffer} + \quad n_C \qquad\qquad (6)$$

Indeed if the dN_{TE}/dt is plotted (Fig. 4.7) for the 1% w/w mucin concentration we find a peak.
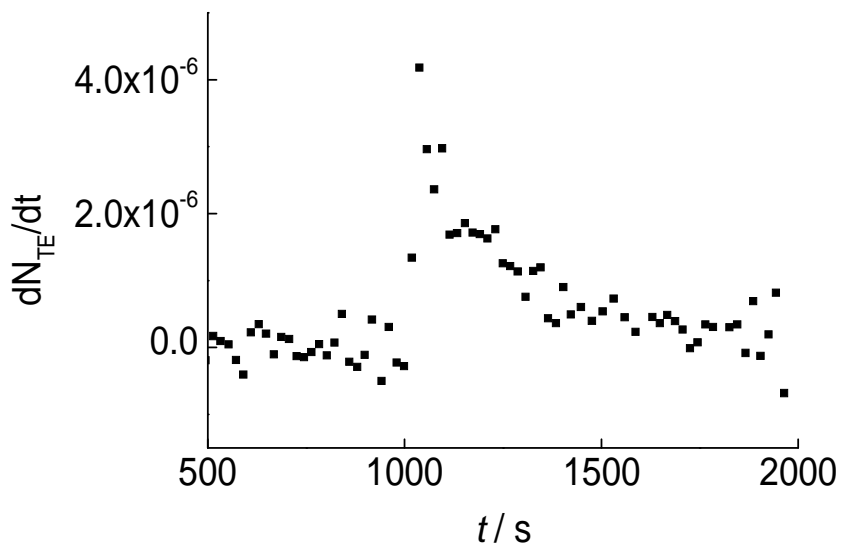
Figure 4.7: dN_{TE}/dt plotted against time for 1.0% mucin adsorption.

Using the corresponding peak N_{TE} value to calculate the n_C we obtain a value of 1.331828 which compares with 1.333110 obtained from the refractometer measurements. When plotting the curve for 1% w/w mucin using 1.331828 as the cover refractive index the shift is almost fully recovered (Fig. 4. 8).
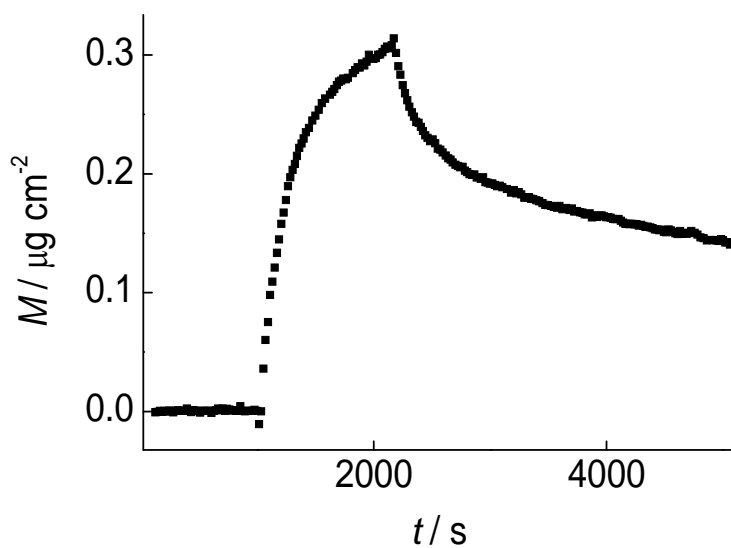
Figure 4.8: Shift recovery. Calculated from the OWLS data, adsorbed on $Si_{0.6}Ti_{0.4}O_2$ from a 1.0% w/w bulk solution against time using the refractive index as 'seen' by the OWLS.

This is not the case for both 3% and 10% w/w solutions with refractive indices 1.340209 and 1.340253 respectively (Fig. 4. 9).
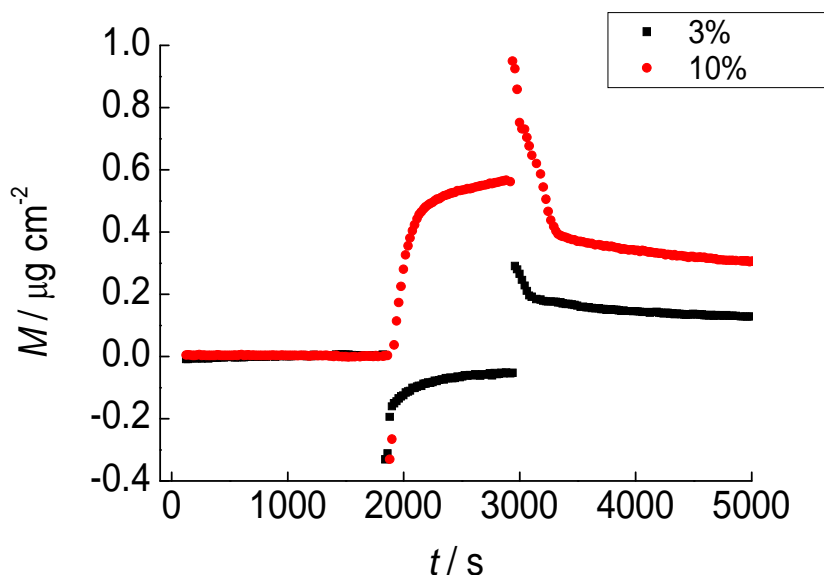
Figure 4.9: Negative mass shift. Calculated from the OWLS data, adsorbed on $Si_{0.6}Ti_{0.4}O_2$ from 1 and 3% w/w bulk solution against time using the refractive index as 'seen' by the OWLS.

The almost complete recovery for the 1% w/w solution is most likely due to this concentration being around the semi-dilute/entangled regime transition point which occurs at ~1 to 2 % w/w concentration. There is certainly an issue with the entangled regime which could be due to entropic depletion.

Asakura and Oosawa, 1954 were the first to suggest that the reduction in entropy of flexible coils close to an interface leads to their repulsion and a reduction in the concentration of the coil in the close vicinity of the interface (entropic depletion) [186]. We consider the case of 3% w/w mucin dissolved in water (see Fig. 4. 5).

The refractive index of the 3 % w/w mucin solution (measured using the refractometer) is 1.33594 (n_m) and the cover medium (water) refractive index 1.331623 (n_O). Buffer n_C is the cover refractive index 'seen' by the propagating

73

mode. It is clear that there is negative mass during the first few experimental points of the adsorption phase (Fig. 4. 5). Indeed the only way to obtain a continuous mass curve is to suppose that $n_C \sim n_O$ which suggests that almost no mucin is present close to the surface (in the 100-200 nm thick sheet monitored by the modes). The mucin concentration near the surface $\varphi(z)$ can be described by

$$\varphi(z) = \varphi_B \tanh^2\left(\frac{\alpha\ z}{\langle s^2 \rangle^{0.5}}\right)$$

(7)

Where φ_B is the polymer concentration in the bulk, the binary mixture constant (2.2) [187] and z the distance from the surface. The concentration of mucin will increase from zero at the surface to the bulk concentration as z increases. The value for z at which the bulk concentration is reached is in the region of the root-mean-square end-to-end distance of the mucin in free solution $\langle s^2 \rangle^{0.5}$ [188, 189].

Using the Rg of 52 nm (calculated by Dr GlebYakbov, [113]) we obtain $\langle s^2 \rangle^{0.5} = 132$ nm with and n_C of 1.334254 which is still too high. It does not recover the shift. We find that to recover the shift fully we must multiply the Rg by a factor of 12 which gives an n_C of 1.331784 for 3% w/w mucin and 1.332134 for 10 % w/w mucin (Fig. 4. 10).
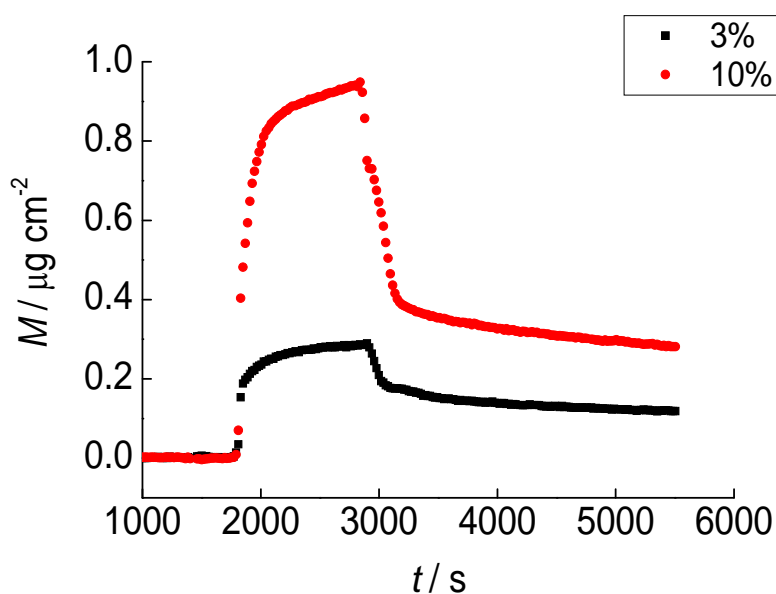
Figure 4.10: Plot of the modified refractive index cover media mass calculations. 3 and 10% w/w bulk solution mucin, adsorbed on $Si_{0.6}Ti_{0.4}O_2$ against time.

For higher concentrations of mucin (3 and 10% w/w) the curves were first determined using the cover refractive indices calculated using either the entropic depletion or direct OWLS analysis. We have already seen that this recovers the shift, all curves could be fitted well using a random sequential desorption process and the fitting parameters are collected in Table 4. 2.

Table 4.2: Adsorption parameters for high concentration mucin

c_b / % w/w	a / nm^2	k_a / mHz cm s^{-1}
1.0	243.2 ± 0.02	1.43 ± 0.02
3.0	199.4 ± 0.02	4.34 ± 0.06
10.0	93.8 ± 0.01	7.52 ± 0.08

As the bulk concentration increases we see a reduction in the molecule area adsorbed at the surface (Table 4. 2). This is analogous to the low concentration mucin results. Most likely this is also due to post adsorption conformational changes on the surface.

75

It is also important to note that the adsorption rate increases as the bulk concentration increases. Taken together these are confusing although if the concentrations are split into sections relating to the dilute (0.001-0.001% w/w), semi-dilute (0.1-1% w/w) and entangled (above 1% w/w) it becomes clear that the adsorption rate is regime specific.

4.1.3   Summary

Adsorption characteristics suggest that at low concentrations the molecules are able to adsorb in an extended conformation. At higher concentrations the large number of molecules makes it impossible for the extended conformation to persist whilst at very high concentrations the molecules entangle. This results in adsorption behaviour unlike that measured previously for both globular and fibrous proteins. The unrealistic negative mass observed when using the bulk refractive index measured with the refractometer is most likely due to entropic depletion.

4.2   Desorption

The following chapter gives details of the desorption characteristics of mucin which provides valuable insight into the behaviour of the molecules at the solid/liquid interface. We confirm the existence of a composite structure and investigate its properties.

4.2.1   Experimental results and discussion

Here we demonstrate that non equilibrium e ects during mucin adsorption lead to the formation of a composite structure. The rst quasilayer adjacent the surface is in equilibrium with the substrate, whereas the second quasilayer is structurally di erent. It is not equilibrated with the underlying layer and its deposition is facilitated due to

76

entanglement trapping. This composite structure would be able to provide the features necessary for e ective lubrication. If indeed entanglement is responsible (as suggested by adsorption) for the mucin layer characteristics this should be re ected in the desorption kinetics.

Visual inspection of the desorption kinetics suggests that they do not follow a simple exponential decay law. In contrast to simple Langmuir (exponential) desorption, mucin follows a stretched exponential (Kohlrausch) kinetic law, $M(t) = M0 \; e^{-(kt)}$, where M0 is the amount of mucin adsorbed at the beginning of desorption (i.e. at the plateau, Fig. 4. 11), and k (desorption rate) and (exponent) [3] are constants.
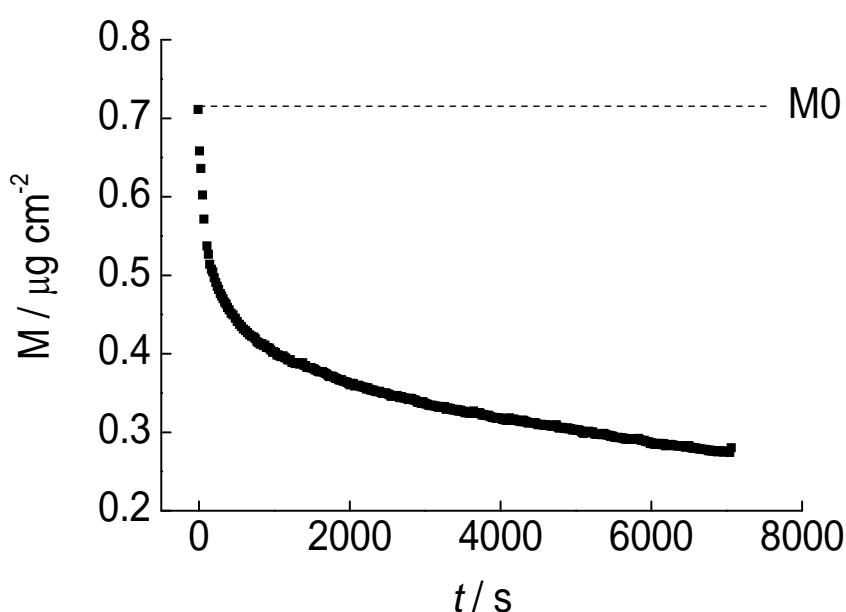
Figure 4.11: Representative plot of mucin desorption from $Si_{0.6}Ti_{0.4}O_2$. The mucin concentration shown is 3% w/w bulk solution against time. MO is the amount of adsorbed mucin at desorption time zero.

---

[3] Note that is between 0 and 1 with 1 being purely exponential desorption.

In order to determine them, the double logarithm of M was plotted against log time for each mucin concentration. At the most dilute concentrations, a single straight line could be tted to the data, but at higher concentrations two lines with distinctly di erent gradients had to be tted. Hence the actual equation used for tting the data was

$$M(t) = M0[f1\ e^{-(k_1 t)^1} + f2\ e^{-(k_2 t)^2}]$$ (8)

where f1 and f2 are the fractions of respectively the rapid initial desorption and the slower subsequent desorption. The boundary between the two adsorption modes could be very easily perceived by eye, especially when plotting the data as logM versus logt and the f values were simply estimated from the intersection of extrapolated straight lines in the vicinity of the boundary. Examples of the ts of eqn (7) are shown in Figure 4. 12.

A
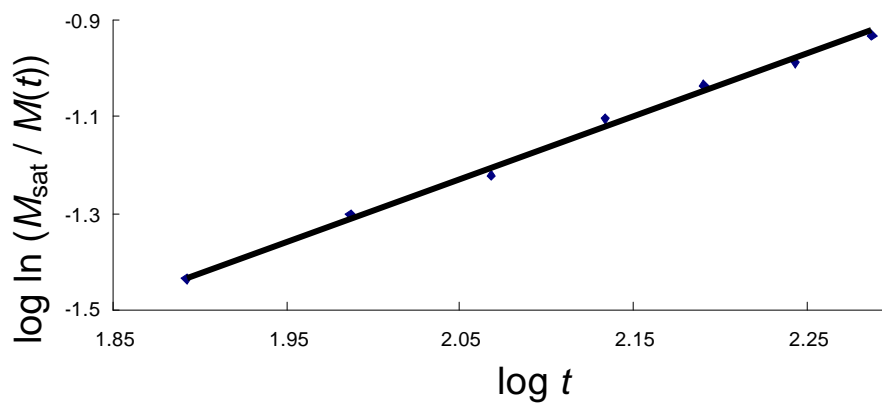
B
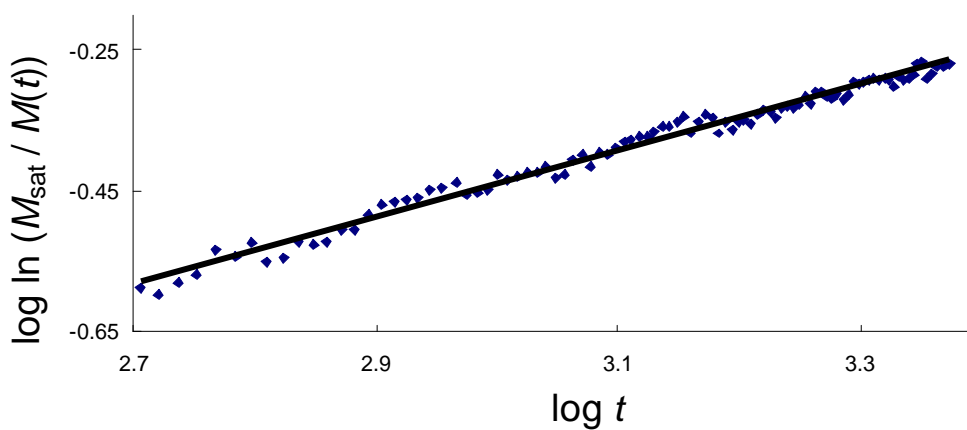
Figure 4.12: Representative plots of the double logarithm of the amount of adsorbed mucin versus the logarithm of time, i.e. in accord with eqn (1). The plots are for desorption of the deposit created from a 3% mucin solution, which could be clearly separated into fast (A) and slow (B) phases.

The parameters characterizing desorption are given in Table 4. 3.

79

Table 4.3: Desorption parameters for different bulk mucin concentrations. Desorption was started 18 min after the start of adsorption. Uncertainties are s.e.m. The uncertainty for f_1 is estimated as +/- 0.04.

c_b %w/w	k_1 /mHz	β_1	f_1	k_2 /mHz	β_2	τ_2
0.0001	0	0	0.00	1.9400	0.837 +/- 0.003	10 min
0.0003	0	0	0.00	0.3870	0.6983 +/- 0.0004	55 min
0.001	0	0	0.00	0.3950	0.6366	65 min
0.01	1	1.20 +/- 0.08	0.14	0.1750	0.4925	3.3 hrs
0.1	0.980 +/- 0.002	1.28 +/- 0.08	0.15	0.1000	0.479 +/- 0.002	6.0 hrs
1.0	0.842	1.29 +/- 0.02	0.28	0.0550	0.473 +/- 0.003	11.3 hrs
3.0	3.940 +/- 0.003	1.50 +/- 0.03	0.41	0.1020 +/- 0.0002	0.213	9.0 days
10.0	5.120 +/- 0.007	1.75 +/- 0.05	0.60	0.2000 +/- 0.0004	0.1874 +/- 0.0005	13.4 days

The Kohlrausch exponents determined by linear least squares tting are also plotted in Figure 4. 13 against the bulk mucin concentrations at which the deposits were created prior to starting desorption. Strikingly, the initial fast desorption, absent at the lower mucin concentrations, shows superexponential kinetics, i.e. an autocatalytic step in the desorption mechanism.
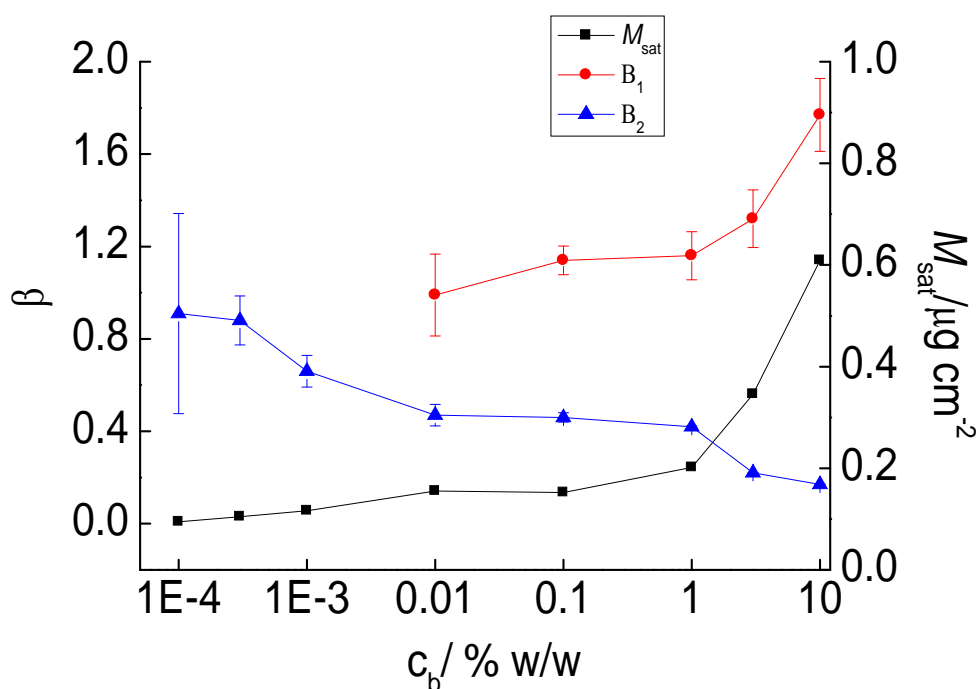
Figure 4.13: Righthand scale: saturation adsorption of mucin dissolved in water on $Si_iTi_iO_2$ plotted against bulk mucin concentration. Lefthand scale: Kohlrausch exponents characterizing mucin desorption from $Si_{0.6}Ti_{0.4}O_2$ in pure water plotted against the bulk concentration of mucin dissolved in water used to create the deposit. Points are connected merely to guide the eye. Error bars denote s.e.m. for [1] and [2], and s.d. for M_{sat}.

A convincing explanation is a sequential, hierarchical process in which a minimum number of units in any level of a hierarchy must change before the next level can decay [190]. This mechanism provides a very natural explanation of the mucin desorption. Mucin is adsorbed via a combination of multiple weak (mainly hydrogen) bonding of the molecules directly to the metal oxide surfaces and entanglement trapping of further mucin molecules with their directly adsorbed congeners. Reversing the trapping process automatically implies hierarchical desorption, and hence Kohlrausch kinetics.

Even the sparse deposits created from the lowest bulk concentrations show Kohlrausch kinetics, albeit with exponents closest to one. This is fully in line with the extended conformation multiply bound to the surface expected from theoretical grounds [184]. A certain number of the surface bound units of mucin must move before, for example, a loop can be created, which is a precursor to further movement leading to desorption. At higher surface concentrations, the adsorbed mucin molecules are somewhat entangled with their neighbours, and the disentanglement necessary before desorption can take place signi cantly contributes to the hierarchical process with correspondingly lower Kohlrausch exponents.

The faster phase appearing at higher concentrations corresponds with the incipient formation of the second layer, whose isolated molecules are relatively weakly bound to the underlying mucin in the rst layer. The appearance of a new process characterized by superexponential desorption shows that a di erent, autocatalytic[4], mechanism operates. At the same time, the second layer adds a further level in the desorption hierarchy, leading to the concomitant reduction in the Kohlrausch exponent for the rst layer.

A signi cant corollary of the diminishing exponents is the rapidly increasing time to equilibrium, which can be quanti ed as

$$ = (1/) / \tag{9}$$

where   is Euler's Gamma function and $= 1/k$. The values calculated from the parameters we have determined are given in Table 4. 3. The inordinately long "equilibration times" mean that under most conditions encountered in living organisms the mucin layers will be far from equilibrium.

---

[4] Note that this does not relate to chemical catalysis and as such denotes purely co-operative behaviour.

Table 4.4: Desorption parameters for di erent bulk mucin concentrations. Desorption was started 60 min after the start of adsorption. Uncertainties are s.e.m.

c_b % w/w	k_1 /mHz	1	f_1	k_2 /mHz	2	2
0.1	1.653	1.37 +/- 0.02	0.27	0.1670	0.466 +/-0.004	4.0 hrs
3.0	4.744 +/- 0.002	1.59 +/- 0.02	0.45	0.192 +/- 0.002	0.188 +/- 0.002	13.5 days

A corollary of the proposed adsorption/desorption mechanism is that di erent kinetics should be observed depending on the interval between achieving saturation adsorption and commencing desorption. This is indeed the case, albeit in a somewhat complicated way. Table 4. 4 presents results from layers allowed to remain at saturation for an extended period. At an intermediate concentration (0.1 % w/w) desorption is actually accelerated, possibly because more molecules arrange themselves in the more rapidly desorbing upper layer. At high concentration there is little e ective di erence.

Further evidence for these time dependent changes in adsorbed layer structure is gained from the force curves measured with the atomic force microscope [191] carried out by Dr Gleb Yakubov (Appendix D. 3). In this experiment, the AFM tip was plunged into the protein layer and then allowed to remain for an interval , following which it was withdrawn. The results are shown in Appendix D. 3. They show how adhesion tends to increase with .

4.2.2   Inhomogeneity

The four layer model enables the extraction of the effective refractive index (N) and thickness of the adsorbed layer and from this the mass can be calculated. For mucin adsorption this model has its limitations as the thickness measured is unrealistic (Fig. 4.14).
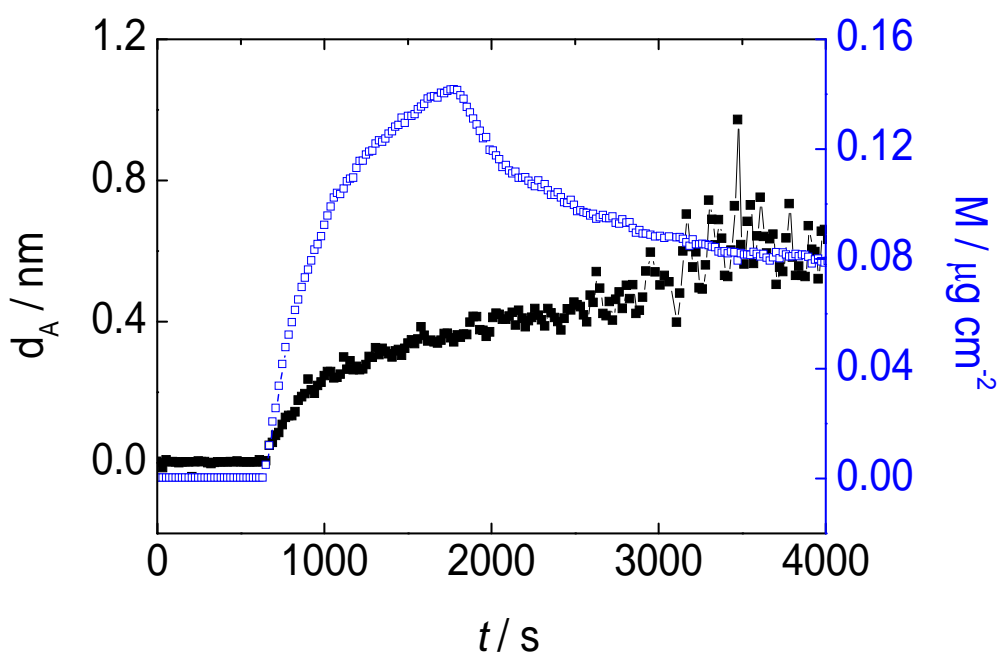
Figure 4.14: Righthand scale: mass adsorption of 0.1% w/w mucin dissolved in water on $Si_{0.6}Ti_{0.4}O_2$ plotted against time. Lefthand scale: calculated thickness of mucin plotted against time.

Here the measured thickness of 0.4 nm cannot be correct as this is smaller than that of a single amino acid (typically ~0.8 nm). [192]
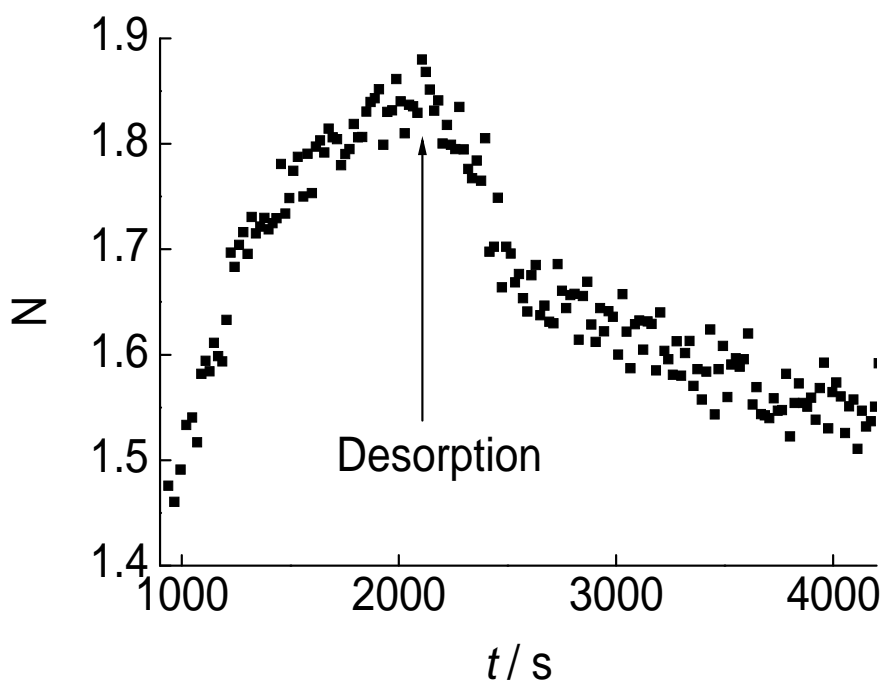
Figure 4.15: Refractive index plotted against time of 0.1% w/w mucin dissolved in water on $Si_{0.6}Ti_{0.4}O_2$.

The measured refractive index (Fig. 4. 15) is not realistic either as bulk measurements of mucin range from 1.33 to 1.34 (Appendix B. 2).

These effects have previously been numerically simulated using ellipsoid spheres and suggestions are that the unrealistic refractive index and thickness somehow balance out to give a mass value which is correct [193]. Therefore the mass is correct for mucin although the thickness and effective refractive index remain unrealistic. This strongly implies that the layer is not homogeneous and that a level of anisotropy exists [194]. When the refractive index is overestimated and the thickness underestimated as is the case here it suggests that a layering (of different refractive indices) [195] is occurring at the surface as opposed to columnar structures [194].

85

4.2.2.1   Hysteresis - low mucin concentrations

To determine further the layer characteristics at different concentrations we plot the effective refractive index against the mass. For very low concentrations of mucin the adsorption starts with a high refractive index, typically around 2 for 0.001% w/w (Fig. 4. 16). During desorption the refractive index of the layer reduces as the mass decreases. A higher 0.1% w/w mucin concentration starts relatively realistic and rises to a very high 1.8. There is a small (just a few data points) of hysteresis occurring although not as large as that seen for concentration above 1% w/w mucin.
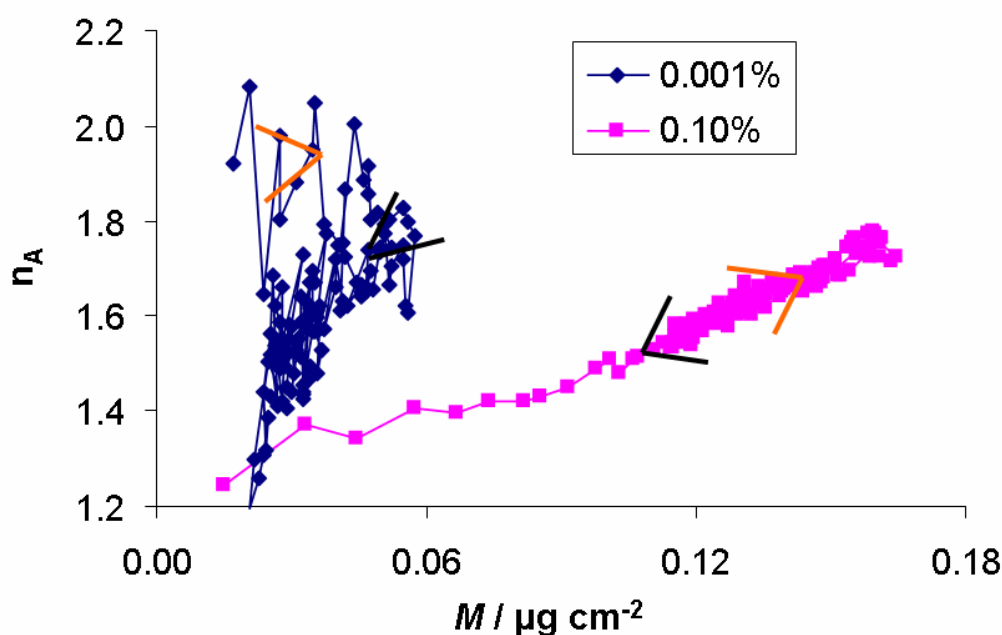
Figure 4.16: Low concentration mucin hysteresis. 0.001% and 0.1% mucin effective refractive index against mass adsorbed. Orange arrows depict adsorption and black arrows desorption.

86

4.2.2.2   Hysteresis – high mucin concentrations

High concentrations of mucin (1% w/w and above) show hysteresis (Fig. 4. 17). Also note that the refractive index of the adsorbed layer is decreasing with increasing concentration. Here it could be that two molecular species (entangled and non-entangled) adsorb. The rapid release of one species, most likely the entangled causes the jump in refractive index with gaps left by the desorbing molecules. These gaps are rapidly filled by the remaining layer which then desorbs in a similar manner for all concentrations (refractive index around 2 decreases slowly).
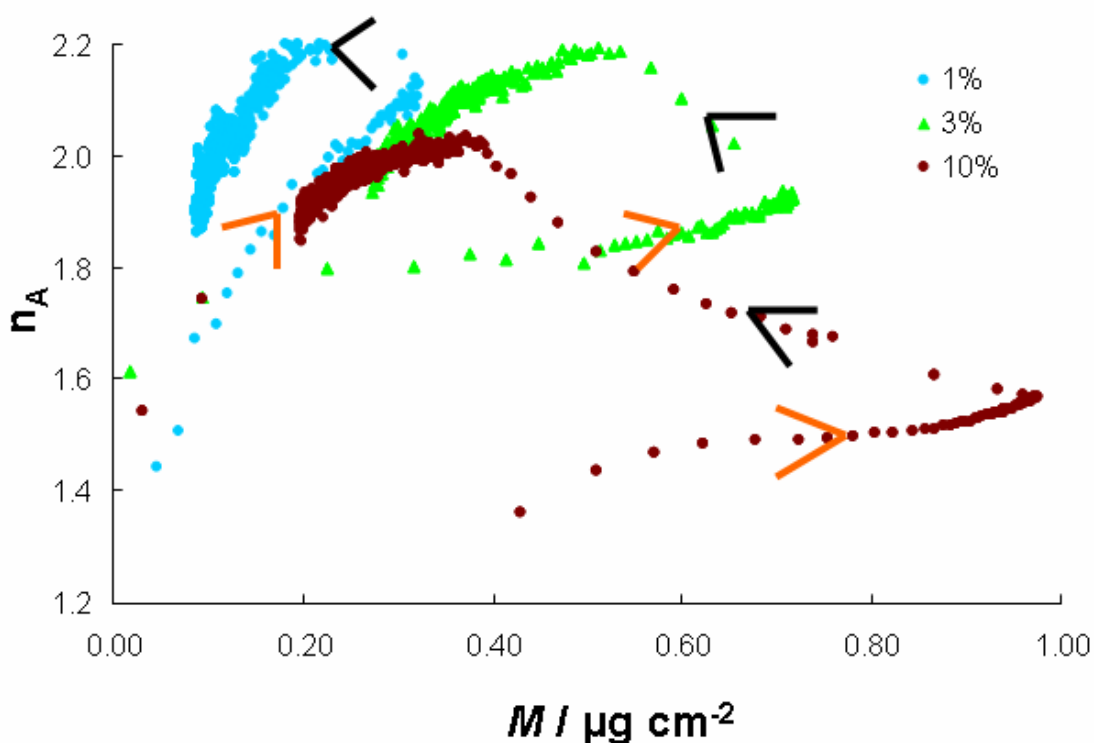
Figure 4.17: High concentration mucin anisotropy. 1, 3 and 10% mucin effective refractive index against mass adsorbed. Orange arrows depict adsorption and black arrows desorption.

4.2.3   Mucin adsorption/desorption model

For the semi-dilute regime many of the molecules are not entangled with each other and therefore adsorb as a single layer (Fig. 4. 18). The molecules most likely stretch out and it is proposed that the high refractive indices are due to the layering of sugars on proteins or the layering of chains on flattened globules.
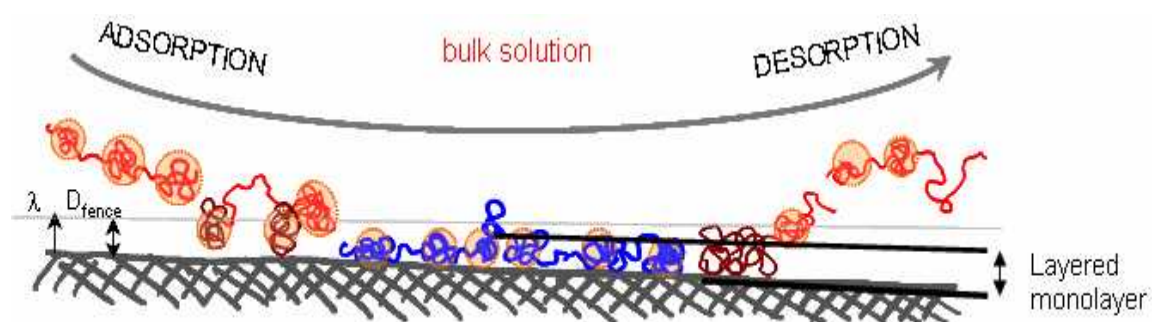
Figure 4.18: Mucin adsorption/desorption model – semi-dilute regime. For the fence Regime D~λ where D is the mean thickness of the layer and λ the Debye Length.

The presence of entangled species at higher concentrations leads to the formation of a bi-layer like structure. Here some of the non-entangled species will still adsorb and the entangled species will also attach (Fig. 4. 19). The lower refractive indices could therefore be due to the formation of columnar like structures in the second layer (see AFM image, Appendix D. 1) which returns to monolayer rapidly after washing.

88
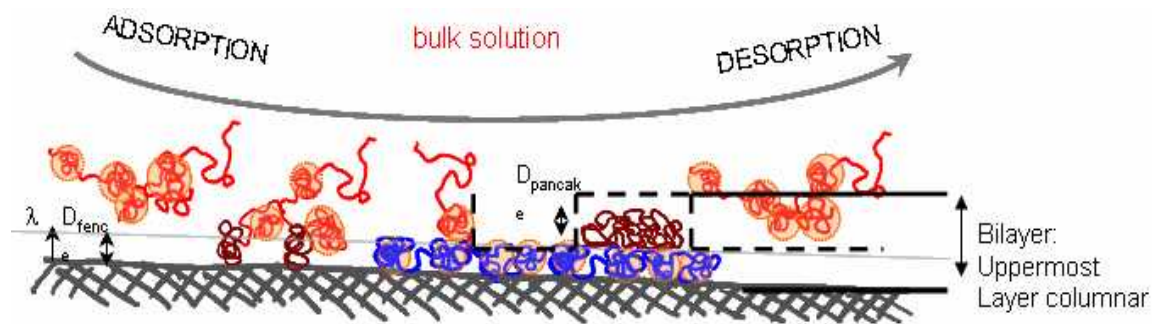
Figure 4.19: Mucin adsorption/desorption model – entangled regime. For the fence Regime D~λ where D is the mean thickness of the layer and λ the Debye Length. For the pancake regime D>>λ.

This forms a layer of adsorbed non-entangled fence molecules and entangled with pancakes molecules. The rapid loss of the pancake molecules is proposed as an explanation of the super-exponential desorption seen.

4.2.4   Summary

In conclusion, insight into the molecular structure of the deposit is given by the desorption kinetics. A main consequence of entanglement is that equilibration times are very long, hence the observed behaviour is mainly governed by the kinetics. The revelation of the qualitatively different deposits created from different bulk mucin concentrations is expected to have important implications for the ability of mucin to lubricate surfaces. In addition the entropic depletion and hysteresis, which were first perceived as problematic have themselves been able to provide clues into the behaviour of mucin at the interface.

4.3 Temperature effects on mucin film characteristics

Irrespective of external temperature, homeotherms such as mammals and birds have body temperatures that range from approximately 36 to 40 ^{o}C. There are however many multicellular organisms inhabiting some of the earth's most hostile environments that are poikilothermic and do not regulate their body temperature, which is therefore close to that of their environment. For example teleosts live in waters that range from close to zero on one extreme to temperatures around 25 ^{o}C and desert ants such as *Cataglyphis bicolor* forage at temperatures that can exceed 60 ^{o}C [96].

It is already well established that the enzymes of microbial extremophiles have subtly di erent amino acid sequences from those of their relatives living at normal temperatures. In other words, nature has solved the problem of altering enzymes to work at di erent temperatures. However, an enzyme adapted to high temperature functions badly at low temperatures, just as the ordinary versions of the enzyme function badly at high temperatures. The enzymes (and other proteins) of poikilothermic organisms require a more sophisticated adaptation that allows them to function over a broad range of temperatures.

Motility is essential for most of the immediate survival needs of multicellular animals, and hence functions such as joint lubrication must fully function across the range of temperatures encountered throughout the life of the organism. We note that mucins are found across all animal phyla, which poses the puzzle as to how they are able to retain the ability to function across a wide temperature range. It is evident that mucin must adsorb in order to function as a lubricant [123]. The same prerequisite applies to its other functions and hence adsorption/desorption characteristics at di erent

temperatures (25.0 to 60.0^{o}C) are investigated here.

4.3.1   Experimental results and discussion

We use Optical waveguide lightmode spectroscopy (OWLS) a "molecular microscope" [185] to provide high resolution kinetic adsorption and desorption data. Dynamic light scattering (DLS), carried out by Dr Gleb Yakubov (Appendix E. 1) is used to establish changes in dissolved mucin conformation at di erent temperatures. The temperature range investigated is 25–60 ^{o}C.

4.3.1.1   Adsorption.

Figure 4. 20 shows typical results. The striking increase in saturated mass M_{sat} with increasing temperature seems counterintuitive because proteins are known to be generally unfolded at higher temperatures. They should therefore occupy more space per molecule and the mass at saturation should be lower. We note, however, that the thermal expansion of only a very small number of proteins (all globular) have in fact been carefully investigated [196].
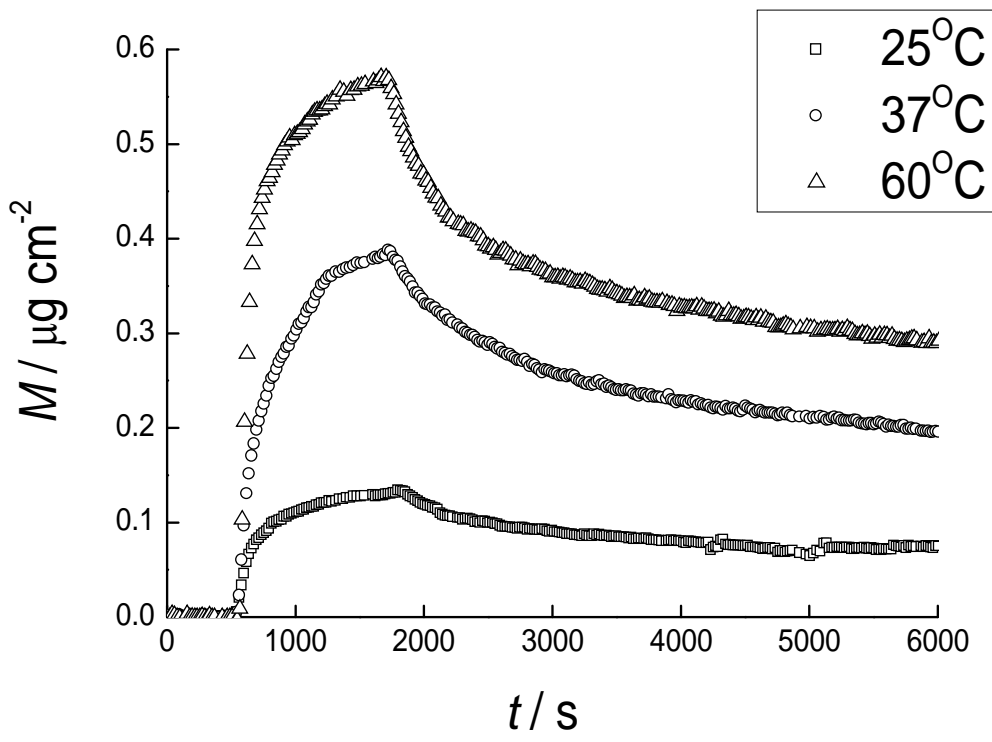
Figure 4.20: Representative plots of the amount of mucin, calculated from the OWLS data, adsorbed on $Si_{0.6}Ti_{0.4}O_2$ from a 0.1% w/w bulk solution against time for 25.0, 37.0 and 60.0 ^oC.

According to the general adsorption equation [162]:

$$dM/dt = k_a c^* \ (M, a) \tag{10}$$

where k_a is the adsorption rate coe cient, c^* is the e ective concentration in the vicinity of the adsorbent surface; for the moment we shall assume that $c^* \sim c_b$), is the available area function and a is the area occupied per molecule. Plots of dM/dt vs M could be very well t ted for all T by a random sequential adsorption process [86]. The tting parameters were (a/m_J) and $k_a c^*$. The fitted parameters, or the practically useful quantities derived from them, are gathered in Table 4. 5.

Table 4.5: Adsorption parameters for 0.1% mucin at different temperatures. The units of M are µg cm s^{-1}. $M_{sat}^{(meas)}$ is the highest observed adsorbed sat amount, and $M_{sat}^{(fit)}$ is the amount calculated from the tted a assuming $_J$ = sat 0.54, appropriate for spheres and spherocylinders. Rh was determined from the dynamic light scattering measurements and D calculated from Rh using the Stokes Einstein relation.

t	$M_{sat}^{(meas)}$	$M_{sat}^{(fit)}$	a/nm^2	k_a/cms^{-1}	Rh/nm	D/cm^2 s^{-1}
25	0.14	0.19	267.0 ± 0.2	1.2×10^{-6}	12	2×10^{-7}
37	0.39 ± 0.02	0.45	113	2.7×10^{-6}	10.5	3×10^{-7}
60	0.53 ± 0.05	0.63	81.5	12×10^{-6}	9	7×10^{-7}

4.3.1.2   Molecular size

From Table 4. 5 it is clear that the adsorption rate increases with temperature, whilst a decrease, corroborating the reduction seen for $M_{sat}^{(meas)}$ as the temperature decreases. Upon closer scrutiny, however, one notices that the values of $M_{sat}^{(t)}$ = $_J$ m/a are signi cantly larger than the $M_{sat}^{(meas)}$ observed directly. The discrepancy is too large to be accounted for by not having allowed adsorption to continue long enough to reach ultimate saturation. It could of course be that we have used too great a value of J , but even very elongated objects only have a value a few percent less than the one we have used [85]. In order to match $M_{sat}^{(t)}$ with $M_{sat}^{(meas)}$ we would need $_J \sim$ 0.3, which does not correspond to any known and investigated shape.

 An obvious question to answer is whether the bulk conformation of the mucin also varies with temperature. Table 4. 5 also reports the hydrodynamic radii obtained from the dynamic light scattering measurements (Appendix E. 1). These also show a marked decrease with increasing temperature. One notes that a $\sim R_h^2$ except for the lowest temperature (25 ^{o}C), where a is almost double the hydrodynamic radius

93

squared.

The thermal contraction of mucin is in sharp contrast to the thermal expansion noted for globular proteins [95]. In fact, Hiebl and Maksymiw concluded that even for these relatively "simple" molecules, the expansion was "anomalous" because of the presence of bound water, with a different thermal expansion coefficient from that of bulk water, and the quantity of which itself diminishes with increasing temperature [197, 198].

Mucin, with its extensive glycosylation (about half of the molecular mass), is very extensively hydrated at room temperature. It could however be that mucin falls into the "natively open" class of proteins (whereas lysozyme and albumin, investigated by Hiebl and Maksymiw, are natively closed) [109]. This would in fact be the most straight forward explanation of the thermal contraction, with complications arising from a redistribution of bound water possibly accounting for the breakdown of the expected relation $a \sim R_h^2$. Mucin is a polyampholyte, and polyampholytic gels composed of triblock copolymers have been shown to contract with increasing temperature. The authors suggest competition between the excluded volume effect (at low temperature) that favours intermolecular interactions between opposed charges and thermal motion as being responsible [199]. Another explanation is that the formation of mucin dimers is promoted at the lowest temperature.

94

4.3.1.3 Adsorption rate.

The adsorption rate coe cient is approximately related to the adsorption activation

energy E_a as follows [88]:

$$K_a \sim D(T) \exp(-E_a/kT) \ ,\tag{11}$$

where D is the mucin di usion coe cient. By plotting these results as ln (k_a/D) vs

1/T, calculating D from the Stokes Einstein relation (Appendix B. 1)

where k_B is Boltzmann's constant and the viscosity, and equating r to Rh, (Fig. 4.

21) yields E_a = 24.5 +/- 0.5 kJ/mol. In terms of energy per area, we have E_a/a =0.35

mJ/m^2, which is within the range of existing measurements for proteins [200].
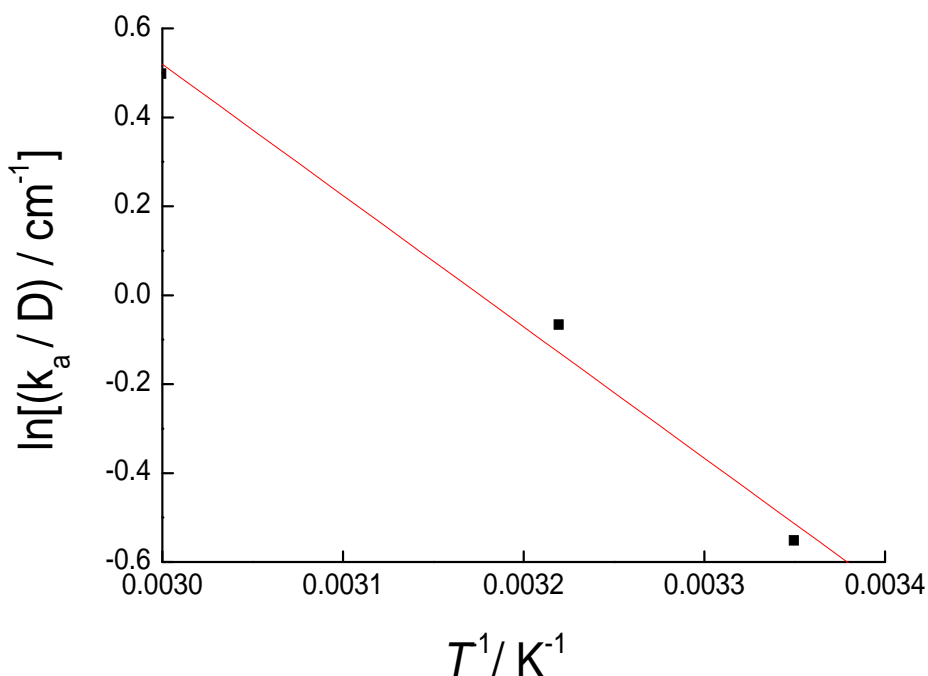
Figure 4.21: Arrhenius plot for adsorption.

4.3.1.4　　　　Desorption.

Mucin has previously (section 4.2.1) been observed to desorb according to a double stretched exponential (Kohlrausch) law [201] and the same behaviour was observed at all temperatures studied. The Kohlrausch law was tted to the experimental data, yielding the parameters given in Table 4. 6. The fact that these two desorption phases are present at all temperatures investigated suggests that the essential functional properties of the composite adsorbed mucin structure are indeed conserved across a wide temperature range.

Table 4.6: Desorption parameters for di erent temperatures. Uncertainties are s.e.m. and errors for f are estimated as +/-0.04. The parameter   =   (1/) / , where   is Euler's Gamma function and   =1/k, is a measure of the "average" relaxation time.

t	f 1	k_1 /mHz	1	K_2 /mHz	2	2
25	0.15	1.29 ± 0.08	0.980 ± 0.002	0.1000 ± 0.001	0.479 ± 0.002	6 hrs
37	0.25	1.34 ± 0.03	1.331 ± 0.001	0.085 ± 0.001	0.423 ± 0.001	9.3 hrs
60	0.3	1.72 ± 0.02	1.310 ± 0.001	0.075 ± 0.001	0.343 ± 0.001	20 hrs

Intriguingly, supposing that the desorption follows a simple Arrhenius behaviour $k_d \sim \exp(-E_d/(k_B T))$, where E_d is the activation energy for desorption, and accordingly plotting ln k_{d_1} and ln k_{d_2} vs 1/T (Figs. 4. 22 and 4. 23) yields apparently normal behaviour for the initial rapid desorption phase, but inverse Arrhenius behaviour for the subsequent slow desorption phase—i.e. desorption decelerates as the temperature is raised.
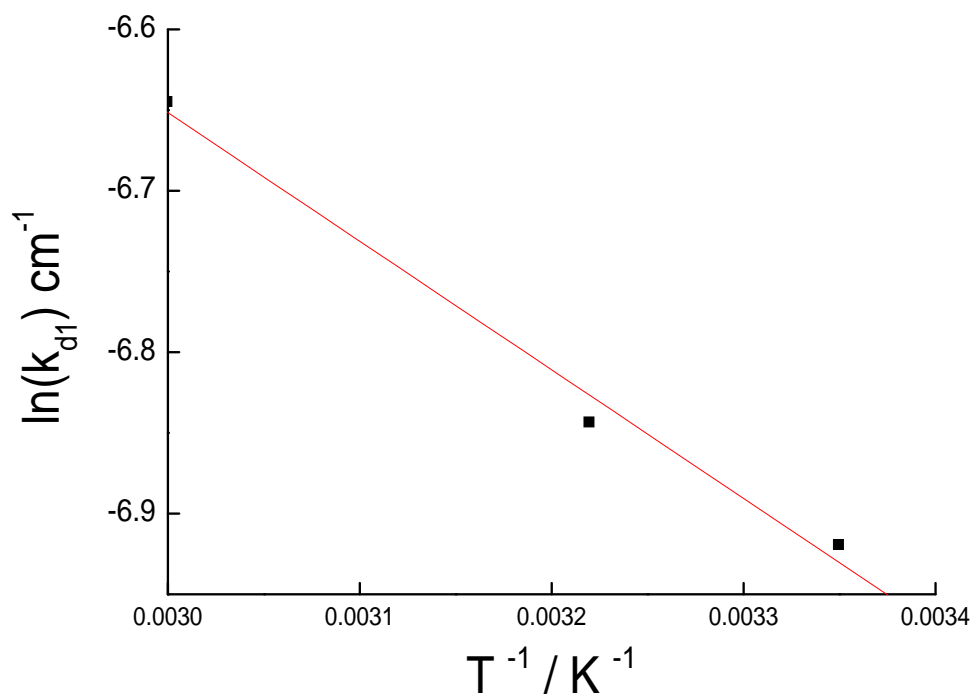
Figure 4.22: Arrhenius plot for desorption (fast phase).
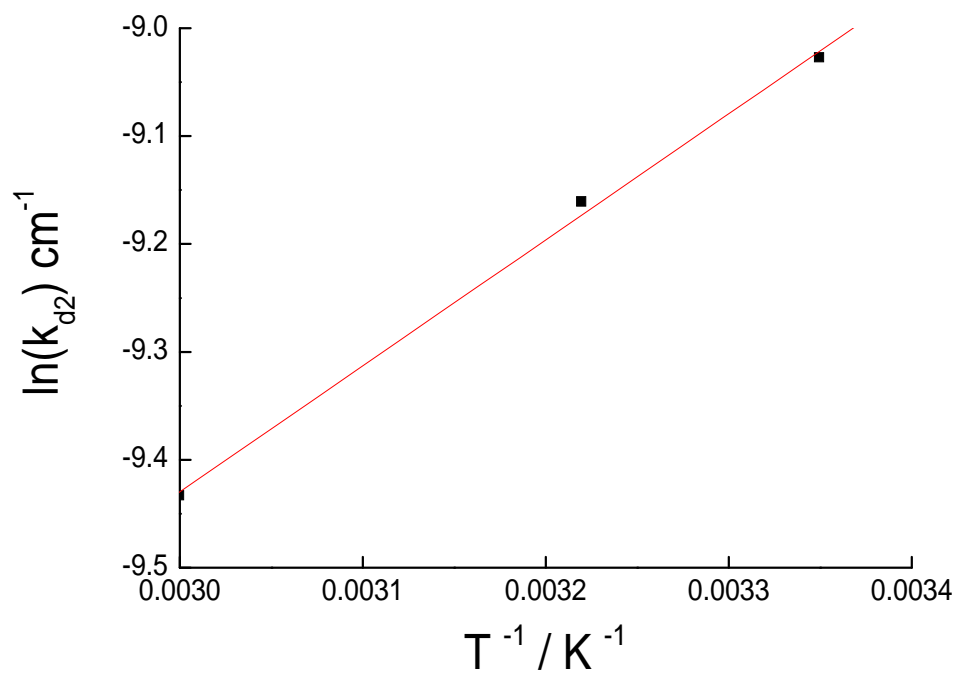
Figure 4.23: Arrhenius plot for desorption (slow phase).

97

Furthermore, the desorption activation energy (E_{d_1}) for the rapidly desorbing layer is only 6.9 kJ/mol, i.e. much lower than E_a! This is incomprehensible from the simple protein adsorption model (e.g. [88]) in which E_d must exceed E_a.

Before addressing these puzzles, we shall recall that our previous investigations established that mucin adsorbs to forms a composite two layered structure with the upper layer desorbing much faster than the layer closest to the substrate [201]. This model provides a very simple explanation of why $E_{d_1} < E_a$: the adsorption activation energy deduced from our measured adsorption kinetics is dominated by the energy of adsorption of the layer closest to the surface, hence the Ansatz $E_d > E_a$ does not apply.

The inverse Arrhenius behaviour observed for the layer adjacent to the substrate recalls the inverse Arrhenius behaviour of enzyme kinetics [202], and hence suggests a much more active adsorption mechanism than that which is usually invoked. According to Blumenfeld's mechanism, the initial (enzyme substrate) binding reaction changes the conformation of the enzyme active site, thereby creating strain between it and the rest of the molecule; the relaxation of this strain then drives the substrate to product reaction, but higher temperatures increasingly decouple the relaxation from driving the reaction, the rate of which therefore decreases. We propose that the initial mucin-substrate (i.e. the adsorbent) reaction creates strain within the molecule, which is used to drive internal conformational changes that, inter alia, facilitate desorption. At higher temperatures this coupling is increasingly broken and the protein remains in a more primitive, difficult-to-desorb conformation.

98

4.3.1.5   Hysteresis and temperature.

Unlike increasing concentration, changing temperature for 0.1% w/w mucin does not result in a measured hysteresis (Fig. 4. 24).
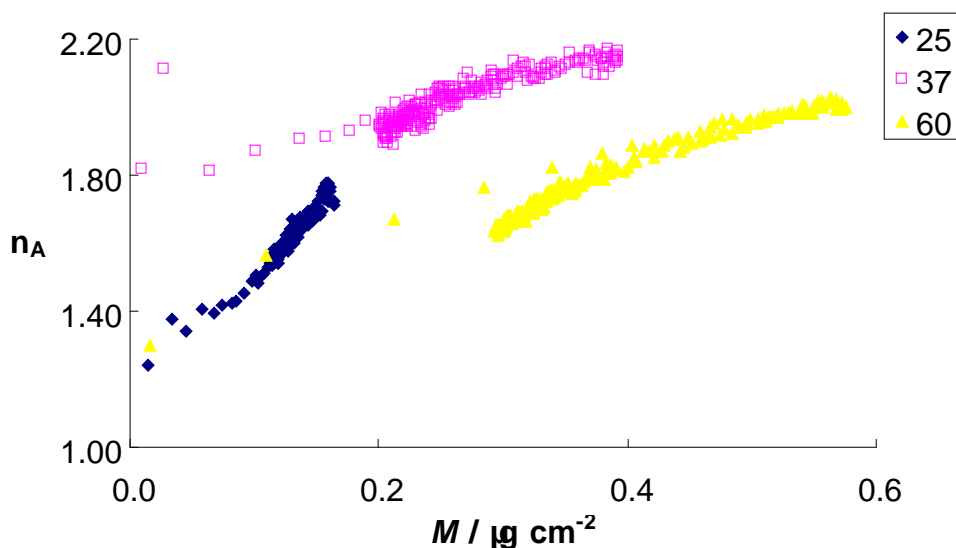
Figure 4.24: Temperature hysteresis. 0.1% w/w mucin refractive index change as a function of adsorbed mass at 25.0, 37.0 and 60.0 $^{\circ}$C.

There is no hysteresis which implies that the structure of the layer is similar for all temperatures i.e. there are no entanglement changes due to temperature. The increase in refractive index as the temperature is increased does suggest that the molecules are in a layered formation. Coupled with the change in molecule size (which becomes smaller) it is suggested that at higher temperatures the molecules form densely packed layers.

4.3.1.6   Summary

The two state adsorption model for porcine gastric mucin previously established at room temperature [200] has been corroborated up to 60 $^{\circ}$C. Mucin has been shown to contract with increasing temperature, a nd retain this contracted conformation upon adsorption. Signi cant and complex conformational changes take place in the adsorbed layer, resulting in an inverse Arrhenius dependence of desorption.

4.4   Salt

Here the effect of the Hofmeister series on mucin adsorption/desorption using sodium fluoride (NaF), sodium chloride (NaCl) and sodium iodide (NaI) are investigated. From the traditional Hofmeister series definition one would expect the kosmotrope, NaF should stabilise the native conformation of the mucin. This could reduce its ability to undergo post adsorption conformational changes and inhibit the formation of the fence/pancake regimes. NaCl is known to shield electrostatic interactions and one would expect that the mass adsorbed increases for this salt. Chaotropic NaI however should destabilise the native structure and in theory reduce the saturated mass. The data discussed in the following section for mucin do not fit these criteria and the possibility of mucin as a natively open protein whereby kosmotrope and chaotrope roles are reversed is presented [108].

4.4.1 Experimental results and discussion

The increase in M_{sat} (Fig. 4. 25) for NaCl solutions suggest that the electrostatic charges are screened.
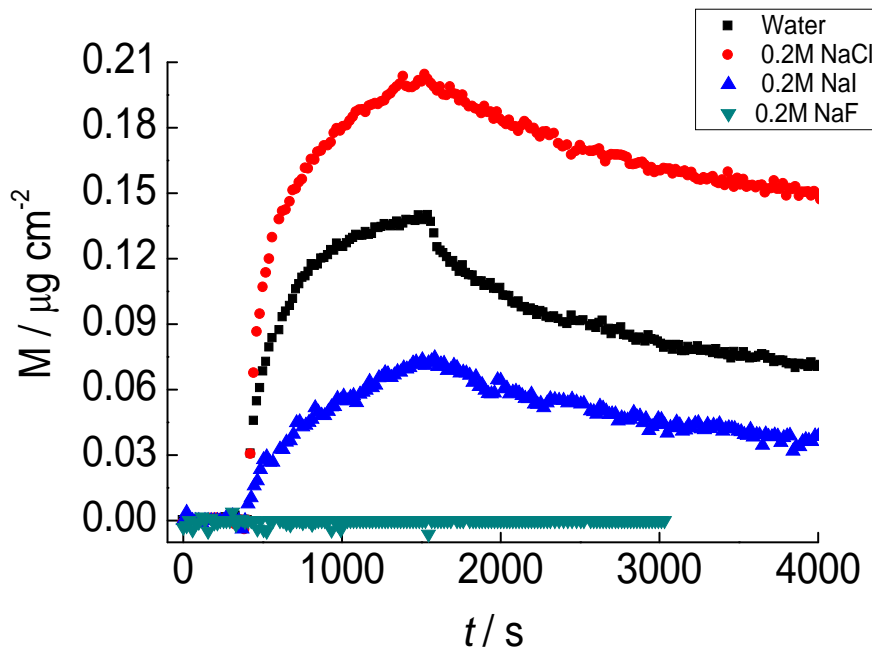
Figure 4.25: Adsorption/desorption of 0.1% mucin dissolved in pure water, 0.2M NaCl, NaI and NaF onto $Si_{0.6}Ti_{0.4}O_2$.

As does the reduction of adsorbed molecule size and adsorption rate (Table 4. 7).

Table 4.7: Adsorption parameters for 0.1% mucin in ultrapure water, 0.2M NaCl, NaI and NaF.

Salt	a / nm^2	k_a / mHz cm s^{-1}
Zero (H_2O)	267.5+/-0.1	1.51 +/- 0.04
Nacl	237.3+/-0.3	3.13 +/- 0.05
NaI	519.2+/-0.7	0.32 +/- 0.05
NaF	0	0

In addition the adsorption rate is much slower than that of mucin in water and the system is less glassy, suggesting that NaCl reduces the interaction with surrounding molecules whilst increasing the substrate interaction (Table 4. 8).

Table 4. 8. Desorption parameters for 0.1% mucin in ultrapure water, 0.2M NaCl, NaI and NaF.

Salt	M_{sat}	k_1 /mHz	1	f 1	k_2 /mHz	2	2
Zero	0.14	1.535+/-0.001	1.47+/-0.02	0.2	0.402+/-0.002	0.2562+/-0.0005	3.6
NaCL	0.20	0	0	0	0.656+/-0.001	0.0736+/-0.0004	5.1
NaI	0.07	0	0	0	0.573+/-0.001	0.1960+/-0.0001	2.3
NaF	0	0	0	0	0	0	0.0

As suggested earlier mucin is thought to belong to the natively open proteins and for these there are some unusual phenomenon predicted [109]. Kosmotropes will destabilise the native conformation whilst chaotropes will stabilise. This would fit for the NaI desorption data (Table 4. 8) as one might expect an increase in 2 as the stabilised molecules interact less with each other, (due to their restricted conformation).

NaF remains an anomaly although it could be that the native conformation is so extensively destabilised that it cannot bind the surface. A further clue to the behaviour could be that the hydrophilic/hydrophobic changes enforced by NaF upon the protein could inhibit the surface adsorption of mucin in NaF. For natively unfolded proteins, kosmotropes should render the protein more hydrophilic and this could drive the retention of the mucin in the NaF solution preventing adsorption to the substrate.

Dynamic light scattering of 0.1% mucin dissolved in water, 0.2M NaCl, NaI and NaF carried out by Dr Gleb Yakubov (Appendix E. 2) provides more evidence for mucin as a natively unfolded protein. Here the NaI (a chaotrope) not only stabilises the protein conformation in the bulk it also slightly reduces its size. NaF has the opposite effect whereby the molecule becomes larger and one can speculate less stable. The large increase for the NaCl could be attributed to the electrostatic screening and consequently the increased freedom in the bulk. One can imagine that this would also enable a greater degree of substrate freedom for NaCl.

4.4.2   Summary.

The chaotropic stabilisation and the kosmotropic de-stabilisation of mucin places it in the natively open protein family. The inhibition of mucin adsorption in the presence of NaF is truly remarkable. One can imagine that for fluoride containing products (i.e. toothpaste) the reduction of mucin close to the interface could elicit a mechanical sensation.

5.0   Function

The primary functions of the mucosa are protective and sensory. Reducing friction via lubrication is the most important factor for protection of the underlying epithelia and mucin as a biolubricator will be discussed here. Mucins role in mucosal sensing is also discussed via its proposed activity during the astringent sensation. Finally cell response to mucin surfaces and mucin surfaces which contain EGCg will be discussed.

5.1   Lubrication – experimental results and discussion

At present ion-ball bearing, brush-brush and poroelastic mechanisms are the accepted phenomena which occur during biolubrication. These mechanisms have been well proven (chapter 2, section 2. 4) and they are not disputed here. An additional mechanism is proposed from studying the lubricating properties of the adsorbed mucin layers with regard to the adsorption-desorption behaviour. These data suggest that the adsorbed layer dynamics are also important for biolubrication. Ball-on-disk tribometry carried out at Unilever by Dr Gleb Yakubov (see Appendix F. 1) using soft surfaces is provided as additional evidence for the importance of the layer dynamics. The observations will be discussed in terms of a new additional lubrication model for biolubrication.

Tribology data for 'smooth' surfaces can be summarised as having a boundary and mixed regime which are concentration dependent (Appendix F. 1, Fig. F. 1). Hydrophobic 'rough' surfaces on the other hand show no concentration dependency in the mixed regime although the boundary regime is concentration dependent. Finally hydrophobic rough surfaces show no facilitation of lubrication. Taken together these

suggest that if the surface roughness is larger than the film thickness then the contact angle dominates i.e. liquid entrainment into the contact. Of more interest are the smooth surfaces as the roughness is comparable with the layer thickness and here there is concentration dependency i.e. the layer properties are important for lubrication.

Mucin has been shown to attach very well to pure waveguides which are hydrophilic. Experiments were also conducted on hydrophobic (silanized) waveguides. The kinetic parameters (Table 5. 1) confirms the similarities with hydrophilic substrates and suggests that the composite two layered structure is formed at hydrophobic surfaces also [201].

Table 5.1: Mucin desorption parameters from silanized $SiTiO_2$ hydrophobic surfaces. Uncertainties are s.e.m.

c_b % w/w	k_1 /mHz	1	f 1	k_2 /mHz	2	2
0.01	1.639+/-0.004	1.27 /-0.08	0.20	0.2967+/-0.0002	0.403+/-0.002	3.0 hrs
0.1	1.535+/-0.001	1.47+/-0.08	0.22	0.2562+/-0.0005	0.402+/-0.002	3.6 hrs
1.0	2.147+/-0.001	1.50+/-0.02	0.40	0.2310+/-0.0004	0.396+/-0.001	4.1 hrs
3.0	2.087+/-0.001	1.51+/-0.03	0.49	0.4463+/-0.0011	0.317+/-0.002	4.6 hrs
10.0	2.314+/-0.003	1.495+/-0.05	0.73	0.5096+/-0.0078	0.301+/-0.002	4.9 hrs

It is also clear that the mass at saturation M_{sat} is higher for hydrophobic surfaces across all concentrations (Table 5. 2) which is probably due to roughening that occurs during silanization [203]. Taken together these data suggest that the two layer structure starts to form at 0.01 % w/w on hydrophobic surfaces (as it does on hydrophilic) although up to 1 % w/w the faster desorbing uppermost layer is small, whereas above 2-3% w/w this layer becomes relatively thick [201].

Table 5.2: Hydrophilic and Hydrophobic saturated mass values for different bulk mucin concentrations after 18 minutes of adsorption time. Errors are S.E.M.

	Hydrophobic		Hydrophilic	
C_b mg/cm^3	M_{sat}	error	M_{sat}	error
0.1	0.130	0.003	0.14	0.05
1.0	0.195	0.004	0.13	0.02
10	0.295	0.039	0.19	0.02
30	0.415	0.032	0.30	0.04
100	0.881	0.013	0.55	0.08

From Appendix F. 1, Fig. F. 4 and F. 5 it appears that as more mass is adsorbed there is less relative change in boundary friction i.e. it becomes less concentration dependant. If one aims to generate an effective lubricant these data suggest that the most important factor is to decrease desorption time and not to increase adsorbed mass per se. We see this effect occurring for mucin. In addition the similar concentration dependent lubricating behaviour of chitosan (Appendix F. 1) suggests that although highly charged, chitosan is a less effective lubricator. Therefore charge may be of secondary importance.

This work highlights certain aspects of biopolymer lubrication that were not previously considered. First the results illustrate the importance of the dynamics of an adsorbed film whereas the majority of previous results [202, 203, 204, 205, 206, 207, 208, 209, 210, 211, 212, 213, 123, 126] were focused on the structure of the film, e.g. brush versus adsorbed configurations. In contrast to structural features, the dynamics can be easily modified at biosynthesis and therefore a number of various properties can be achieved with a relatively minor degree of post modifications. For mucins these modifications are related to the glycosylation of the protein chain. Even small

variations in composition can significantly alter the lubricating functionality of the molecules.

5.1.1 Summary

Mucin has been shown to facilitate lubrication between hydrophobic PDMS surfaces leading to a reduction in the boundary friction coefficient. The lubrication behaviour of mucin was found to be concentration dependent. It is proposed that local adsorbed film dynamics (composite layer structure) are crucial for lubrication, which, thus far have not been investigated for biolubrication. Also highlighted is the importance of surface roughness on observed lubrication behaviour. If roughness is much larger than the thickness of the adsorbed film the mixed regime is dominated by the contact angle. On the other hand if the roughness is comparable with the thickness of the adsorbed film then the film properties should impact on mixed regime, and dominate boundary lubrication. This is indeed the case for mucin. The lubrication of chitosan is also concentration dependent, albeit much weaker than mucin suggesting that the adsorbed film dynamic properties are of primary importance for effective lubrication.

5.2 Astringency

The most pertinent example of oral mechanical stimulation is astringency, a dry, puckering sensation. It is a diffuse surface phenomenon, taking many seconds to develop and has been linked to a reduction in saliva's lubricating properties [7, 8, 9]. Here mucin adsorption/desorption characteristics are evaluated in the presence of EGCg. These data suggest that EGCg stabilises the mucin layer, although above a critical concentration the mucin layer breaks down. We show how this concentration switch is related to the astringent perception evaluated in the literature. The presence of a temperature switch is more difficult to interperate and the possibilities are discussed.

5.2.1 Experimental results and discussion

Optical waveguide lightmode spectroscopy is used in to measure the adsorption/desorption characteristics. Dynamic light scattering (DLS) carried out at Unilever Colworth by Dr Gleb Yakubov confirm the OWLS findings (Appendix F. 2).

5.2.1.1 Concentration switch

First the adsorption/desorption characteristics of 0.1% w/w and 3% w/w mucin solutions mixed with EGCg are investigated. Next the influence of epicatechin (EC) and finally the affects on an established layer of mucin are investigated by flowing 0.1% mucin mixed with EGCg and EGCg alone (in water) over an already established 0.1% w/w mucin layer adsorbed onto the waveguide.

5.2.1.2   Mucin + EGCg adsorption onto pure waveguides

The adsorption/desorption curves show clearly that more mass is adsorbed when EGCg is added to the mucin solution. There are two possibilities, either the EGCg is incorporated into the adsorbed layer or the EGCg controls the adsorption of the mucin molecules at the interface. These possibilities, as will become apparent are difficult to determine. Also note that at very high concentrations (1% w/w EGCg) the layer breaks down (Fig. 5. 1).
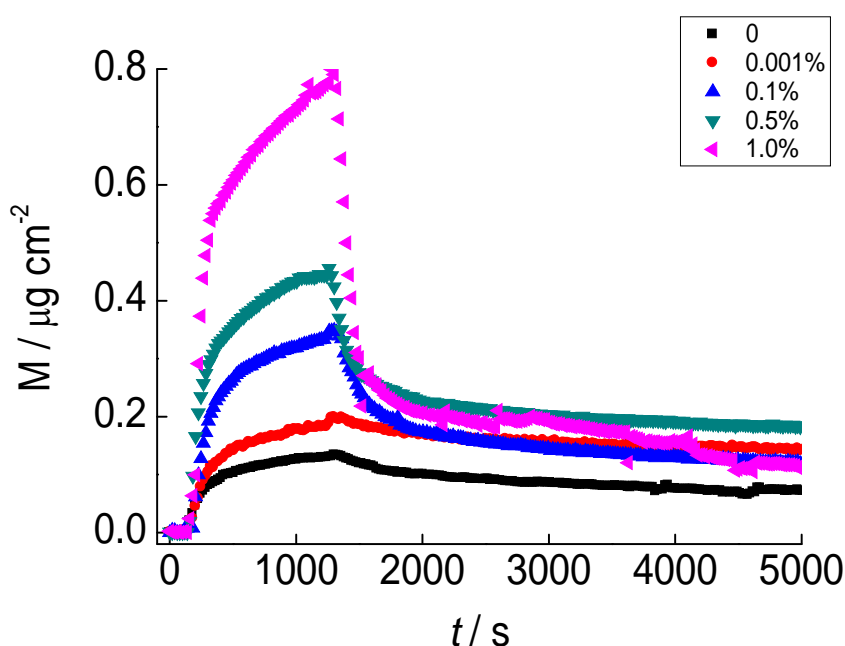
Figure 5.1: Typical result of mucin adsorption/desorption. 0.1% w/w mucin pre-mixed with EGCg concentrations spanning 0.001 to 1% w/w.

The dynamic light scattering (carried out by Dr Gleb Yakubov, Appendix F. 2) clearly suggests that mucin forms aggregates in solution and possibly complexes with the EGCg. However this does not necessarily mean that the EGCg molecules will be incorporated into the layer upon adsorption. In order to investigate further the

adsorption kinetics (Table 5. 3orption kinetics (Table 5. 4) were plotted using the analytical techniques which were previously used for mucin solutions alone.

Table 5.3: Adsorption parameters for 0.1% mucin mixed with varying concentrations of EGCg (0.01-1.0%). Uncertainties are s.e.m.

EGCg concentration (% w/w) dissolved in 0.1% mucin	a / nm^2	k_a / mHz cm s^{-1}
0	268.0 ± 0.2	1.20 ± 0.04
0.01	257.4 ± 0.4	2.12 ± 0.08
0.1	194.3 ± 0.4	4.62 ± 0.07
0.5	169.0 ± 0.3	4.84 ± 0.05
1.0	105.2 ± 0.6	4.94 ± 0.07

From Table 5. 3 one can see that higher concentrations of EGCg result in a smaller adsorbed molecule at the surface suggesting that the EGCg is collapsing the mucin at the interface. Note that this behaviour is in stark contrast to that which occurs in the bulk whereby the complex size increases with increasing EGCg concentration (Appendix F. 2). Investigating the desorption kinetics (Table 5. 4) should provide additional information on the structural properties of the layers derived from mucin + EGCg solutions.

Table 5.4: Desorption parameters for 0.1% mucin mixed with EGCg. Uncertainties are s.e.m.

EGCg concentration	M_{sat}	k_1 /mHz	1	f 1	k_2 /mHz	2	2
0	0.14	2.147+/-0.004	1.50+/-0.04	0.15	0.1750+/-0.0001	0.4975+/-0.0001	3.3
0.01	0.22	3.940+/-0.006	1.51+/-0.06	0.20	0.1890+/-0.0001	0.4170+/-0.0035	4.4
0.1	0.34	3.222+/-0.004	1.63+/-0.07	0.25	0.2097+/-0.0001	0.2539+/-0.0026	29.0
0.5	0.45	5.351+/-0.012	1.78+/-0.07	0.52	0.1798+/-0.0003	0.1928+/-0.0014	208.1
1.0	0.76	7.286+/-0.007	2.16+/-0.08	0.75	3.3550+/-0.2129	0.2456+/-0.0014	2.2

It is clear that a concentration switch occurs, whereby the addition of EGCg no longer increases desorption time (tau) above 0.5% w/w (Table 5. 4). Increasing the

concentration of EGCg (up to 0.5 % w/w) results in a reduction of 2 which suggests that the system is increasingly glassy. It could be that at 1% w/w EGCg the concentration is so high that it collapses the mucin molecules (see also size changes, Table 5. 3) thereby affecting their adsorption/desorption characteristics.

For 3% mucin concentrations there is again an increase in Msat as seen for 0.1% (Fig. 5. 2). Indeed it is also clear that the addition of EGCg has a similar effect as seen for the semi-dilute regime.
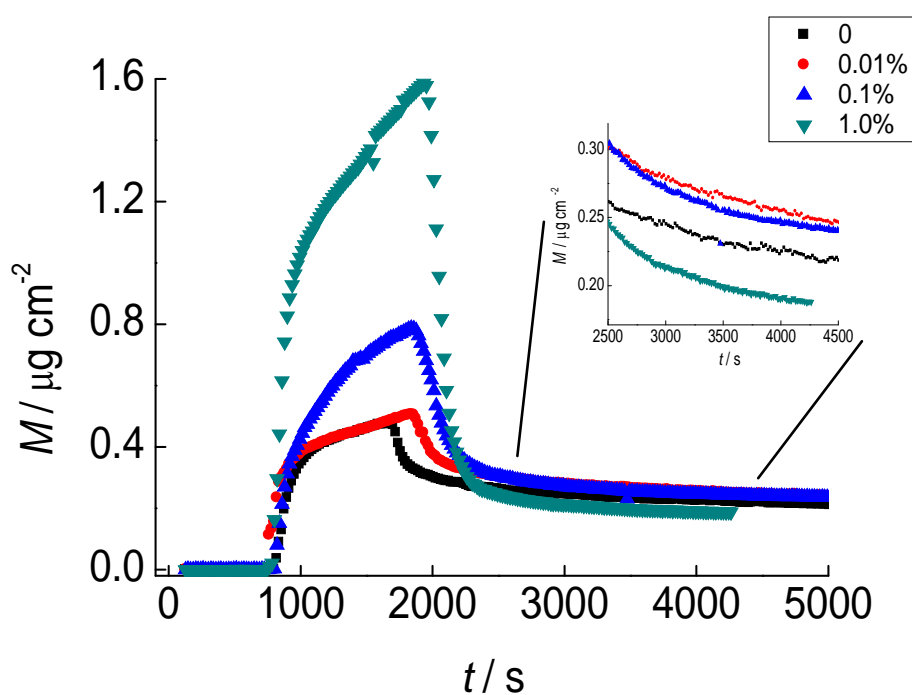
Figure 5.2: Mucin adsorption/desorption. 3% w/w mucin mixed with 0.01, 0.1 and 1.0% EGCg. Inset is expanded view of slow phase desorption.

Most striking are the effects of EGCg on the area occupied by the adsorbed mucin molecules (Table 5. 5). For 1% w/w EGCg this value is approximately $1/10^{th}$ the value for EGCg free solutions.

111

Table 5.5: Adsorption parameters for 3% mucin mixed with varying concentrations of EGCg (0.01-1.0%).

EGCg concentration (% w/w) dissolved in 3 % mucin	a / nm^2	k_a / mHz cm s^{-1}
0	199.0 ± 0.2	4.37 ± 0.03
0.01	90.5 ± 0.7	5.75 ± 0.02
0.1	46.7 ± 0.3	16.6 ± 0.04
1.0	27.4 ± 0.4	22.8 ± 0.05

There is no doubt that this reduction in adsorbed area effects the desorption kinetics and contributes to the rapid depletion of the layer at 1% w/w EGCg (Table 5.6).

Table 5.6: Desorption parameters for 3% mucin mixed with EGCg. Uncertainties are s.e.m.

EGCg concentration	M_{sat}	k_1 /mHz	1	f 1	k_2 /mHz	2	2
0	0.14	3.940+/-0.003	1.5+/-0.03	0.41	0.10+/-0.002	0.2130+/-0.0001	9 days
0.01	0.22	3.444+/-0.001	1.41+/-0.04	0.45	0.08+/-0.001	0.2379+/-0.0035	5 days
0.1	0.34	2.604+/-0.004	1.33+/-0.04	0.50	3.55+/-0.012	0.1848+/-0.0026	19 hrs
1.0	0.76	2.579+/-0.006	1.28+/-0.06	0.76	177.54+/-0.356	0.1374+/-0.0014	5 hrs

It is therefore possible that the presence of EGCg in the bulk will either collapse or cross-link with the mucin or that its presence drives the aggregation of mucin molecules. Most likely at very high concentrations the EGCg collapses the mucin molecules as the layer is drastically affected (both 0.1 and 3.0% w/w mucin). The adsorbed molecule area is a critical factor affecting layer characteristics as for all 0.1% w/w mucin + EGCg; with the exception of 1% w/w EGCg is increased. The opposite is true for 3% w/w mucin whereby even the lowest concentration of EGCg reduces .

112

Mucin therefore appears to form complexes (micelles) in the bulk which incorporate into an adsorbed layer (Fig. 5. 3). There is however the possibility that mucin is not incorporated into the adsorbed layer.
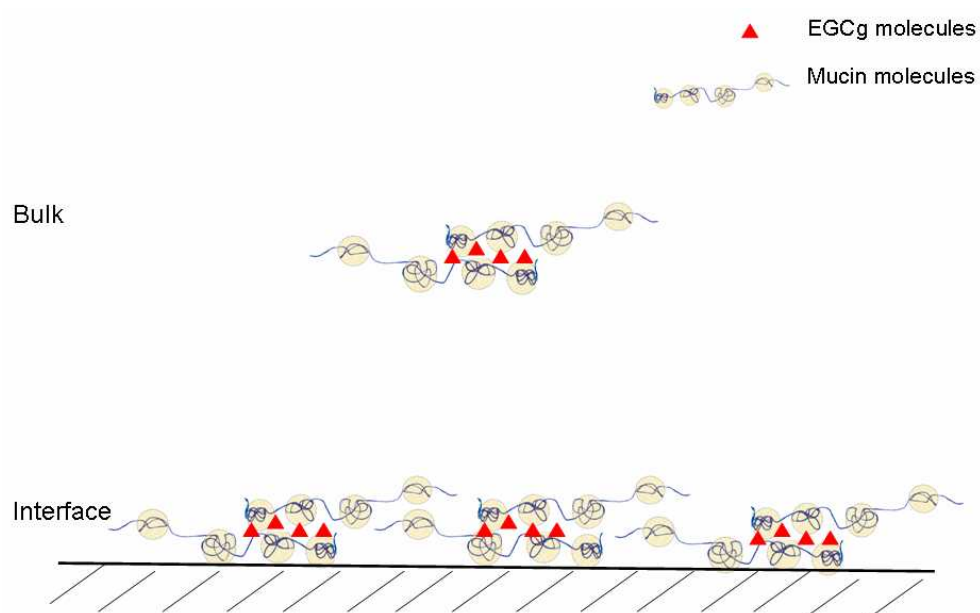
Figure 5.3. Mucin + EGCg behaviour in the bulk and at an interface. Mucin forms complexes with EGCg in the bulk and it is most likely that the EGCg bound to the mucin is also incorporated into the adsorbed film at the interface.

5.2.1.3   Mucin + EC adsorption onto pure waveguides

In order to determine if the galloyl group were important we investigated adsorption/desorption using epicatechin (EC) as this catechin does not have the galloyl group. As is the case for mucin + EGCg solutions the absorbed mass for mucin mixed with EC is much higher than that of mucin alone (Fig. 5. 4). Note that it was only possible to investigate one concentration due to experimental constraints.

113
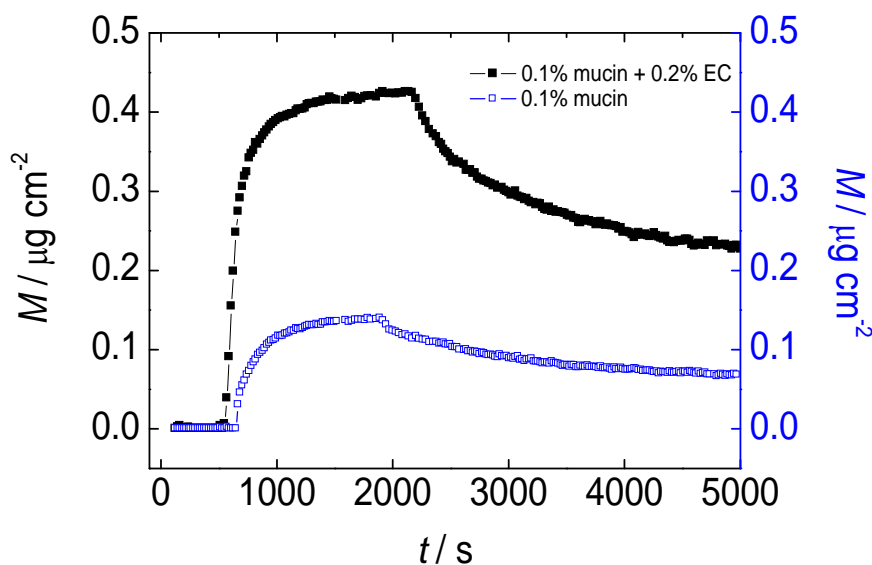
Figure 5.4: Adsorption/desorption plot for 0.1% w/w mucin in water and 0.1% w/w mucin mixed with 0.1% w/w 0.2 % w/w EC.

However differences in behaviour become apparent when investigating the kinetics. The molecule area, a, is much smaller for solutions containing EC (Table 5. 7) than those of EGCg (Table 5. 3). This suggests that even for this low concentration of EC the mucin molecules are collapsed as is the case for much higher concentrations of EGCg + mucin.

Table 5.7: Adsorption parameters for 0.1% w/w mucin mixed with 0.2% w/w EC. Uncertainties are s.e.m.

EC concentration (% w/w) dissolved in 0.1% mucin	a / nm^2	k_a / mHz cm s^{-1}
0.2	97.7 ± 0.6	5.64 ± 0.08

It is therefore hypothesised that the mucin molecules do not complex with the EC and instead are collapsed. Examining the desorption kinetics it is clear that the M_{sat} before

114

desorption is much higher for mucin + EC solutions (Table 5. 8) than for mucin + EGCg, indeed one would need 0.5% w/w EGCg to have a similar effect (Table 5. 4). The 1 and k_{d1} are almost identical suggesting a similar process occurs here. 2 is interesting as it is only slightly smaller than mucin alone and is much higher than that of 0.1% w/w EGCg mixed with mucin (Table 5. 3) and could imply that structure of the adsorbed layer is similar to that of the mucin only layer, albeit with more molecules at the interface, i.e. EC collapses the mucin molecules in the bulk and is not incorporated into the layer.

Table 5.8: Desorption parameters for 0.1% w/w mucin mixed with 0.2% w/w EC. Uncertainties are s.e.m.

EC concentration	M_{sat}	k_1 /mHz	1	f 1	k_2 /mHz	2	2
0.2	0.42	2.029+/-0.002	1.47+/-0.05	0.20	0.1186+/-0.0001	0.4198+/-0.0001	6.8

Low EC concentration therefore has little impact on the characteristics of the adsorbed mucin layer when compared with low EGCg concentration.

5.2.1.4   Mucin + EGCg adsorption onto established mucin layers

Further clues are provided by investigating EGCg and mucin + EGCg flowed over an already established mucin layer (Fig. 5. 5).

115
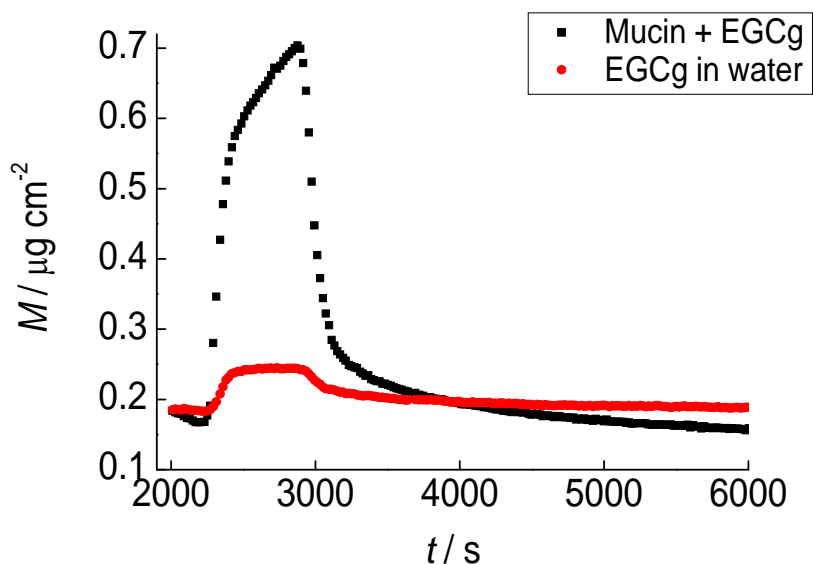
Figure 5.5: Typical results of 0.1% w/w mucin in water and 0.1% w/w mucin mixed with EGCg flowed over 0.1% mucin layer.

Clearly the large mucin+ EGCg complexes in the bulk contribute to the larger adsorption seen, although after washing very little remains. EGCg has a dramatic effect on the desorption characteristics (Table 5. 9).

Table 5.9: Desorption parameters for EGCg mixed with water and 0.1% mucin mixed with EGCg flowed over an established 0.1% w/w mucin layer. Uncertainties are s.e.m.

Concentration EGCg	M_{sat}	k_1 /mHz	1	k_2 /mHz	2	2
0	0.14	2.147+/-0.001	1.50+/-0.02	0.1750+/-0.0001	0.4925+/-0.0001	3.3
0.01	0.16	1.910+/-0.001	1.00+/-0.16	0.0259+/-0.0003	0.4223+/-0.0016	30.9
0.1	0.26	1.610+/-0.002	1.04+/-0.18	0.0030+/-0.0001	0.1906+/-0.0015	2 yrs
0.5	0.38	1.783+/-0.007	1.04+/-0.32	0.0024+/-0.0001	0.0837+/-0.0020	>2yrs
1	0.4	2.067+/-0.010	1.02+/-0.11	0.0169+/-0.0002	0.0698+/-0.0040	>2yrs
Concentration EGCg in 0.1% mucin						
0	0.14	2.147+/-0.001	1.50+/-0.02	0.1750+/-0.0001	0.4925+/-0.0001	3.3
0.01	0.26	2.100+/-0.001	1.51+/-0.28	0.1589+/-0.0001	0.4801+/-0.0016	3.8
0.1	0.33	2.010+/-0.001	1.49+/-0.08	0.1440+/-0.0002	0.3223+/-0.0017	13.2
0.5	0.59	5.653+/-0.007	1.38+/-0.21	4.1410+/-0.0064	0.1602+/-0.0015	76.3
1	0.75	6.227+/-0.004	1.68+/-0.08	4.3450+/-0.0089	0.1576+/-0.0014	88.8

116

For EGCg in water flowed over the mucin layer there is a small residual increase in mass after washing which stabilises the layer to such an extent that is 2 years (and above) for high concentrations. It does not desorb. Most likely it is forming a layer which covers the underlying mucin, constraining the molecules and preventing desorption from the surface. If the EGCg molecules bind only the PRO-PRO-ARG regions (as is the case for proline rich proteins) then one would expect very little EGCg adsorption (as this site may also bind the substrate). EGCg must also bind other mucin regions.

For EGCg dissolved into a 0.1% w/w mucin solution the effect is much less. This must be due to the formation of mucin/EGCg complexes which inhibits EGCg activity with the adsorbed layer. Indeed at low concentrations of EGCg there is virtually no effect on desorption kinetics whilst at higher concentrations the EGCg has a greater effect. At high concentrations there will be excess EGCg molecules available which will be able to interact with the adsorbed layer, suppressing desorption as is seen for EGCg in water solutions.

From these data it is most likely that the mucin molecules complex with EGCg molecules at low concentrations. At high concentrations the mucin molecules may be collapsed. If the molecules aggregate in the bulk this should occur by either cross-linking or molecule collapse [214]. We can confirm this by investigating the bulk behaviour using dynamic light scattering and atomic force microscopy (carried out at Unilever by DR Gleb Yakubov, Appendix F. 2). The radius of gyration (R_g) for this mucin is 52 +/- 5 nm and a daisy bead conformation with hydrodynamic radius (R_h) of 10 nm +/- 2 nm. If the molecule collapse scenario were true one would not expect to see the daisy bead behaviour and instead globule dynamics should be observed.

117

Using polyelectrolyte approximation the hydrodynamic radius ($R_h = 0.77* R_g = 40 +/- 4$ nm) and polymer coil approximation ($R_h = 0.67* R_g = 35 +/- 3$ nm) to calculate the globule dynamics one can see that collapsed mucin molecules are only present in the bulk at concentrations above 0.5% w/w and that below that typical daisy bead R_h values are observed.

Individual collapsed molecules are therefore only present at concentrations above 0.5% w/w suggesting that at low concentrations interactions can occur (probably via cross-linking) whereas at higher concentrations mucin molecules can be collapsed by the presence of a high quantity of EGCg molecules. We suggest cross-linking as at low concentration we do not see flocculation which would be expected for molecule collapse (136, 215). It is clear that mucin clearly interacts with EGCg (Appendix F. 2) and that high concentrations deplete the mucin layer.

5.2.1.5   Summary

We therefore suggest that galloyl group catechins impact heavily on mucosal behaviour and in particular the mucin components. The build up of EGCg molecules at the surface of the oral mucosa could be responsible for the initial astringency feeling [134] whereby the bound molecules evoke a strain on the underlying cells or free nerve endings. Consequently the time taken to build up the coating is analogous with the slow onset of the sensation [7, 8] and as the concentration of EGCg increases beyond a critical value the surface coating breaks down and the astringency feeling is lost.

EC also interacts with mucin although via a different mechanism as functional characteristics of the mucin layer are not affected. The galloyl ring is therefore thought to be responsible.

Mucin molecules could be forced (by the surrounding EGCg molecules) into entangled conformations which adsorb in a similar manner as those adsorbed from EGCg free solutions. Alternatively mucin may complex with EGCg and be incorporated into the adsorbed layer in a manner which does not affect the mucin/substrate binding site.

5.2.2   Temperature switch

As has been already discussed the effect of temperature is an important parameter for studying mucin behaviour and combining with EGCg should provide further information. There is a temperature switch. Adsorbed mass increases with temperature up until 37 $^{\circ}$C where it decreases (Fig. 5. 6).
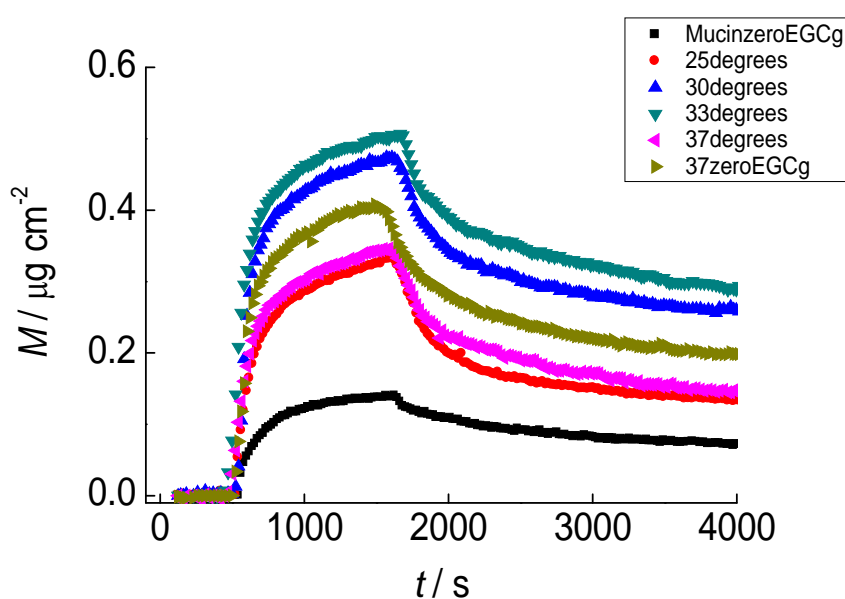
Figure 5.6: Mass time plot for 0.1% w/w mucin mixed with EGCg (0.1% w/w) solutions at different temperatures.

119

This is corroborated by the adsorption parameters fitted using RSA (Table 5. 10). It is important to note that the size of the adsorbed area for the molecule decreases up to 37 ^{o}C at which point it increases.

Table 5.10: Adsorption characteristics. 0.1% w/w mucin mixed with 0.1% w/w EGCg and absorbed at different temperatures on to a $SiTiO_2$ substrate.

T	EGCg % w/w	a / nm^2	k_a / mHz cm s^{-1}
25	0	268.0 ± 0.4	1.23 ± 0.04
37	0	113.4 ± 0.4	2.76 ± 0.05
25	0.1	196.6 ± 0.7	4.62 ± 0.07
30	0.1	137.4 ± 0.8	4.85 ± 0.03
33	0.1	116.0 ± 0.3	5.02 ± 0.03
37	0.1	168.2 ± 0.2	2.73 ± 0.06

This behaviour has a profound effect on the desorption behaviour (Table 5. 11). Instead of seeing an increase for   as the temperature increases (as we would expect for mucin only) there is a decrease in   .

Table 5.11: Desorption characteristics for 0.1% w/w mucin and 0.1% w/w mucin + EGCg solutions at temperatures ranging from 25.0 to 37.0 ^{o}C.

t	EGCg % w/w	M_{sat}	k_1 /mHz	1	f 1	k_2 /mHz	2	2
25	0	0.14	0.980+/-0.002	1.29+/-0.15	0.15	0.1	0.479+/-0.002	6 hrs
37	0	0.39	1.310+/-0.002	1.34+/-0.08	0.25	0.1+/-0.02	0.423+/-0.003	9 hrs
25	0.1	0.34	3.222+/-0.004	1.63+/-0.12	0.25	0.2+/-0.01	0.21+/-0.001	29 hrs
30	0.1	0.46	1.197+/-0.005	1.30+/-0.38	0.32	0.1+/-0.03	0.312+/-0.001	27 hrs
33	0.1	0.51	1.268+/-0.002	1.39+/-0.07	0.37	0.1+/-0.01	0.396+/-0.001	10 hrs
37	0.1	0.35	2.082+/-0.003	1.79+/-0.16	0.36	0.2+/-0.01	0.398+/-0.004	4 hrs

The differences seen at different temperatures could be attributed to an effect imposed on the mucin, the EGCg molecule or both. The major influence of temperature

increase is most likely on the mucin molecule as EGCg is stable (at temperature below 70 ^{o}C) for many hours [216]. Earlier we saw that the mucin bulk and adsorbed molecule size decrease as temperature is increased (Chapter 4, section 4. 3).

The mucin molecules are obviously getting smaller as the temperature increases (Table 4. 5, chapter 4, section 4. 3). When EGCg is added to mucin at the lowest temperature (25 ^{o}C) the molecule size is also reduced (Table 5. 10). It is sufficient to presume that this is occurring for the intermediate (30 and 33 ^{o}C) temperatures as the adsorbed molecule size is smaller. At 37 ^{o}C the adsorbed molecule size increases.

The 2 exponent is a measure of the memory of the system and when EGCg is added (25 ^{o}C) the system becomes glassier (Table 5. 10). This may be due to cross-linking which adds a further step to the desorption process. As the temperature is increased the system becomes less stretched suggesting that the EGCg has less effect and at 37 ^{o}C the exponent is close to that of an EGCg free mucin solution.

It would seem from this data that astringency will have greater impact on organisms that have body temperatures below 37 ^{o}C and it is interesting to speculate evolutionarily as to why plants have evolved these molecules in such a way that they impact on the mucosa of homeothermic animals less vigorously. One possible reason could be seed dispersal. A high percentage of the seed coat is polyphenol [217] and land based homeotherms tend to have greater territories than poikilotherms. The reduced astringent perception (by homeotherms with body temperatures ~36-40 ^{o}C) may have had clear evolutionary advantages for those plants that were dispersed by homeotherms.

121

5.2.3   Summary

We show that adding polyphenol increases adsorbed mass of mucin at the solid-water interface and that increasing temperature increases the adsorbed mass further. At a critical temperature (37 ^{o}C) there is a switch whereby the saturated mass decreases. This suggests that polyphenol-mucin interactions (and not only polyphenol-protein) are also be involved in the astringent perception.

5.3   Cell spreading

This section will first introduce the initial experimental data which produced results that were difficult to interperate. In turn this led to the design of the second experimental data set and it is shown here that EGCg can control (via the substrate) cell spreading.

5.3.1   Initial experiments

Initially the affects of catechin on cell morphology were first investigated by growing cells on waveguides (on-line) and adding 100µl EGCg (Fig. 5. 7). The cells used were murine 3T3 fibroblasts (Appendix C. 1).
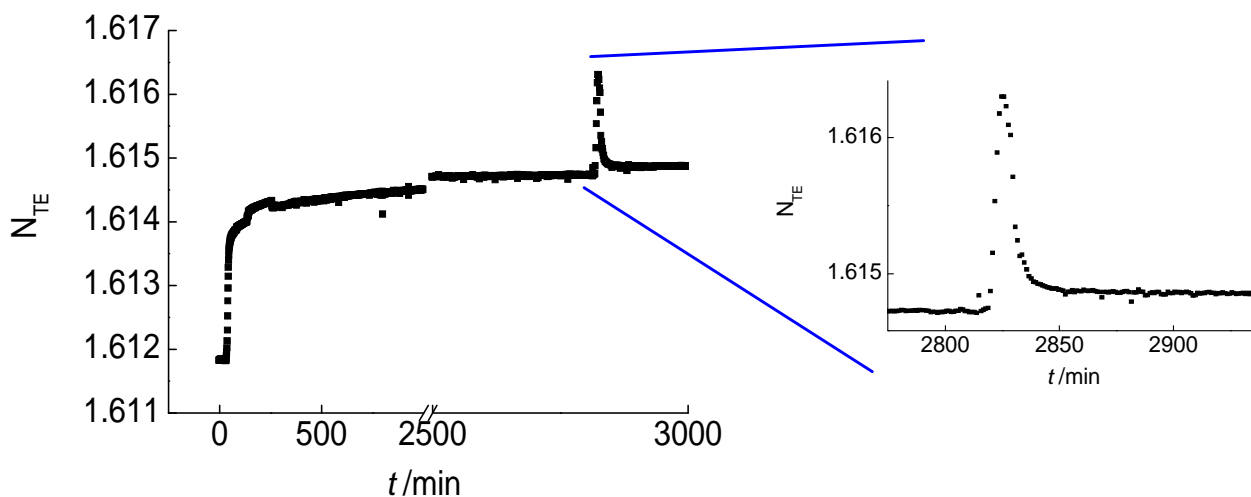
Figure 5.7: 3T3 fibroblast cells grown online. Buffered medium and serum were first flowed onto the waveguide (DHS: Dulbecco's media containing Hepes and Serum) (first curve). Cells were then added, the flow stopped (to allow cells to attach, second small curve) and then restarted. Restarting the flow causes the signal to drop slightly. Cells were then spread over many hours and 100 μl EGCg is injected (1.0% w/w) at around 2,800 minutes and washed with DHS (expanded area).

The results were inconclusive when analysing the data as it was not possible to determine if the results were a cell or substrate response (Fig. 5. 8).
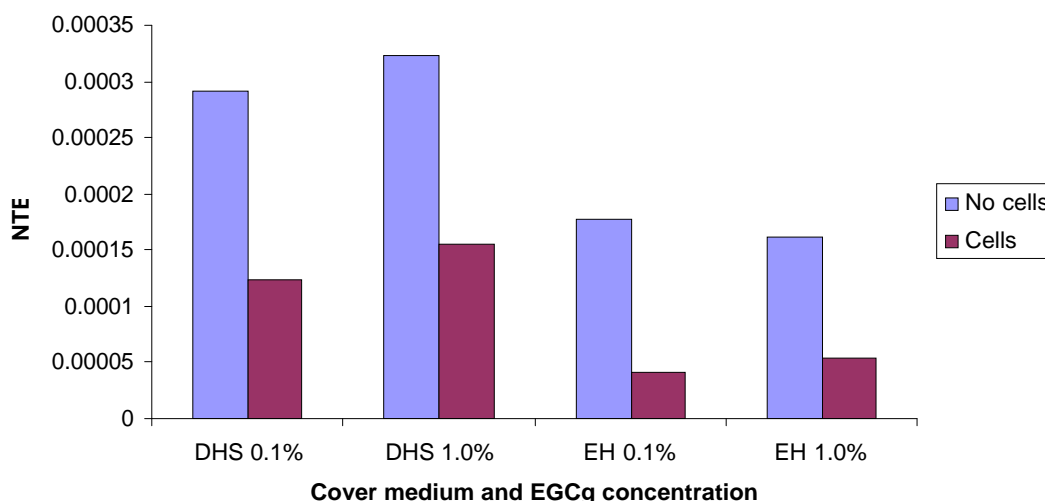
Figure 5.8: N_{TE} for EGCg added to cell-free and cell-established substrates. EGCg is either added in buffered medium + 10% serum (DHS) directly to cells. Or the cells are washed for 15 minutes with 0.1M Hepes buffer and then EGCg in Hepes (EH) applied.

The N_{TE} was measured for both cell covered substrates and substrates which had no cells attached. To eliminate the effect of the proteins in serum the experiments were also carried out using Hepes buffer (and also phosphate buffer). The results were still inconclusive. EGCg added to cell free substrates have a larger N_{TE} suggesting increased adsorption of EGCg on these surfaces (Fig. 5. 8). This could indicate that the differences for substrates which contain cells are due to the reduced area available for EGCg surface binding (as the cells are covering the substrate). Initial experiments using cells in phosphate buffered saline (PBS) and 0.1% w/w EGCg, using phase microscopy suggested that the cells would 'round up' and reduce their contact with the surface (Fig. 5. 9). These experiments were also carried out using 10mM Hepes with 0.1% w/w EGCg giving the same result.

124
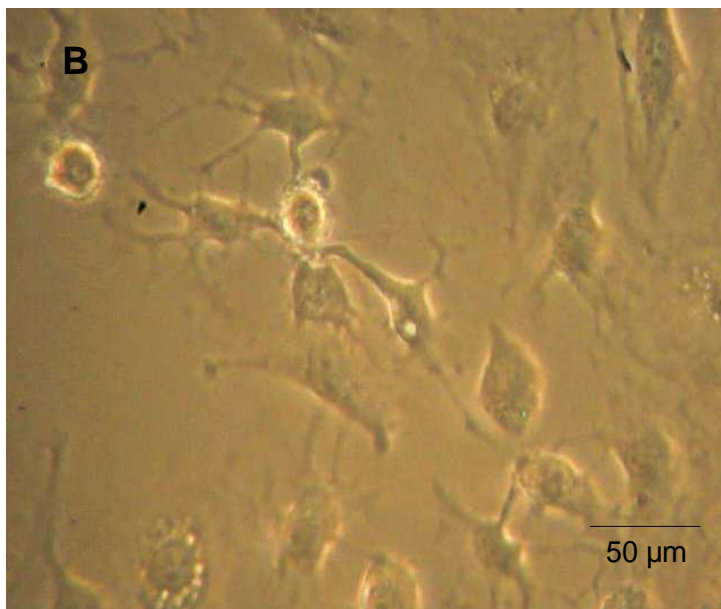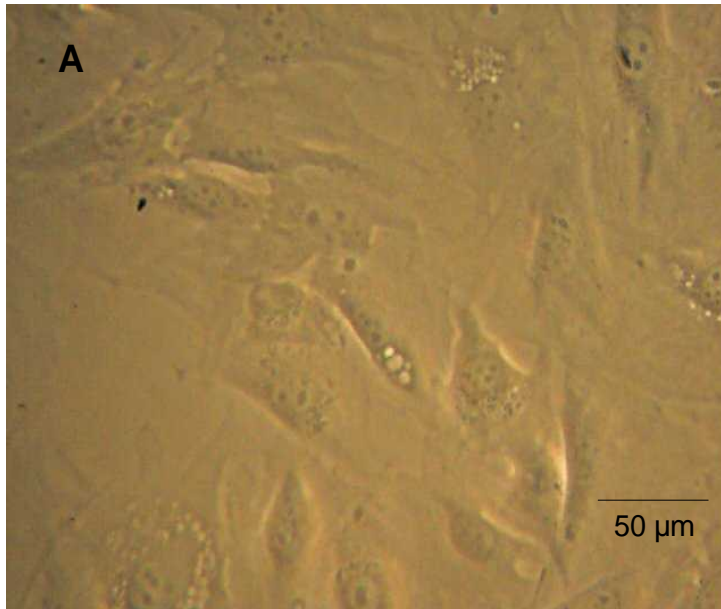
Figure 5.9: 3T3 fibroblast cells in PBS with 0.1% w/w EGCg. At the beginning of the experiment cells show normal morphology (A) but after 30 minutes incubation with EGCg (B) cells round up and reduce in size.

If they are rounding up on the waveguide we would expect a decrease in N_{TE}. This is not the case as we see an increase in the signal suggesting more material at the surface

125

(Fig. 5. 8). It could be that the cells are releasing material onto the substrate or that EGCg is binding the substrate. This approach produced too many variables.

The inconclusive results required a new approach to the problem. If we could not measure the affect of EGCg in solution then it would be best to incorporate the EGCg into the substrate. This also caused some problems as EGCg does not bind to the waveguide directly (Fig. 5. 10).
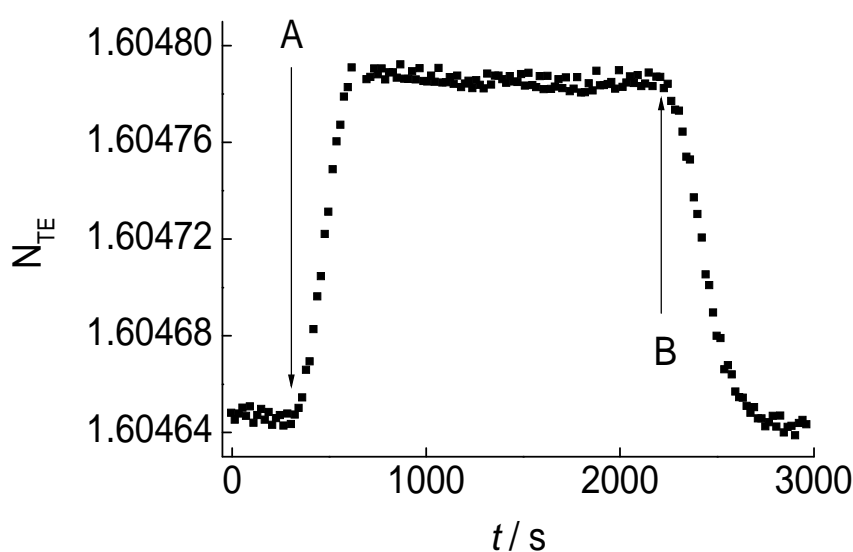
Figure 5.10: EGCg adsorption onto a bare waveguide. Initially a water baseline is established after which the EGCg is added (first rising curve, point a). The return of the curve to the same position after washing (second curve, point b) implies no adsorption has taken place.

Therefore incorporating EGCg into the mucin layer may enable a response from the cells.

126

5.3.2   Polyphenol control of cell spreading

Tissue engineering applications such as wound repair and tissue growth strive to mimic the assimilatory role of natural substrata whilst designers of biomedical coatings (such as those of certain implants and surgical instruments) may seek to assimilate or inhibit protein and cell attachment [218]. One way to inhibit is to use natural systems and of particular interest in this regard are the mammalian repulsive mucus barriers that actively remove invading cells from the mucosa [122]. The major macromolecular component of the mucosal layer is mucin, a family of heavily glycosylated, high molecular weight glycoproteins with carbohydrate side chains that make up some 50-80 % of the molecule by weight [123, 219].

Fibroblast and keratinocyte cultures grown on mucin-coated substrata adhere poorly when compared with oxidised polystyrene (tissue culture polymers) or mucin surfaces that have their O-linked carbohydrates removed [220]. Indeed the sugar moieties seem to play a pivotal inhibitory role, as cellulose-coated [221, 222] and dextran sulphate-coated surfaces (even when over-coated with fibronectin) [223] inhibit cell spreading.

Catechins are a group of plant polyphenol flavonoids found in many fruits and vegetables and persist in beverages such as tea [7, 224]. Epigallocatechin gallate (EGCg) found at high concentrations in green tea and is known to cause flocculation of saliva and complexes with salivary proline-rich-proteins [136]. It has been suggested [225] and we have also seen from this work that polyphenols may form aggregates with salivary glycoproteins.

The attachment and spreading kinetics of fibroblast cells onto mucin and modified mucin + EGCg substrates using laser scanning confocal microscopy and OWLS are

investigated. We find that cell attachment and spreading on the mucin substrate is greatly reduced when compared with poly-L-lysine controls whilst mucin + EGCg substrates restore (at least in part) cell spreading.

5.3.3   Experimental results and discussion

Using dynamic light scattering we have found increasing mucin hydrodynamic radius (R_h) with increasing EGCg concentration (Appendix E, Fig E 6). The complex forms a micelle or aggregate most likely in a similar manner to that of proline-rich-protein/polyphenol interactions [136].

The structure of adsorbed glycoprotein films with and without EGCg using optical waveguide lightmode spectroscopy (OWLS) [174, 175] much more aggregated mucin + EGCg adsorbs than mucin alone (Fig. 5. 1, Chapter 5, section 5.2.1.2). For mucin and mucin + EGCg, desorption occurs in two distinct phases, 'fast' and 'slow'. The 'fast' phase disappears before cells are attached and we are only interested in the slow phase. This behaviour signifies a change in the mechanical properties, e.g. viscoelasticity of the layer [226]. It is most likely that EGCg cross-links the mucin, reducing the viscoelasticity of the layer [227]. Note that poly-L-lysine adsorbs irreversibly.

The attachment and spreading kinetics of fibroblasts are investigated using OWLS, a molecular microscopy technique that has been previously been used to measure the attachment and spreading of cells. Behaviour is dramatically different for mucin and mucin + EGCg layers (Fig. 5. 11). The sigmoidal kinetics corresponds to cell spreading [163]. The rate of physico-chemical association and initial spreading on mucin (0 – 10 minutes) is an order of magnitude smaller than that with mucin +

EGCg or with PLL. We can see that mucin sharply inhibits spreading compared with PLL, but the mucin + EGCg layer is practically as good an early spread-promoting substrate as PLL (Fig. 5. 11).
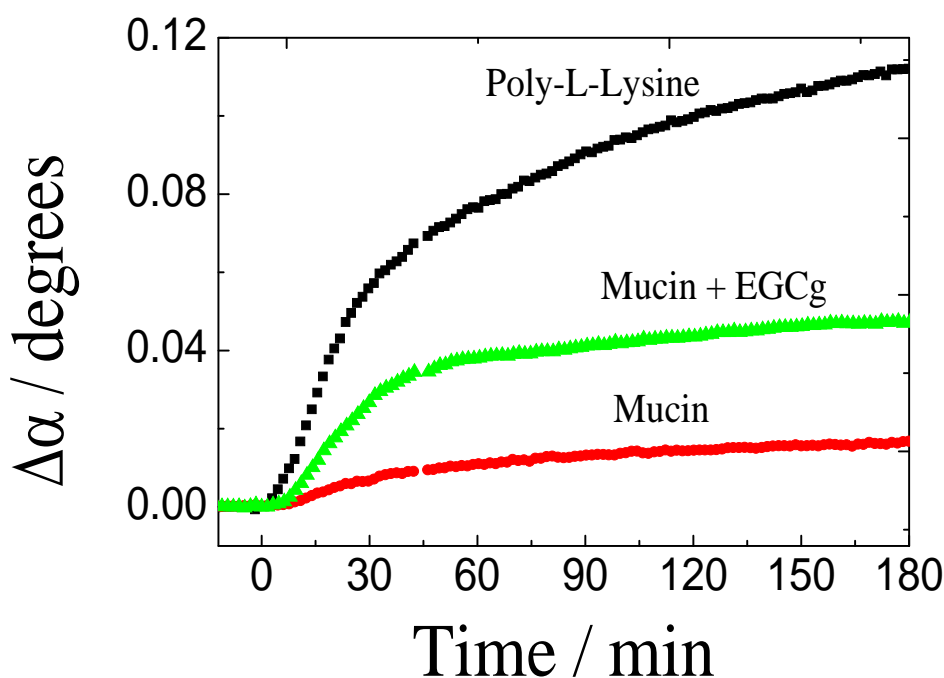
Figure 5.11: Cell-substrata interactions monitored by OWLS (monitored as mean incoupling peak position shift with time). Fibroblasts spread on 0.1% PLL in water (top curve), 0.1% (w/w) mucin in water (lower curve) and 0.1% mucin + 0.1% EGCg in water (middle curve). Cells were added at time 0. 0-10minute data were fitted with linear least square fits yielding (PLL) $1.7x10^{-3} \pm 2x10^{-5}$, (mucin + EGCg) $1.1x10^{-3} \pm 5x10^{-5}$ (mucin) $1.7x10^{-4} \pm 9x10^{-5}$. For the interval 10 -30 minutes values were, (PLL) $2.1x10^{-3} \pm 9x10^{-5}$, (mucin + EGCg) $1x10^{-3} \pm 2x10^{-5}$ and (mucin) $3x10^{-4} \pm 2x10^{-5}$

Confocal microscopy of cells living on identical substrates shows the organelle distribution of the cell (Fig. 5.12). Confirming the OWLS data mucin clearly inhibits spreading compared with PLL, but the inhibition is abolished by the admixture of EGCg and after 60 minutes the cells on mucin + EGCg are virtually indistinguishable from those on PLL. Yet Mucin + EGCg substrata do not lead to long term cell

spreading as after 3 hours mucin and mucin + EGCg both look rather similar (Fig. 5. 11, lower row), and by then   is practically stationary (Fig. 5. 11).
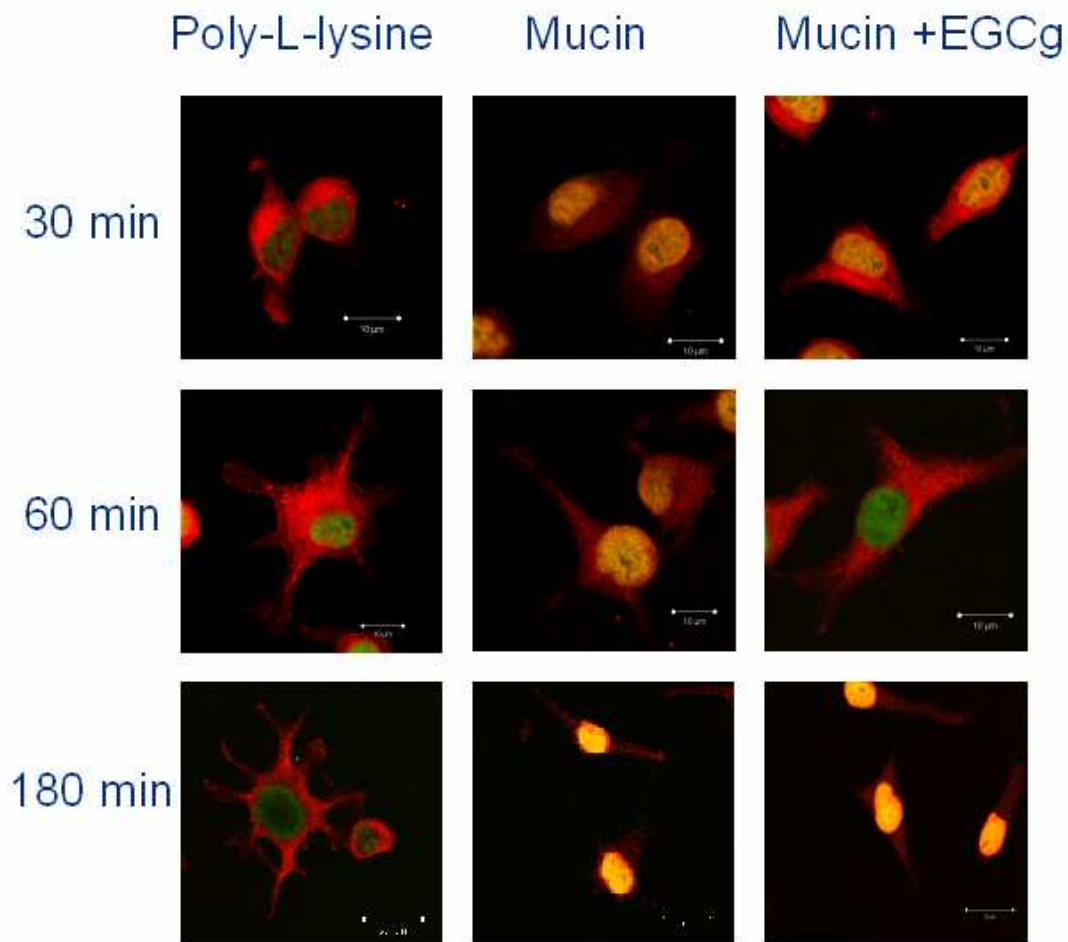
Figure 5.12: Confocal microscopy images of fibroblast cells on poly-L-lysine, mucin and mucin/EGCg substrates after 30, 60 and 180 minutes. Sytox (green) stains the nucleus and Alexa Fluor555A stains mitochondrial biotin, yellow indicates red on green staining. All images x400 magnification with both 30 minute and 60 minute images zoomed (x4.5). White scale bars in the lower right hand corner correspond to 10μm for 30 and 60 minute images and 50μm for 180 minutes. The 180 minute images are not zoomed and show typical overall cell coverage.

130

The possibility of EGCg leaching out of the substrate and leaving the cells on pure mucin was excluded by our failure to detect any free EGCg in the cover medium surrounding the cells using high performance liquid chromatography, with a detection limit of 1μg/ml (carried out at Silsoe campus by Iva Chianella, see Appendix F. 3). OWLS and confocal microscopy data both support the conclusion that spreading is inhibited by mucin as with cellulose coated substrates [221, 223] and the inhibition is initially abolished for the mucin + EGCg aggregate layer.

Analysing the OWLS peak width provides further evidence of the above as the surface coverage, defined as the fraction of substratum covered by cell material (up to 150 nm above the surface for our experimental conditions) is obtained. The resonance peak width increases up to a surface coverage of 50% of randomly placed objects and then decreases as the coverage increases further [177]. The peak width data confirms that the covered area is largest for PLL, less for mucin + EGCg and smallest for mucin (Fig. 5. 13).
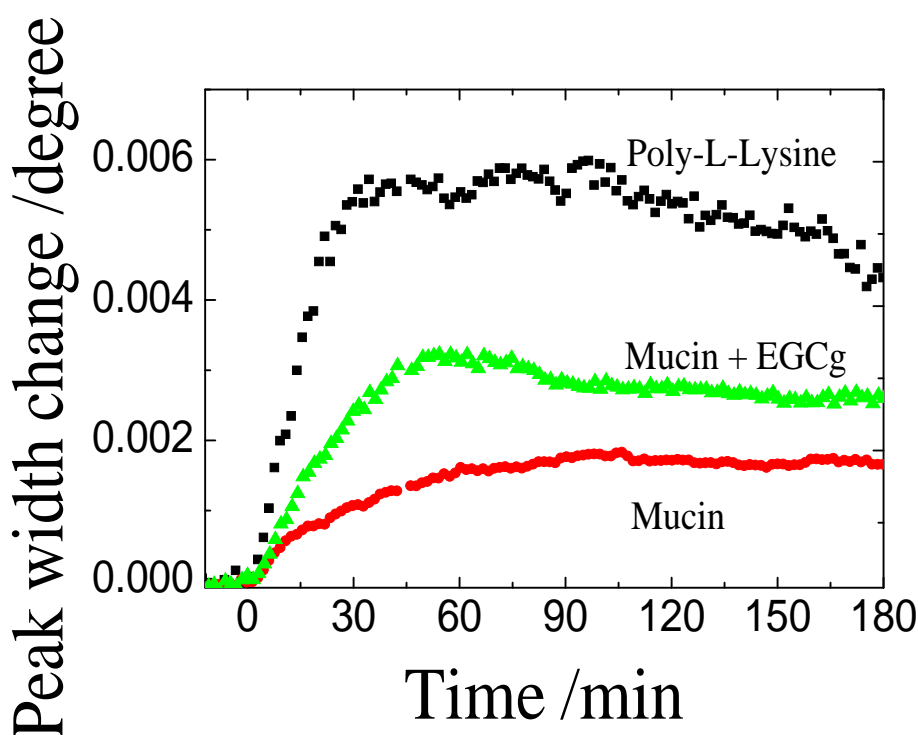
Figure. 5.13: Cell-substrata interactions monitored via OWLS (incoupling peak width). Fibroblasts spread on 0.1% PLL in water (top curve), 0.1% (w/w) mucin in water (lower curve) and 0.1% mucin + 0.1% EGCg in water (middle curve). Cells were added at time 0. Notice that PLL and mucin + EGCg both reach a maximum peak width, which declines beyond 50%, whereas on mucin they never get that far. Linear least square fits to the interval 0-30 minutes gave rates of $2x10^{-4} \pm 8x10^{-6}$ deg/min and $9x10^{-5} \pm 3x10^{-6}$ deg/min for PLL and mucin + EGCg respectively. Mucin alone yields two phase, a fast initial are $(7x10^{-5} \pm 3x10^{-6}$ deg/min) and a subsequent slow are $3x10^{-5} \pm 1x10^{-6}$ deg/min.

For PLL and mucin + EGCg the initial rate of incoupling peak width change increases linearly over the first 30 minutes whereas the mucin substrates exhibit two-phase coverage kinetics, initially fast and then slows (Fig. 5. 13). The incoupling peak position change suggests movement of optically refractive material, either intra-cellular (e.g. the nucleus or cyto-skeletal components) or extra-cellular towards the substratum (Fig. 5. 11) and area covered (Fig. 5. 13) are key factors for long term cell

132

viability. This is clear if one compares   for PLL and mucin + EGCg at 60 minutes (Fig. 5. 11), the 50% coverage point (from Fig. 5. 13). There is a twofold increase in   for PLL, implying more highly optically refractive material is localised close to the surface for this substratum.

5.3.4   Summary

Fibroblast cell attachment and spreading is greatly reduced on mucin coated substrates when compared with PLL and? can be countered by a polyphenol flavonoid, EGCg. Cell attachment and spreading responds to substrate rigidity [228 229] and the flavonoid-induced restoration of cell activity may be due to structural changes in the layer which alter the viscoelastic properties. On the other hand, upon contacting the substrate fibroblasts, and many other cell types will modify it by synthesising and releasing onto the surface proteins required for the extracellular matrix [230]. For mucin substrates the properties of the layer could inhibit mechanoreceptive feedback mechanisms essential for increasing coverage. Also the increase in   for mucin substrates (10-30 minutes) suggests that more material is being localised close to the surface even as the surface coverage stops increasing. It is therefore most likely that the substrate properties are the dominant influence on initial cell spreading.

6.0   Future work

The aim of the final section is to suggest some possible future areas of research and highlight areas that may either reinforce this work or answer any questions which were not addressed. The evidence that mucin adsorbs in a composite layer is strong and using additional techniques to confirm its presence is most likely not necessary. Of interest however would be further investigations into the structure which give further insights into the dynamics of the adsorbed layer. A possibility here is to use modified waveguides capable of exciting additional modes. These should give more information (such as a realistic thickness) and as such would help with the anisotropy conundrum.

Many biological systems which utilise mucin prevail across diverse temperature and salt conditions i.e. fish inhabit both freshwater and marine environments and indeed some will migrate from one to the other. This work has shown that mucin is able to adapt to its environment, with the exception of NaF, maintaining its functional characteristics. An obvious follow on from these experiments is to investigate mucin at different temperatures with different salt concentrations.

An area which we have not investigated at all is heavy metals and their impact on mucin behaviour. In addition to mucosal secretions mucins are also released onto the skin (during perspiration). The presence of heavy metals in many cosmetic products (for example anti-perspirants) suggests that these molecules would be of interest. Indeed if the metals impact on mucin behaviour they may also provide additional structural information, as with the salt experiments.

134

The work with polyphenols could be extended to include other members of the catechin family and indeed many other flavonoids which have therapeutic properties. The timeframe and objectives for this work did not enable extensive experimental investigations into the effect of the complete catechin family.

The surprising recovery of the cell spreading on mucin + EGCg substrates requires further work. We cannot state categorically that EGCg is incorporated into the layer although all the evidence at present suggests it is. It is important to first determine if this is the case. Once clarified, what is it about the mucin + EGCg substrates that the cells prefer? Most likely as mentioned in the text the viscoelasticity changes making the substrate increasingly responsive to the cells. Here it would first be interesting to grow cells on surfaces where the EGCg concentration in solution has been varied. Note here tough that the layer will collapse above a critical EGCg concentration.

Appendix A

Optical waveguide lightmode spectroscopy: principle and fitting (RSA).

A. 1 Reflection, refraction and total internal reflection

When light travels across medium of differing refractive indices (for example F and C) some light will be reflected back and some will be refracted. This is commonly known as Snells law although Harriot had initially discovered it sometime before Snell [] (Fig. A. 1).

$$n_F \sin \theta_F = n_C \sin \theta_C \qquad\qquad (A\ 1)$$

where n_F and n_C are the refractive indices of media F and C respectively where $n_C > n_F$. θ_F is the angles of incidence and θ_C the angle of refraction.

136
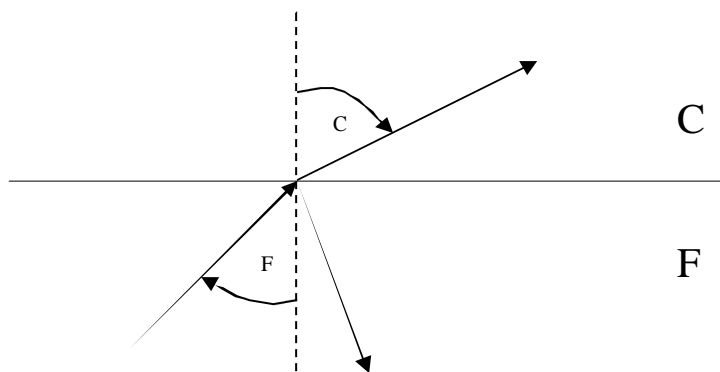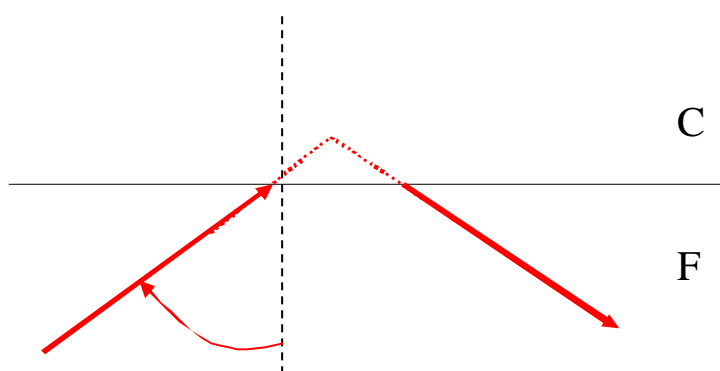
Figure A. 1: Refraction, reflection and total internal reflection. A. Light travelling into media F (dark arrow) will refract into media C and reflect back into media F with the C/F relationship dependent on the angle of incidence $_F$. B. Total internal reflection (red arrow) will occur above a critical incidence angle, here no light is rerfracted. The Goos-Hánchen shift is shown as the dotted red lines.

Above a critical angle ( ), total internal reflection will occur. This only occurs when the light is travelling from a high to low refractive index material. The light confined within two reflecting interfaces will travel as a standing wave between the surfaces and as an evanescent wave beyond (Fig. A. 2). The light penetrates into C before returning to F, resulting in a phase shift, D [170].

137
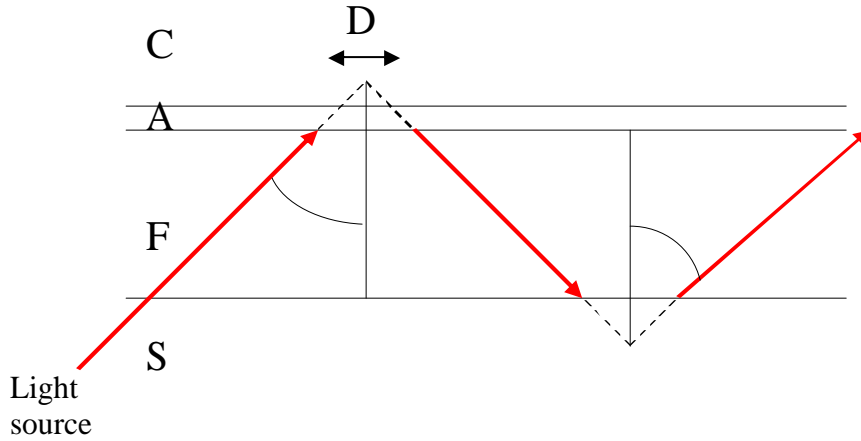
Figure A. 2: Laser light travelling through an optical waveguide. Light is confined within a high refractive index film (F) and will penetrate into the surrounding low refractive index material (S and C). A denotes an adsorbed adlayer, D the phase shift and   the angle of incidence.

A. 2 Waveguide and adlayer parameter calculations

A three layer model is used to calculate the waveguide parameters

$$\pi m = \frac{2\pi}{\lambda}\sqrt{n_F^2 - N^2}\, d_F - \arctan\left[\left(\frac{n_F}{n_S}\right)^{2p}\sqrt{\frac{N^2 - n_S^2}{n_F^2 - N^2}}\right] - \arctan\left[\left(\frac{n_F}{n_C}\right)^{2p}\sqrt{\frac{N^2 - n_C^2}{n_F^2 - N^2}}\right] \text{(A 2)}$$

where

p=1 and N=N_{TM} for TM mode   (A 3)

p=0 and N=N_{TE} for TE mode.

138

where TM is the transverse magnetic component of the propagating light, TE the transverse electric component and p the mode.

Adsorption of material onto the surface will form an adlayer (A, Fig. 15) with the parameters characterised using the four layer mode equation [77, 172]. The refractive index of the adlayer, n_A is calculated using

$$n_A = \left(\frac{\frac{FM(N_{TM})}{A(N_{TM})} - d_F}{\frac{FE(N_{TE})}{A(N_{TE})} - d_F} \left(\frac{1}{n_C^2} + \frac{1}{n_F^2} - \frac{1}{N_{TM}^2} \right) - \frac{1}{n_C^2} + \frac{1}{N_{TM}^2} \right)^{-\frac{1}{2}}$$ (A 4)

and the thickness, d_A calculated using

$$d_A = \left(\frac{FE(N_{TE})}{A(N_{TE})} - d_F \right) \left(\frac{n_F^2 - n_C^2}{n_A^2 - n_C^2} \right)$$ (A 5)

where

$$A(N) = \frac{2\pi}{\lambda} \sqrt{n_F^2 - N^2}$$ (A 6)

$$FM(N) = \arctan\left(\frac{n_F^2}{n_S^2} \sqrt{\frac{N^2 - n_S^2}{n_F^2 - N^2}} \right) + \arctan\left(\frac{n_F^2}{n_C^2} \sqrt{\frac{N^2 - n_C^2}{n_F^2 - N^2}} \right)$$ (A 7)

$$FE(N) = \arctan\left(\sqrt{\frac{N^2 - n_S^2}{n_F^2 - N^2}} \right) + \left(\sqrt{\frac{N^2 - n_C^2}{n_F^2 - N^2}} \right)$$ (A 8)

139

A. 3 Random sequential adsorption

As molecules adsorb onto a surface their shape will impact on the available surface for further adsorption. After a time adsorption will stop as the surface becomes jammed. This is the jamming limit (J) (e.g. a sphere has J ~ 0.547). The available area is at first close to one but as the molecules start to adsorb the surface becomes more occupied and the corrections become increasingly prominent [85]. At a certain point the surface cannot accommodate further adsorption, despite there being space, and the jamming limit is reached [68, 81, 82, 83, 84, 86].

The equation used for fitting is

$$\phi(M,a) = (1 - x^3)/(1 - 0.812x + 0.2336x^2 + 0.0845x^3) \qquad \text{(A 9)}$$

where $x = \dfrac{\theta}{\theta_J}$, θ being related to M by $M = \theta\, m/a$, where m is the mass per molecule, and θ_J is the jamming limit.

Appendix B

Determination of wall shear rate and refractive index increment (dn/dc).

B. 1 Wall shear rate

The diffusion boundary distance ( ) is calculated using [185]

$$\delta = \left(\frac{3}{2}\right)^{2/3} \left(\frac{DC}{F}\right)^{1/3} \qquad \text{(B 1)}$$

where F is the volumetric flow rate, C a constant (dependent on characteristics of the tube) and D the diffusivity calculated using the Stokes Einstein relation

$$D = \frac{k_B T}{4\pi r \eta} \qquad \text{(B 2)}$$

B. 2 Refractive index increment.

The refractive index (R I) increment of mucin in water at 25 $^{\circ}$C, 37 $^{\circ}$C and 60 $^{\circ}$C were determined by plotting R I against bulk concentration (c_b) plots with the slope of the fit equating to the dn/dc [174].
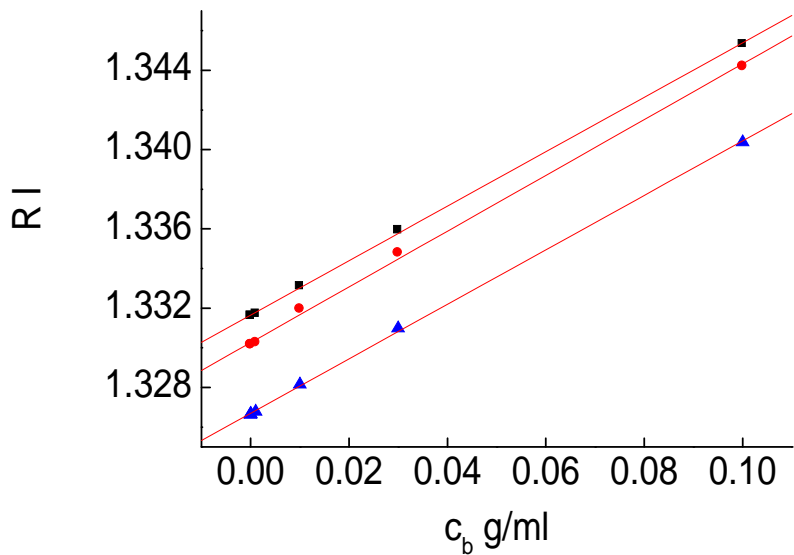
Figure B.1: dn/dc for mucin at 25 ^{o}C (top), 37 ^{o}C (middle) and 60 ^{o}C (bottom) in water.
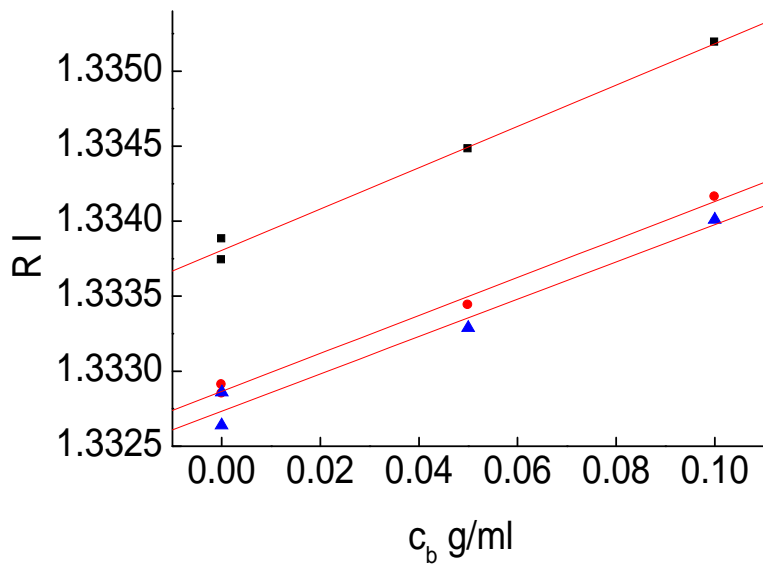
Figure B.2: dn/dc for NaCl (top), NaF (middle) and NaI (bottom).

142
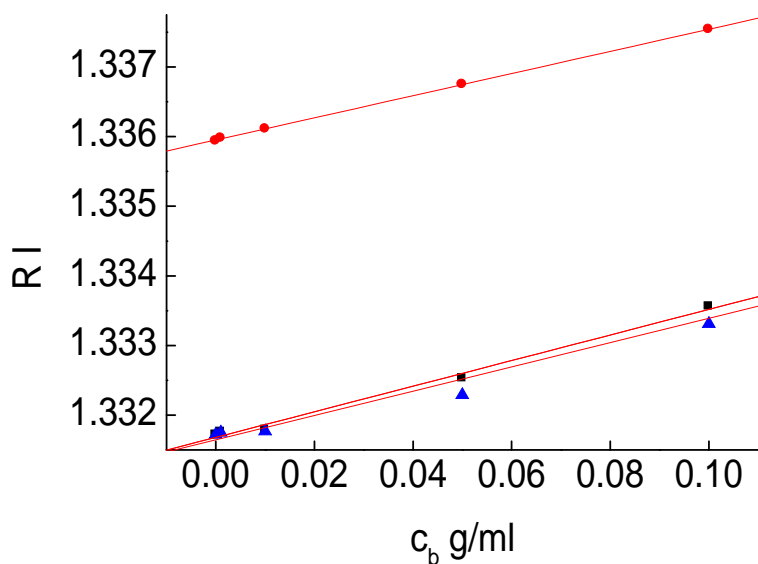
Figure B.3:. dn/dc for 3% w/w mucin + EGCg (top), 0.1% w/w mucin + EGCg (middle) and 0.1% mucin + EC (bottom).

The dn/dc for all solutions are collected in Table B. 1.

Table B.1: dn/dc for all solutions used.

Solvent	T (^{o}C)	dn/dc
Water	25	0.138
Water	37	0.141
Water	60	0.138
0.2M NaCl	25	0.146
0.2M NaF	25	0.128
0.2M NaI	25	0.132
EGCg 0.1% mucin	25	0.184
EGCg 3% mucin	25	0.159
EC	25	0.156

143

Appendix C

Preparation techniques

C. 1 Cell culture

3T3 growth media

Dulbeccos Modified Eagles Medium (DMEM)

10% Foetal Bovine Serum (FBS)

For experiments outside the incubator 3T3 growth medium is supplemented with

hepes Z1 buffer.

Z1 buffer

For 1 litre of Z1 buffer 10mM hepes and 0.688 ml of 6M NaOH were mixed. pH 7.4

MGM growth media

DMEM

10% FBS

0.1% penicillin streptomycin

0.2% glutamine

Cells were supplemented with Z1 buffer for experiments performed outside the

incubator [233].

DMEM recipe

Dulbecco's Modified Eagle Medium (D-MEM) (1X) liquid (high glucose)

Contains GlutaMAX I, 4500 mg/L glucose and 110 mg/L sodium pyruvate.

Catalog Number: 31966021 was used. Recipe is provided below.

COMPONENTS	Molecular Weight	Concentration (mg/L)	Molarity (mM)
Amino Acids			
Glycine	75	30	0.400
L-Alanyl-L-Glutamine	217	862	3.97
L-Arginine hydrochloride	211	84	0.398
L-Cystine 2HCl	313	63	0.201
L-Histidine hydrochloride-H2O	210	42	0.200
L-Isoleucine	131	105	0.802
L-Leucine	131	105	0.802
L-Lysine hydrochloride	183	146	0.798
L-Methionine	149	30	0.201
L-Phenylalanine	165	66	0.400
L-Serine	105	42	0.400
L-Threonine	119	95	0.798
L-Tryptophan	204	16	0.0784
L-Tyrosine	181	72	0.398
L-Valine	117	94	0.803
Vitamins			
Choline chloride	140	4	0.0286
D-Calcium pantothenate	477	4	0.00839
Folic Acid	441	4	0.00907
i-Inositol	180	7.2	0.0400
Niacinamide	122	4	0.0328
Pyridoxine hydrochloride	204	4	0.0196
Riboflavin	376	0.4	0.00106
Thiamine hydrochloride	337	4	0.0119
Inorganic Salts			
Calcium Chloride (CaCl2-2H2O)	147	264	1.80
Ferric Nitrate (Fe(NO3)3"9H2O)	404	0.1	0.000248
Magnesium Sulfate (MgSO4-7H2O)	246	200	0.813
Potassium Chloride (KCl)	75	400	5.33
Sodium Bicarbonate (NaHCO3)	84	3700	44.05
Sodium Chloride (NaCl)	58	6400	110.34
Sodium Phosphate monobasic (NaH2PO4-2H2O)	154	141	0.916
Other Components			
D-Glucose (Dextrose)	180	4500	25.00
Phenol Red	376.4	15	0.0399
Sodium Pyruvate	110	110	1.000

145

C. 2 Waveguide cleaning

Cleaning protocols were established throughout the course of the work. To remove weak (concentrations up to 0.1 % w/w) mucin solutions from the waveguide surfaces Roche was used. The rinse step involves filling the centrifuge tube with fresh water and pouring out.

Roche Protocol

Sonicate in water for 10 minutes at 50 ^{o}C

Rinse

Rinse

Sonicate in Roche 'Cobas Integra' solution for 10 minutes at 50 ^{o}C

Rinse

Rinse

Rinse

Dry with filtered nitrogen

O_2 plasma treated at 20 mW for 2 minutes

For higher concentrations of mucin (up to 3%) Roche was not good enough at removing the extremely well bound layer. A Sodium dodecyl sulphate step was introduced into the protocol.

SDS – Roche Protocol

Sonicate in water for 10 minutes at 50 ^{o}C

Rinse

Rinse

Sonicate in SDS for 10 minutes at 50 ^{o}C

Rinse

Rinse

Rinse

Sonicate in Roche 'Cobas Integra' solution for 10 minutes at 50 ^{o}C

Rinse

Rinse

Rinse

Dry with filtered nitrogen

O$_2$ plasma treated at 20 mW for 2 minutes

At very high mucin concentration (10%) and for mucin + EGCg solutions the layer formed was very stable and chromesulphuric acid was used to clean.

Chromesulphuric acid

Fully submerge in chromesulphuric acid for 3 minutes

Dip in potassium hydroxide (KOH)

Sonicte in water (room temerature) changing water frequently

Dry with filtered nitrogen

O$_2$ plasma treated at 20 mW for 2 minutes

Appendix D

Supporting information: second layer formation

D.1 Atomic force microscopy of mucin layer

Images were obtained using an MFP3DIO instruments (Asylum Research, California) integrated within an inverted optical microscope. NSC36/AL BS (tip radius ~10 nm, resonant frequency f = 140–170 kHz, Micromash, Estonia) silicon tips were used. A drop of 0.1% w/w mucin solution was placed onto the substrate, glass microscope slides pretreated for 2 min in oxygen plasma, and kept for 20 min before rinsing with pure water. The sample was then immersed in 10 mM NaCl for intermittent contact imaging at room temperature.

AFM image shows entangled regime mucin layer. Here the raised areas (coloured blue) are proposed as the second layer which is sitting on the layer adsorbed adjacent the surface.
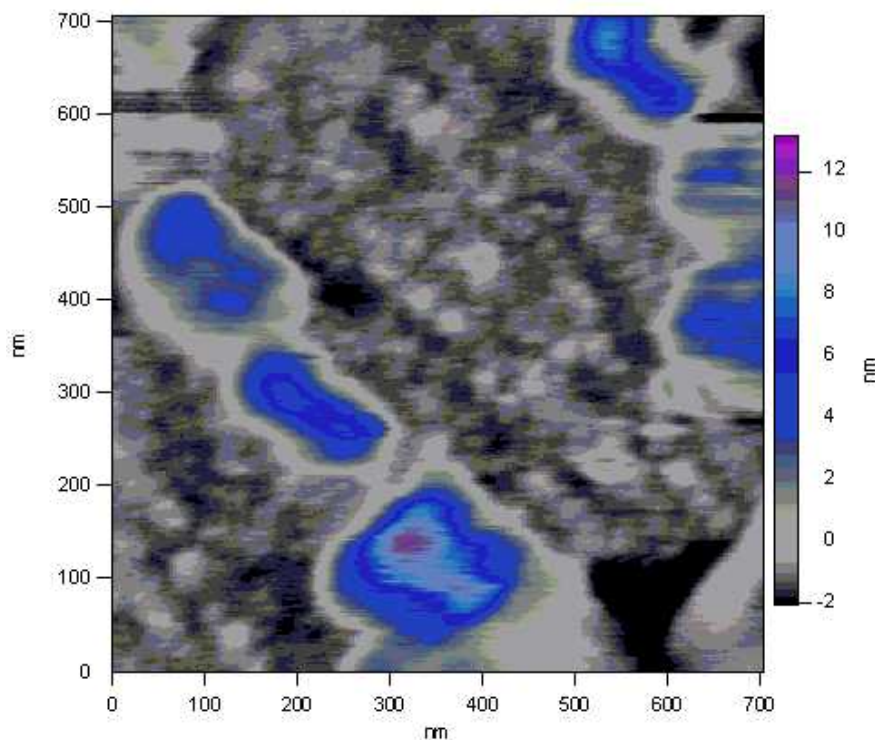
Figure D.1: AFM image of 3% mucin concentration dissolved in water and adsorbed onto mica.

D. 2 Microrheometry

Polystyrene latex particles (radius r = 274 nm) were chosen to be non-interacting with mucin with a size substantially bigger then the mesh size of a semi-dilute mucin solution. The particles were added to solutions of mucin covering the concentration range from 0.01–10 weight % (it is experimentally impracticable to measure the deposition at much lower or much higher bulk concentrations because the solutions become indistinguishable from pure water and extremely viscous respectively) in pure water and the Brownian movement monitored via phase contrast optical microscopy and particle tracking software. The recorded two-dimensional trajectories were converted to mean square displacements and plotted against trajectory duration. The intercept of this graph with the y axis yields the di usion coe cient, from which the

149

viscosity of the solution could be obtained from the Stokes Einstein relation. Speci c viscosity was de ned by the relation $\eta sp = (\eta - \eta water)/\eta water$.
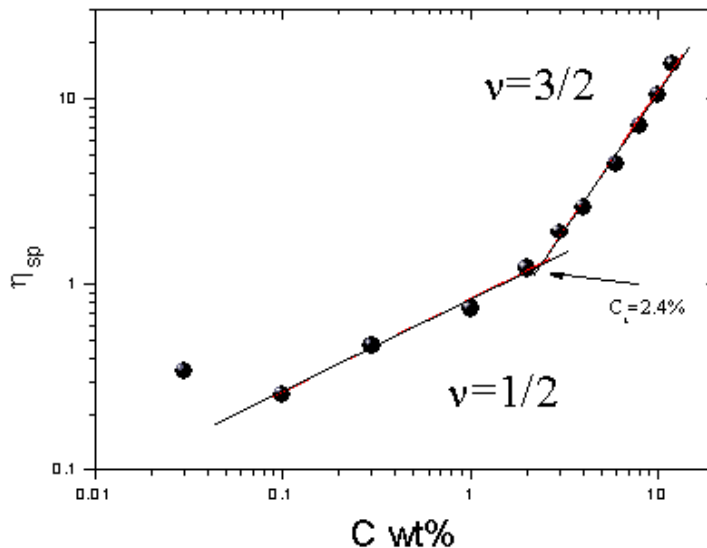
Figure D. 2: Plot of log (speci c viscosity) against log(bulk mucin concentration). Straight lines are least squares ts. The slopes are 1/2 and 3/2.

C. 3. Force distance AFM measurements

Force vs separation curves measured between a hydrophilic glass colloidal probe (radius 14.1 µm) glued to ae rectangular tipless silicon cantilever (Mikromash, Estonia, spring constant k = 0.346 N/m) and a plasma treated glass cover slip surface previously immersed in 0.1% mucin solution (bulk viscosity 0.96 mPa s) in 1 mM NaCl as a background electrolyte. Force curves were obtained using a constant approach load of 93 nN and an approach speed of 360 nm/s to minimise hydrodynamic force [191].

150
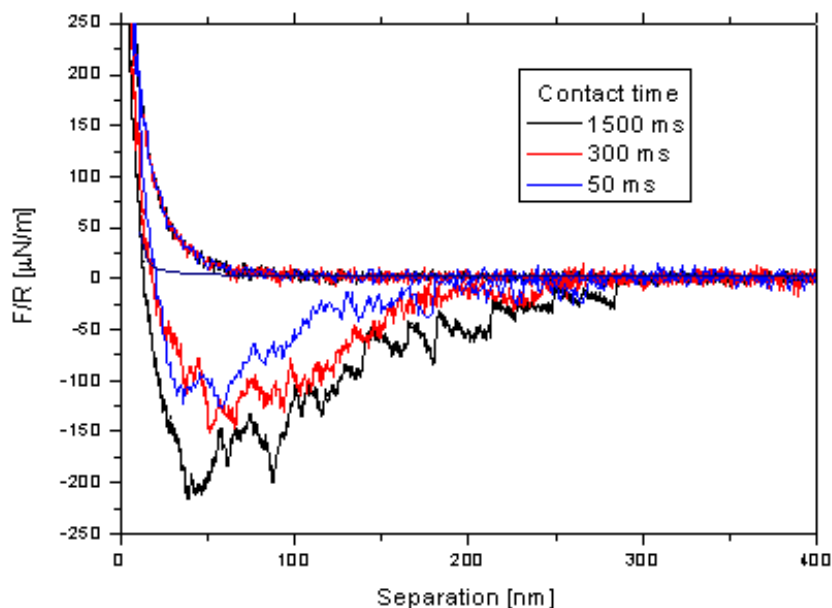
Figure D.3: Typical force vs separation curves were obtained at three di erent contact

dwell times were applied: 1.5 s (black); 300 ms (red); and 50 ms (blue). Upper traces:

extension; lower traces, retraction. The thicker solid line represents the theoretical

contribution from the hydrodynamic force assuming Reynolds squeeze ow with stick

boundary conditions.

Appendix E

Supporting information: layer structure

E. 1 Dynamic light scattering: temperature

Dynamic light scattering (DLS). Measurements to determine the hydrodynamic radius Rh of dissolved mucin were carried out using a PCS 4700 goniometer system (Malvern Instruments, UK) with dedicated software. A laser (wavelength = 488 nm and power = 20.4 mW) was used to ensure consistent incident beam intensity without overheating the sample. Initial measurements were performed for 10 scattering angles between 30 and 120 ^{o}. Measurements were carried out across a temperature range of 12.2–60 C.
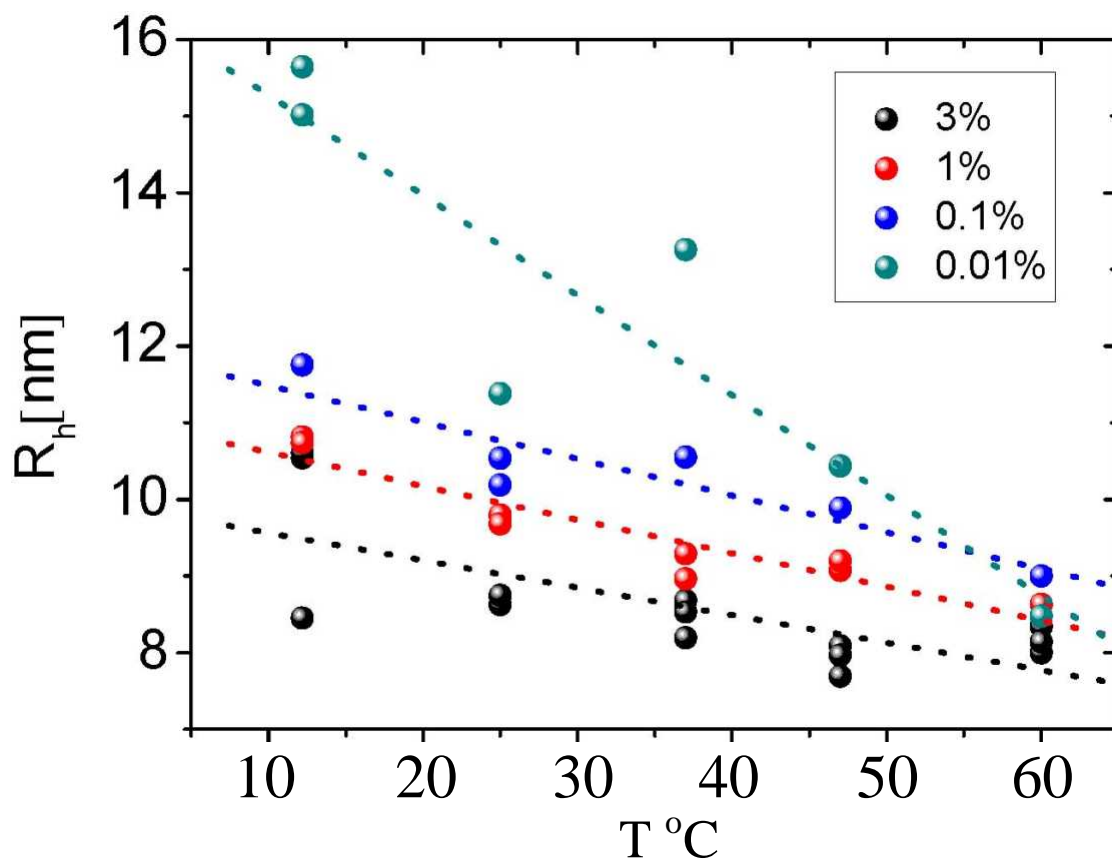
Figure E.1: Concentration – temperature size dependency of mucin in water.

E. 2 Dynamic light scattering: salts

Experimental set up and technique used was the same as that for E. 1. The experimental data is presented in Table E 1. From these measurements two species were determined. Rh small relates to the globule (beads) whilst Rh big relates to the overall molecule size.

Table E. 1: Mucin - salt size relation determined using DLS. Rh small relates to the globules and Rh large the overall molecule dimensions.

	Rh (small)	Rh (big)
NaI	8.4	29.2
NaF	12.9	72.4
NaCl	13.6	115.6
DIW	10.1	34.9

153

Appendix F

Supporting information: function

F. 1 Lubrication

Tribological measurements were made with both mucin and chitosan with 'smooth' and 'rough' tribopair surfaces.

Methods

Preparation of mucin and chitosan solutions

Pharmaceutical grade porcine gastric "Orthana" mucin was purchased from A/S Orthana Kemisk Fabrik (Kastrup, Denmark). "Orthana" mucin is used in a saliva substitute formulation "Saliva Orthana"™ and originates from the linings of pork stomach. The molecular weight of mucin Orthana is 546 kDa and it adopts a daisy chain structural confirmation in the bulk [113]. The commercial preparation was extensively dialysed to remove all salts and other low molecular weight additives and finally lyophilized and stored for use as required. All solutions were made by dissolving weighed portions of the lyophilized material in demineralised water. The sample was shaken for 2 hours and subsequently filtered through a Sartorius "Minisart" filter (200nm pore size). The solutions were used immediately after preparation.

Chitosan (ChitoClear ®, Primex Ingredients ASA, Norway), Acetic acid (99.99+%, Aldrich, UK) and Sodium Chloride (99,98%, Riedel-de-Haen, UK) were used without further purification.

The following solutions were utilised:

1. Mucin aqueous solutions with concentrations in the range between 0.1 mg/ml and 100 mg/ml.

2. Chitosan 0.1, 1.0 and 10 mg/ml aqueous solutions with addition of 0.2M NaCl, and acetic acid to the pH=4.

Water was purified using a commercial water purification system that comprises of two units: SG reverse osmosis pre-cleaning unit and Barnstead NANOpure Diamond equipped with semiconductor-grade ion-exchange resins, ultrafilter (0.2 µm) and UV oxidation chamber. The deionised water had a resistivity 18.2 MOhm.

Tribological measurements using Mini Traction Machine

Tribological measurements were carried out on a Mini Traction Machine (MTM) (PCS Instruments Ltd., UK). This technique has been described in previous studies [234]. Briefly, friction forces between a disk and a loaded ball (applied normal force L) are measured as a function of speed using a force transducer on the ball. Ball and disk are both driven by separate motors so that any slide-to-roll-ratio (SRR) can be adjusted:

$$SRR = \frac{V_{ball} - V_{disk}}{(V_{ball} + V_{disk})/2}.$$

The velocities determine the entrainment speed (U) defined as

155

$$U = (V_{ball} + V_{disk})/2$$

For each entrainment speed the measurements were performed using both conditions $V_{ball} > V_{disk}$ and $V_{ball} < V_{disk}$, thus keeping the SRR constant. The average of the two measurements was taken, enabling evaluation of F_f free from the offset errors in the lateral force measurement and also removing the contribution from the rolling friction. The measured friction force was used to calculate the friction coefficient (μ), defined as

$$\mu = \frac{F_f}{L}$$

In a typical experiment the friction coefficient μ was measured five times for every U, starting at high speed and then step-wise reducing it. The presented data are an average of all measurements. The ball and disk were immersed in the polymer test solution for at least ½h before starting each measurement. Each tribopair was only used for one liquid and then stored. For low polymer concentrations < 1 mg/ml a longer 1h equilibration time was used. As a control of a steady state in polymer adsorption we were monitoring a hysteresis in the Stribeck curves. If hysteresis was less then the scatter of the data we have assumed that steady state was reached, and measurements were qualified.

Surfaces used in tribological measurements

PDMS elastomer (Sylgard ®, silicone elastomer, Dow Corning, MI, US) was used for surfaces with a range of surface properties for tribological measurements. Disks of varying roughness were used, while the roughness of the ball was kept constant. Hydrophilic PDMS surfaces were prepared by treating surfaces with in oxygen plasma for 5-7 min. The properties of the surfaces are listed below:

- Hydrophobic "smooth" surfaces (RMS $= 8.6 \pm 1$ nm, peak-to-valley difference = 300 nm, contact angle ~$100 \pm 10°$).

- Hydrophobic "rough" surfaces (RMS = 382 nm, peak-to-valley difference $= 27$ µm, contact angle ~$100 \pm 10°$).

- Hydrophilic "rough" surfaces (RMS = 382 nm, peak-to-valley $= 27$ µm, contact angle~$40 \pm 15°$).

Results

Stribeck (1902) introduced the velocity dependence of friction in the presence of liquid whereby at high velocities an elastohydrodynamic (EHL) fluid film regime (red shaded area, Fig. E 1) forms that prevents the surfaces from coming into contact and for this regime the fluid hydrodynamics can be described using the Reynolds equation. Conversely boundary lubrication or nanofriction (a lubricating film of less than 100 nm) is characterised at low speeds (non-shaded area, Fig. F. 1) and is the separation of solids at the molecular level whereas the mixed regime (Grey shaded area, Fig. E 1) occurs when the roughness of the surface is comparable with the film thickness at those velocities between the EHL and boundary [151]. For 'smooth

157

hydrophobic surfaces mucin facilitates lubrication in both the boundary and mixed regimes (Fig. F. 1)
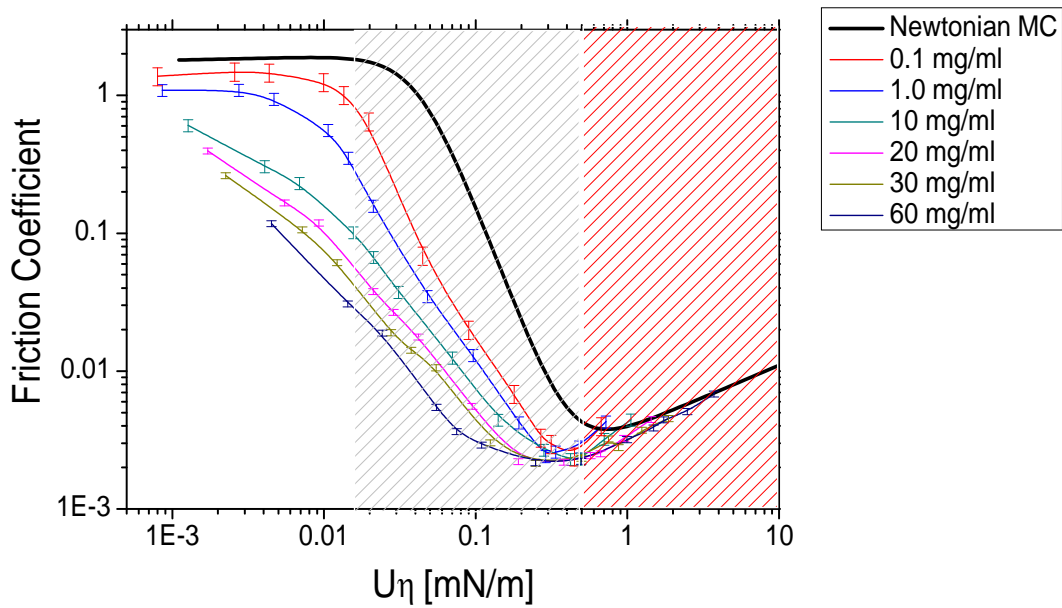
Figure F. 1: Stribeck curves at room temperature for a smooth hydrophobic tribopair (disk r.m.s. roughness ~ 8.6 nm) for various mucin bulk concentrations. The master curve is the solid black line. Non – shaded area denotes boundary regime, grey shaded area mixed regime and red shaded area hydrodynamic regime.

Rough surfaces effectively extend the boundary regime and mucin lubricates in a concentration dependent manner in the boundary regime (Fig. F. 2).
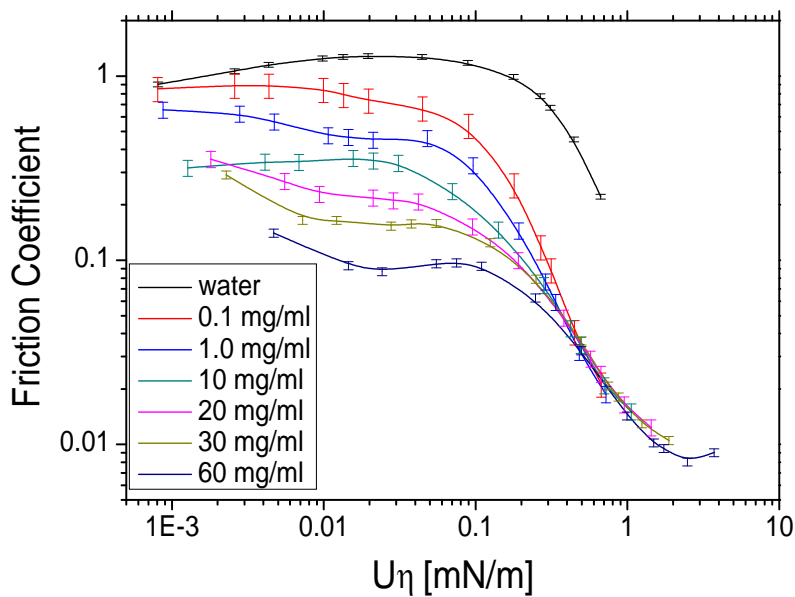
Figure F. 2: Stribeck curves at room temperature for a rough hydrophobic tribopair (disk RMS. roughness ~ 382 nm) for various mucin bulk concentrations. Master curve is the black line.

For rough surfaces rendered hydrophilic it is clear that mucin does not facilitate lubrication as all concentrations collapse onto the master curve (Fig. F. 3).
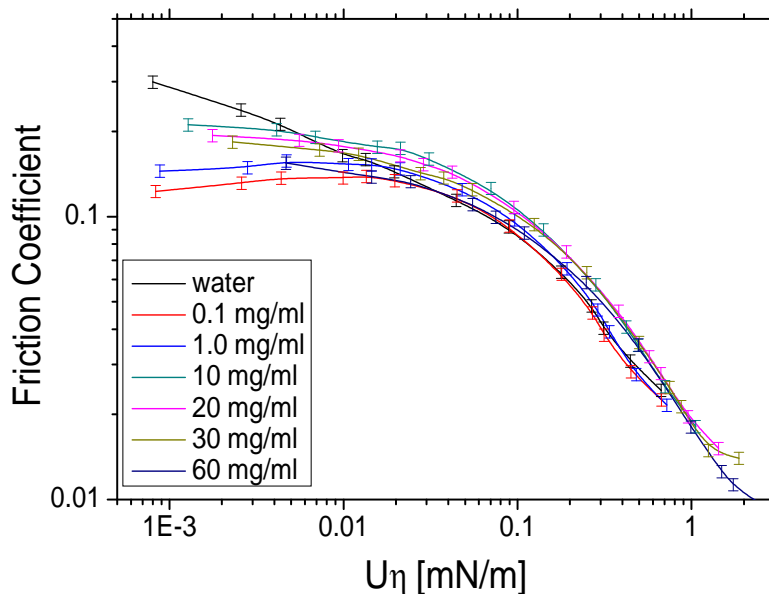
Figure F. 3: Stribeck curves at room temperature for a rough hydrophilic tribopair (disk RMS roughness ~ 382 nm) for various mucin bulk concentrations.

The correlation of saturated mass (Fig. F 4) and time for desorption (Fig. F 5) with friction reduction should give us an insight into which process is the most important for effective mucin lubrication. Total mass adsorbed or the dynamics of the layer?

160
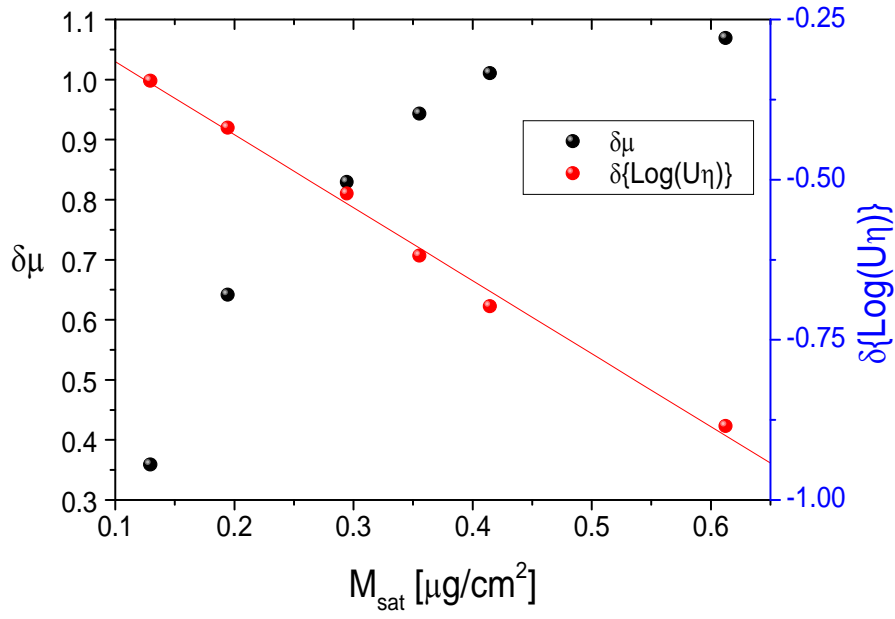
Figure F. 4: Correlation between saturated adsorbed mass and the observed $U\eta$ shift ($\delta\{\log(U\eta)\}$) and boundary friction drop ($\delta\mu_B$).
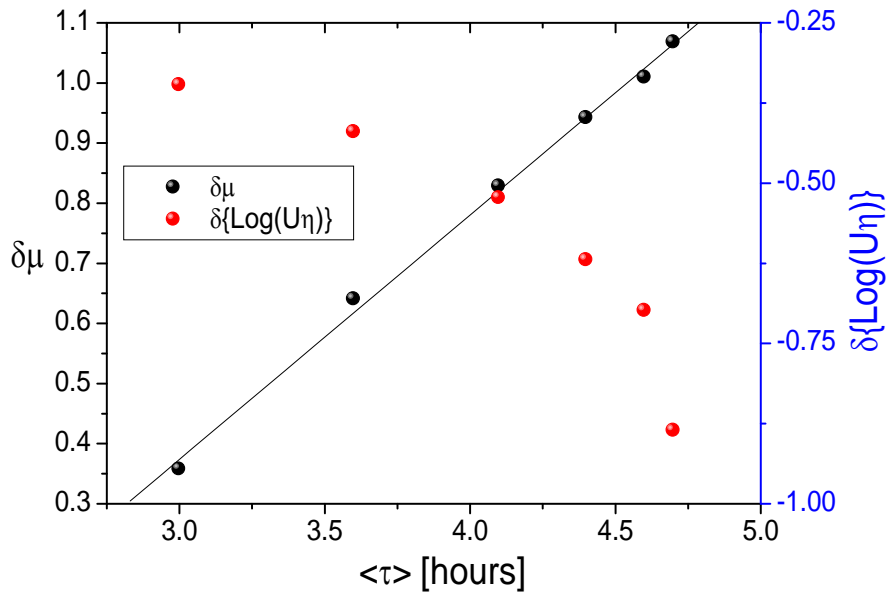
Figure F. 5: Correlation between desorption characteristic time and the observed $U\eta$ shift ($\delta\{\log(U\eta)\}$) and boundary friction drop ($\delta\mu_B$).

F. 2 Astringency

Dynamic light scattering for mucin solutions with varying concentrations of EGCg suggest complexes are formed (Fig. F 6).
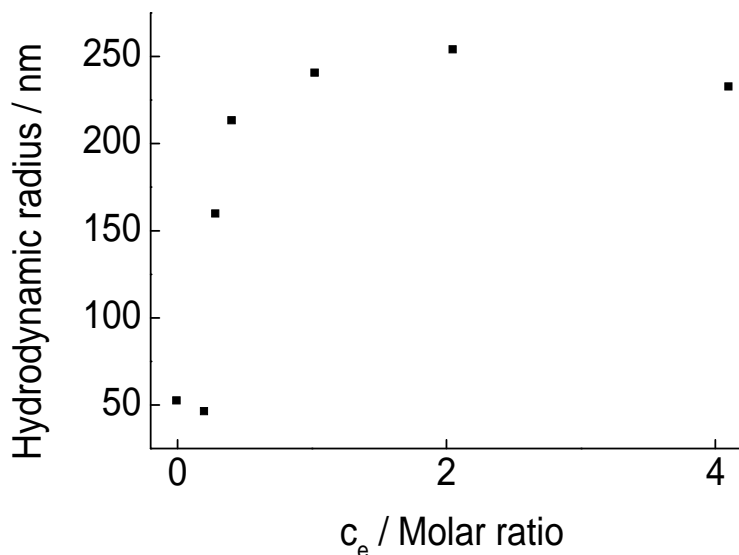
Figure F. 6. Glycoprotein aggregate size-polyphenol concentration relationship. 3% (w/w) mucin solution with varying concentrations (c_e) of EGCg.

F. 3 HPLC determination of free EGCg

Several concentrations (1-0.001 mg/ml) of EGCg in water were used to characterise the peak and build a calibration curve. The detection limit was 1µg EGCg/ml. Cell cover media were injected and tested using the same method as for standard solutions. The mobile phase consisted of AcN/10 mM KH_2PO_4 (20/80, v/v) at pH 4.70 with a flow rate of 0.5 ml/min, injection volume of 10 µl and UV detection at 206 nm [235]. Figure F. 7 shows the retention time for EGCg alone dissolved in water.
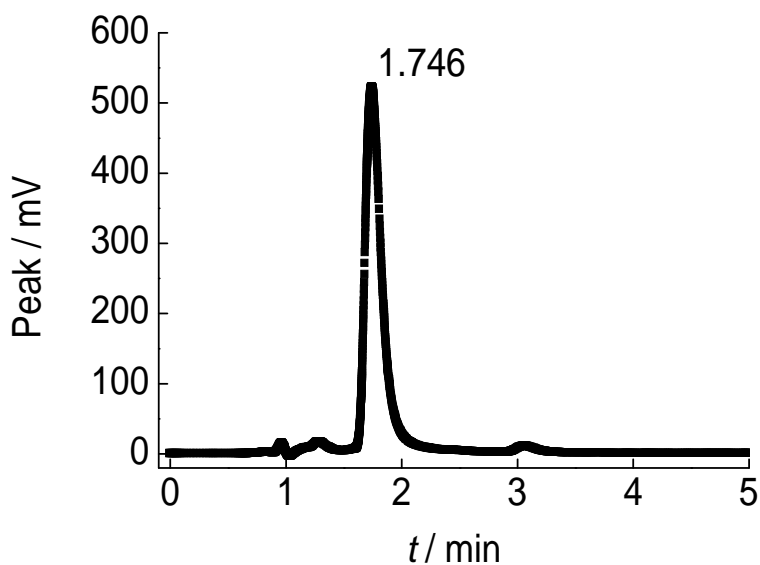
Figure F. 7: EGCg retention time. 1mg/ml stock EGCg solution diluted 1:50.

Free EGCg could not be detected in the surrounding media of cells grown on mucin + EGCg (Fig. F 8), mucin (Fig. F 9) or PLL (Fig. F 10) substrates.
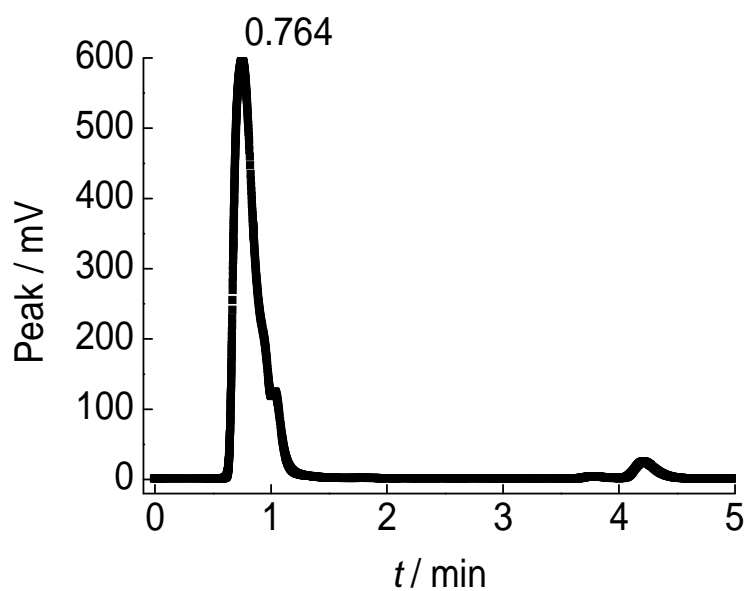
Figure F. 8: Retention time of species in media from cells grown on mucin + EGCg substrates.

163

Note that there is a peak with retention time 0.764 minutes (Fig. E 8). This is most likely the phenol red in the cell culture media. There is no EGCg peak (1.746 minutes).
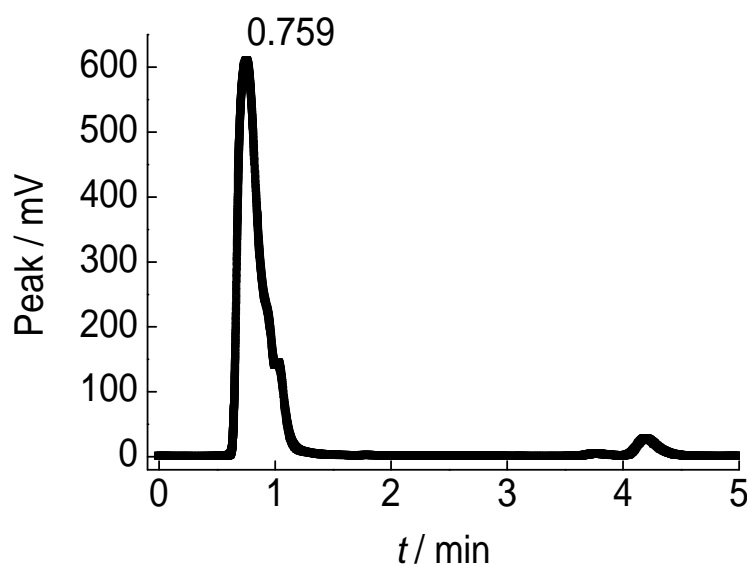
Figure F. 9: Retention time of species in media from cells grown on mucin substrates.
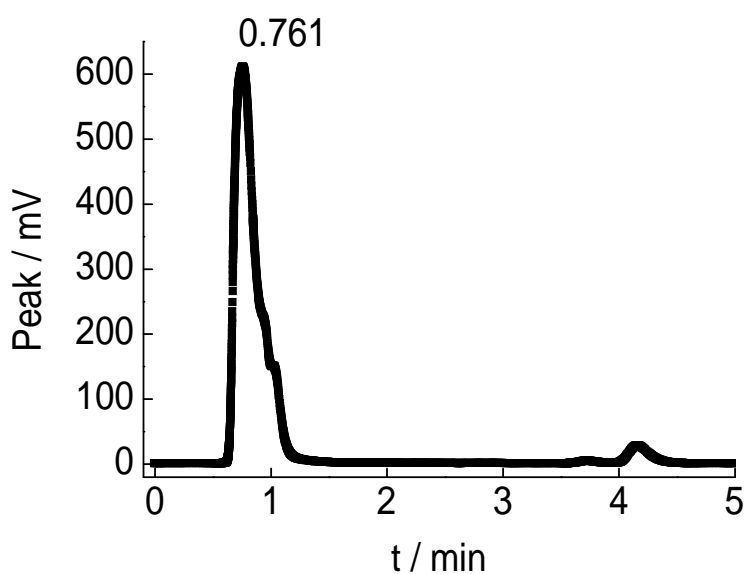
Figure F. 10: Retention time of species in media from cells grown on PLL substrates.

164

Finally as a positive control EGCg was added to the PLL cover solution and run over the column. It is clear that if EGCg were in the solutions taken from the cell experiments it would have been easy to detect (Fig. F11).
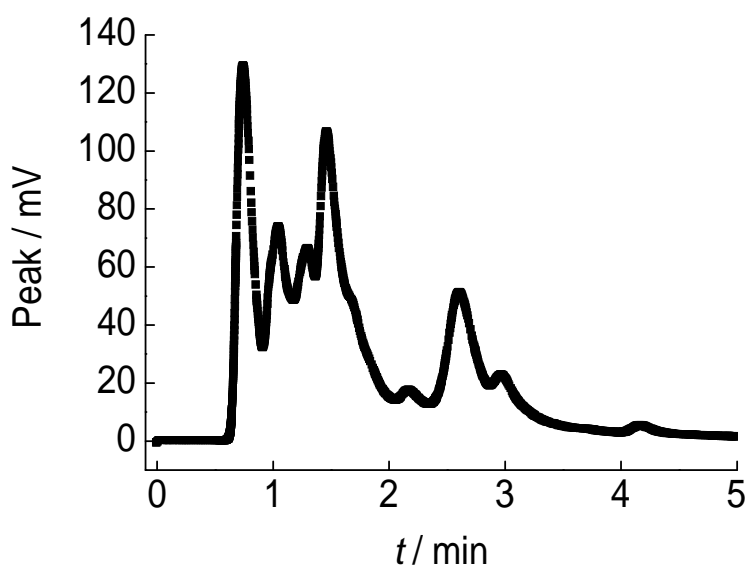
Figure F. 11: Retention time of species in media spiked with 20µl EGCg 1:10 dilution.

References

1. Department of health. (2006). Citing internet resources.

   http://www.dh.gov.uk/PublicationsAndStatistics/ document number 4138630.

   (accessed 15th September 2006)

2. World health organisation. (2006). Citing internet resources.

   http://www.who.dk/obesity (accessed 15th September 2006)

3. Blonz, E. R. You are what you ate: The biosetpoint hypothesis. *Med.*
   Hypotheses. **67** (2006) 270–275.

4. Hamill, O. P. and Martinac, B. Molecular basis of mechanotransduction in
   living cells. *Physiological. Rev.* **81** (2001) 685–740.

5. Green, B. J. Oral astringency: A tactile component of flavour, *Acta.*
   Psychologic. **84** (1993) 119–125.

6. Edwards, C. M. B., Corkery, P. P. and Edwards, A. V., Submandibular
   responses to stimulation of the parasympathetic innervation in anesthetized
   sheep. *J. App. Physiology.* **95** (2003) 1598–1605

7. Kallithraka, S., Bakker, J. and Clifford, M. N. Evidence that salivary proteins
   are involved in astringency. *J. Sensory. Studies.* **13** (1998) 29–44.

8. Valentova, H., Skrovankova, S., Panovska, Z. and Pokorny. Time-intensity studies of astringent taste. *J. Food. Chem.* **78** (2002) 29–37.

9. Lawless, H. T., Corrigan, C. J. and Lee, C. B. Interactions of astringent substances. *Chemical. Senses.* **19** (1994) 141–154.

10. Stratton, R. J. The impact of nutritional support on appetite and food uptake. *Clinical. Nutr.* **20** (2001) 147–152.

11. Warwick, Z. S., Hall, W. G., Pappas, T. N. and Schiffman, S.S. Taste and smell sensations enhance the satiating effect of both a high carbohydrate and high fat meal in humans. *Physiol. Behav.* **53** (1993) 553–563.

12. LeBlanc, J. and Soucy, J. Interactions between postprandial thermogenesis, sensory stimulation of feeding and hunger. *Am. J. Physiol.* **271** (1996) 936–940.

13. Stratton, R. J., Nugent, A., Rutgers, C. and Elia, M. The effect of chewing nutritive and non-nutritive material (modified sham feeding) on subsequent appetite sensations and food intake. *Proc. Nutr. Soc.* **58** (1999) 20.

14. Meyer, E., Overney, R. M., Dransfeld, K. and Gyalog, T. Nanoscience: Friction and rheology on the nanometer scale. World scientific Singapore. (1998) 99–115.

15. Weiss, J., Takhistov, P. and McClements, J. Functional materials in food nanotechnology. *J. Food. Sci.* **7**1 (2006) 107–116.

16. Chen, H., Weiss, J. and Shahidi, F. Nanotechnology in neutraceuticals and functional foods. *Food. Tech.* **60** (2006) 30–36.

17. Dziezak, J. D. Microencapsulation and encapsulated ingredients. *Food. Tech.* **42** (4) 136–151.

18. Schrooyen, P. M. M., van der Meer, R. and De Kruif, C. G. Microencapsulation: its application in nutrition. *Proc. Nutr. Soc.* **60** (2001) 475–479.

19. Birt, D. F. Phytochemicals and cancer prevention form epidemiology to mechanism of action. *J. Am. Dietetic. Assoc.* **106** (2006) 20–21.

20. Fang, J-Y., Lee, W-R., Shen, S-C. and Huang, Y-L. Effects of liposome encapsulation of tea catechins on their accumulation in basal cell carcinomas. *J. Dermatological. Sci*. **42** (2006) 101–109.

21. Yang, C. S., Lambert, J. D., Ju, J., Lu, G. and Sang, S. Tea and cancer prevention: Molecular mechanisms and human relevance. *Toxicol. App. Pharmacology.* (2006) In press.

22. Semo, E., Kesselman, E., Danino, D. and Livney, D. Casein micelle as a natural nano-capsular vehicle for nutraceuticals. *Food. Hydrocolloids*. **21** (2007) 936–942.

23. McClements, D. J. and Decker, E. A. Lipid oxidation in oil-in-water emulsions: impact of molecular environment on chemical reactions in heterogeneous food systems. *J. Food. Sci.* **65** (2000) 1270–1282.

24. Garti, N. and Benichou, A. Recent developments in double emulsions for food applications. In: J Sjoblom, Editor, Encyclopedic handbook of emulsion technology. New York. Marcel Dekker (2001) 377–407.

25. Garti, N. Double emulsions – scope, limitations and ne achievements. *Coll. Surf. A: Physiochemical and engineering aspects.* **123**–**124** (1997) 233–246.

26. Gu, Y. S., Decker, A. E. and McClements, D. J. Production and characterisation of oil-in-water emulsions containing droplets stabilized by multilayer membranes consisting of beta-lactoglobulin, carrageenan and gelatin. *Langmuir*. **21** (2005) 5752–5760.

27. Mun, S., Decker, E. A. and McClements, D. J. Influence of droplet characteristics on the formation of oil-in-water emulsions stabilized by surfactant-chitosan layers. *Langmuir*. **21** (2005) 6228–6234.

28. Decher, G. Fuzzy nanoassemblies: toward layered polymeric multicomposites. *Science*. **277** (1997) 232–237.

29. Lunt, J. Large-scale production, properties and commercial applications of polylactic acid polymers. *Polym. Degrad. Stab*. **59** (1998) 145–152.

30. Riley, T., Govender, T., Stolnik, S., Xiong, C. D., Garnett, M. C., Illum, L. and Davis, S. S. Colloidal stability and drug incorporation aspects of micellar-like PLA-PEG nanoparticles. *Coll. Surf. B*. **16** (1999) 147–159.

31. Mathew, A. P. and Dufresne, A. Morphological investigation of nanocomposites from sorbitol plasticized starch and tunicin whiskers. *Biomacromolecules*. **3** (2002) 609–617.

32. Uyama, H., Kuwabara, M., Tsujimoto, T., Nakano, M., Usuki, A. and Kobayashi, S. Green nanocomposite from renewable sources: plant oil-clay hybrid materials. *Chem. Mater.* **15** (2003) 2492–2494.

33. Park, H. M., Lee, W. K., Park, C. Y., Cho, W. J. and Ha, C. S. Enviromentally friendly polymer hybrids: part I mechanical, thermal and barrier properties of the thermoplastic starch/clay nanocomposites. *J. Mater. Sci.* **38** (2003) 909–915.

34. Risbud, M., Hardikar, A. and Bhonde, R. Growth modulation of fibroblasts by chitosan-polyvinyl pyrrolidone hydrogel: implications for wound management. *J. Biosci*. **25** (2000) 25–31.

35. Juang, R. S. and Shao, H. J. A simplified equilibrium model for sorption of heavy metal ions from aqeuos solutions on chitosan. *Water. Res*. **36** (2002) 2999-3008.

36. Warheit, D. B. What is currently known about the health risks related to carbon nanotube exposure? *Carbon*. **44** (2006) 1064–1069.

37. Graveland-Bikker, J. and de Kruff, C. G. Self-assembly of hydrolysed alpha-lactalbumin into nanotubes. *FEBS. J*. **272** (2005) 550.

38. Graveland-Bikker, J. and de Kruff, C. G. Unique milk protein-based nanotubes: food and nanotechnology meet. *Trends. Food. Sci. Technol.* **17** (2006) 196–203.

39. Graveland-Bikker, J., Schaap, I. A. T., Schmidt, C. F. and de Kruff, C. G. Structural and mechanical study of a self-assembling protein nanotube. *Nano. Lett.* **6** (2006) 616–621.

40. Graveland-Bikker, J., Fritz, G and Glatter, O. Growth and structure of – lactalbumin nanotubes. *J. Appl. Chrystallogr*. **39** (2006) 180–184.

41. Keogh, M. K., O'Kennedy, B. T., Kelly, J., Auty, M. A., Kelly, P. M. and Fureby, A. Stability to oxidation of spray-dried fish oil powder encapsulated using milk ingredients. *Food. Chem. Toxicol*. **66** (2001) 217–224.

42. Denning, M. F. Epidermal keratinocytes: regulation of multiple cell phenotypes by multiple protein kinase C isoforms. *Int. J. Biochem. Cell. Biol.* **36** (2004) 1141–1146.

43. Alonso, L. and Fuchs, E. Stem cells of the skin epithelium. *Colloquium.* **100** (2003) 11830–11835.

44. Webb, A., Li, A. & Pritinder, K. Location and phenotype of human adult keratinocyte stem cells of the skin. *Differentiation.* **72** (2004) 387–395.

45. Green, J. H. *An introduction to human physiology* (4th edition), Oxford University press. (1976) London.

46. Menon, G. K. New insights into skin structure: scratching the surface. *Adv. Drug. Delivery. Rev.* **54** (2002) 3–17.

47. Houssay, B. A. *Human physiology* (2nd edition), McGraw-Hill. (1955) New York.

48. Rhodin, J. and Dalhamn. Electron microscopy of collagen and elastin in lamina propria of the tracheal mucosa of rat. *Exp. Cell. Res.* **9** (1955) 371–375.

172

49. Thomas, C. C. Current concepts of the histology of oral mucosa. *British. J. Oral. Surgery.* **10** (1972–1973) 102–103.

50. Walsh, M. D., Young, J. P., Leggett, B. A., Williams, S. H., Jass, J. R. and McGuckin, M. A. The MUC13 cell surface mucin is highly expressed by human colorectal carcinomas. *Human. Pathology*. **38** (2007) 883–892.

51. Thomson, H. J., Busuttil, A., Eastwood, M. A., Smith, A. N. and Elton, R. A. The submucosa of the human colon. *J. Ultrastructure. Mol. Struc. Res.* **96** (1986) 22–30.

52. Ibanez, C., Shields, S. A., El-Etr, M., Leonelli, E., Magnaghi, V., Li, W-W., Sim, F. J., Baulieu, E-E., Melcangi,R. C., Schumacher, M. and Franklin, R. J. M. Steroids and the reversal of age-associated changes in myelination and remyelination. *Prog. Neurobiol*. **71** (2003) 49–56.

53. Simon, A. M. Gap junctions: more roles and new structural data. *Trends. Cell. Biol.* **9** (1999) 169–170

54. Bell, J., Bolanowski, S. and Holmes, M. H. The structure and function of pacinian corpuscles. *Progr. Neurobiol.* **42** (1994) 79–128.

55. Maeda, T., Ochi, K., Nakakura-Ohshima., Youn, S. H. and Wakisaka, S. The ruffini ending as the primary mechanoreceptor in the periodontal ligament: its

morphology, cytochemical features, regeneration, and development. *Crit. Rev. Oral. Biol. Med*. **10** (1999) 307–327.

56. Boulais, N. and Misery, L. Merkel cells. *J. Am. Acad. dermatology.* **57** (2007) 147–165.

57. Stryer, L. Biochemistry. W. H. Freeman and Company. New York. (1997).

58. Rocco, M., Carson, M., Hantgan, R.R., McDonagh, J. and Hermans, J. Dependence of the shape of the plasma fibronectin molecules on solvent composition. Ionic strength and glycerol content. *J. Biol. Chem*. **258** (1983) 14545–14549.

59. Rocco, M., Infusini, E., Giovanna Daga, M., Gogioso, L. And Cuniberti, C. Models of fibronectin. *EMBO*. **6** (1987) 2343–2349.

60. Cotterill, R. Biophysics: An Introduction. John Wiley & Sons Ltd. Chichester, England. (2002).

61. Horbett, T. A. Principles underlying the role of adsorbed plasma proteinsin blood interactions with foreign material. *Cardiovasc. Pathol.* **2** (1993) 137–148.

62. Brash, J. L. and Horbett, T. A. Proteins at interfaces; an overview, in Proteins at interfaces II; Fundamentals and applications. Horbett, T.A and Brash, J.L, editors. American chemical society. Washington D C. (1995).

63. Haynes, C. A. and Norde, W. Globular proteins at solid/liquid interfaces. *Coll. Surf. B: Biointerfaces*. **2** (1994) 517–566.

64. Ramsden, J.J. Puzzles and paradoxes in protein adsorption. *Chem. Soc. Rev.* **24** (1995) 73–78.

65. Israelachvili, J. Intermolecular and Surface Forces. Academic Press, London. (1992).

66. Norde, W. Adsorption of proteins from solution at the solid/liquid interface. *Adv. Coll. Int. Sci*. **25** (1986) 267–340.

67. Tilton, R. D. Biopolymers at Interfaces, volume 110 of Surfactant Science Series. Marcel Dekker, New York. (2003).

68. Ramsden, J. J. Concentration scaling of protein deposition kinetics. *Phys. Rev. Lett.* **71** (1993) 295–298.

69. Guemouri, L., Ogier, J. and Ramsden, J .J. Optical properties of protein monolayers during assembly. *J. Chem. Phys*. **109** (1998) 3265–3268.

175

70. Guemouri, L., Ogier, J., Zekhnini, Z. and Ramsden, J. J. The architecture of bronectin at surfaces. *J. Chem. Phys*. **113** (2000) 8183–8186.

71. Van Tassel, P. R., Guemouri, L., Ramsden, J. J., Tarjus, G., Viot, P. and Talbot, J. A particlelevel model of irreversible protein adsorption with a postadsorption transition. *J. Coll. Int. Sci*. **207** (1998) 317–323.

72. Malmstem, M. Ellipsometry studies of the effect of surface hydrophobicity on protein adsorption. *Colloids. Surf. B*. **3** (1995) 297–308.

73. Vroman, L. and Adams, A. L. Findings with the recording ellipsometer suggesting rapid exchange of specific plasma proteins at liquid/solid interfaces. *Surf. Sci*. **16** (1969) 438–446.

74. Malmstem, M., Blomberg, E., Claesson, P., Calstedt, I. and Ljusegren, I. Mucin multilayers on hydrophobic surfaces studied with ellipsometry and surface force measurements. *J. Coll. Int. Sci*. **151** (1992) 579–590.

75. Malmstem, M., Claesson, P. and Siegel, G. Forces between proteoheparan sulphate layers adsorbed at hydrophobic surfaces. *Langmuir*. **10** (1994) 1274–1280.

76. Malmstem, M. and Siegel, G. Electrostatic and Ion-binding effects on the adsorption of proteoglycans. *J. Coll. Int. Sci*. **170** (1995) 120–127.

77. Ramsden, J. J. Experimental methods for investigating protein adsorption kinetics at surfaces. *Quart. Rev. Biophys.* **27** (1995) 41–105.

78. Schaaf, P., Voegel, J-C and Senger, B. Irreversible deposition/adsorption processes on solid surfaces. *Ann. De. Phys*. **23** (1998) 1–89.

79. Ward, A. F. H. and Tordai, L. Time-dependence of boundary tensions of solutions I. The role of diffusion in time-effects. *J. Chem. Phys.* **14** (1946) 453.

80. Langmuir, I. The adsorption of gases on plane surfaces of glass, mica and platinum. *J. Am. Chem. Soc*. **40** (1918) 1361–1403.

81. Evans, J. W. Random and cooperative sequential adsorption. *Rev. Mod. Phys*. **65** (1993) 1281–1329.

82. Swendsen, R. H. Dynamics of random sequential adsorption. *Phys. Rev. A*. **24** (1981) 504–508.

83. Ramsden, J. J., Bachmanova, G. I. and Archakov, A. I. Kinetic evidence for protein clustering at a surface. *Phys. Rev. E.* **50** (1994) 5072–5076.

84. P. Lavalle, G., Gergely, A., Lustig, and V. Ball. Critical analysis of the apoferritin adsorption at solid-liquid interfaces in the framework of a particular adsorption model. *J. Chem. Phys*. **113** (2000) 8212–8224.

85. Ricci, S. M., Talbot, J., Tarjus, G. and Viot, P. Random sequential adsorption of anisotropic particles. II. Low coverage kinetics. *J. Chem. Phys*. **97** (1992) 5219–5228.

86. Schaaf, P. and Talbot, J. Surface exclusion effects in adsorption processes. *J. Chem. Phys*. **91** (1989) 4401–4409.

87. Feder, J. and Giaever. Adsorption of ferritin. *J. Coll. Int. Sci.* **78** (1980) 144–154.

88. Ramsden, J.J. Kinetics of protein adsorption. In biopolymers at interfaces. Dekker, New York. (1998) 321– 361.

89. Van der Plancken, L., van Loey, A and Hendrickx, M. E. Effect of heat-treatment on the physico-chemical properties of egg white proteins: A kinetic study. *J. Food. Eng*. **75** (2006) 316–326.

90. Szabelski, P., Cavazzini, A., Kaczmarski, K., Liu, X., Van Horn, J. and Guiochon, G. Experimental studies of pressure/temperature dependence of protein adsorption equilibrium in reversed-phase high-performance liquid chromatography. *J. Chromatogr. A*. **950** (2002) 41–53.

91. Kondo, A. and Urabe, T. Temperature dependence of activity and conformational changes in alpha-amylases with different thermostability upon adsorption of ultrafine silica particles. *J. Coll. Int. Sci*. **174** (1995) 191–198.

92. Urry, D. Physical chemistry of biological free energy transduction as demonstrated by elastic protein-based polymers. *Phys. Chem. B.* **101** (1997) 11007–11028.

93. Debelle, L., and Alix, A. The structures of elastins and their function. *Biochimie*. **81** (1999) 981–994.

94. Urry, D., Hugel, T. Seitz, M. Gaub, H. Sheiba, L. Dea, J. Xu, J. and Parker, T. Elastin: a representative ideal protein elastomer. *Phil. Trans. R. Soc. Lond. B.* **357** (2002)169–184.

95. Tsai, A. M., Udovic, T. J. and Neumann, D. A. The inverse relationship between protein dynamics and thermal stability. *Biophysical. J*. **81** (2001) 2339–2343.

96. Gehring, W.J. and Wehner, R. Heat shock protein synthesis and thermal tolerance in Cataglyphis, an ant from the sahara desert. *Proc. Natl. Acad. Sci*. **92** (1995) 2994–2998.

97. Pugh, L.G., Corbett, J.L. and Johnson, R.H. Rectal temperatures, weight losses and sweat rates in marathon running. *J. Appl. Physiol.* **23** (1976) 347–352.

98. Maron, B., Wagner, J.A. and Horvath, S.M. Thermoregulatory responses during competitive marathon running. *J. Appl. Physiol.* **42** (1977) 909–914.

99. Buckberg, G.D. Update on current techiques of myocardial protection. *Ann. Thorac. Surg.* **60** (1995) 805–814.

100. Averbukh, I.Sh., Blumenfeld, L.A., Kovarsky, V.A., and Perelman, N.F. A model of the mechanism of enzyme action in terms of protein conformational relaxation. *Biochimic. Biophys. Acta.* **873** (1986) 290–296.

101. Alben, J.O., Beece, D., Bowne, S.F., Doster, W., Eisenstein, L., Frauenfelder, H., Good, D., McDonald, J.D., Marden, M.C., Moh, P.P., Reinisch, L., Reynolds, A.H., Shyamsunder, E, and Yue, K.T. Infrared spectroscopy of photodissociated carboxymyoglobin at low temperatures. *Proc. Natl. Acad. Sci*. **79** (1982) 3744–3748.

102. Schaaf, P., Dejardin, P., Johner, A. and Schmitt, A. Thermal denaturation of an adsorbed fibrinogen layer studied by reflectometry. *Langmuir*. **3** (1987) 1128–1131.

103. Elofsson, U. M., Paulsson, M. A., Sellers, P. and Arnebrant, T. Adsorption during heat treatment related to the thermal unfolding/aggregation of -lactoglobulins A and B. *J. Coll. Int. Sci.* **183** (1996) 408–412.

180

104.   Arnebrant, T., Barton, K. and Nylander, T. Adsorption of -lactoalbumin and -lactoglobulin on metal surfaces versus temperature. *J. Coll. Int. Sci.* **174** (1995) 10–

105.   Debye, P. and Huckel, E. 'The theory of electrolytes. I. lowering of freezing point and related phenomena'. *Physikalische Zeitschrift.* **24** (1923) 185–206.

106.   Vig, I. and Agram, I. The effect of salts on the oxygen affinity of haemoglobin. *FEBS Lett.* **90** (1978) 247–249.

107.   Collins, K. D. and Washabaugh, M. W. The Hofmeister effect and the behaviour of water at interfaces. *Q. Rev. Biophys.* **18** (1985) 323–422.

108.   Cacace, M. G, Landau, E. M. and Ramsden, J. J. The Hofmeister series: salt and solvent effects on interfacial phenomena. *Q. Rev. Biophys.* **30** (1997) 241–277.

109.   Dér, A., Kelemen, L., Fábián, L., Taneva, S. G., Fodor, E., Páli, T., Cupane, A., Cacace, M. G. and Ramsden, J. J. Interfacial water structure controls protein conformation. *J. Phys. Chem. B*. **111** (2007) 5344–5350.

110.   Kamiyama, Y. and Israelachvili. J. Effect of pH and salt on the adsorption and interactions of an amphoteric polyelectrolyte. *Macromol.* **25** (1992) 5081–5088.

111.   Dobrynin, A. V, Colby, R. H and Rubenstein, M. Polyampholytes. *J. Poly. Sci: Part B: Polymer physics*. **42** (2004) 3513–3538.

112.   Dobrynin, A. V., Rubenstein, M. and Obukhov, S. P. Cascade transition of polyelectrolytes in poor solvents. *Macromol*. **29** (1996) 2974–2979.

113.   Yakubov, G. E., Papagiannopoulos, A., Rat, E., Easton, R. L. and Waigh, T. A. Molecular structure and rheological properties of short-side-chain heavily glycosylated porcine stomach mucin. *Biomacromolecules*. (2007) In press.

114.   Boris, D. C. and Colby R. H. Rheology of sulfonated polystyrene solutions. *Macromol.* **31** (1998) 5746–5755.

115.   Dobrynin, A. V., Rubenstein, M. and Joanny, J. F. Adsorption of a polyampholyte chain on a charged surface. *Macromol*. **30** (1997) 4332–4341.

116.   Khan, M. O., Akesson, T. and Jonsson, B. Simple approach to polyampholytes based on chain polarizabilities. *J. Chem. Phys.* **116** (2002) 3917–3924.

117.   Katchlasky, A. and Miller, I.R. Polyampholytes. *J. Polym. Sci.* **13** (1954) 57–68.

118.   English, A. E., Mafe, S., Manzanares, J. A., Yu, X., Grosberg, A. Y. and Tanaka, T. J. Equillibrium swelling properties of polyampholytic hydrogels. *J. Chem. Phys.* **104** (1996) 8713–8720.

119.   McCormick, C. L. and Salazar, L. C. Water soluble copolymers: 44. Ampholytic terpolymers of acrylamide with sodium 2-acrylamido-2-methylpropaesulphonate and 2-acrylamido-2-methylpropanetrimethyl-ammonium chloride. *Polymer*. **33** (1992) 4384–4387.

120.   Roussel, Ph. and Delmotte, Ph. The diversity of epithelial secreted mucins. *Curr. Organic. Chem.* **8** (2004) 413–437.

121.   Perez-Vilar, J. and Hill, R. L. The structure and assembly of secreted mucins. *J. Biol. Chem*. **274** (1999) 31751–31754.

122.   Bansil, R., Stanlet, E and LaMont, J. T. Mucin biophysics. *A. Rev. Physiol.* **57** (1995) 635–657.

123.   Lee, S., Mueller, M., Rezwan, K. and Spencer, N. D. Porcine gastric mucin (PGM) at the water/poly(dimethylsiloxane) (PDMS) interface: in uence of pH and ionic strength on its conformation, adsorption and aqueous lubrication properties. *Langmuir*. **21** (18) 8344–8353.

124.   Proctor, G. B. and Carpenter, G. H. The function of salivary proteins and the regulation of their secretion by salivary glands. *Biomed. Rev.* **9** (1998) 3–5.

125. Berg, C. H., Rutland, M. W. And Arnebrant, T. Lubricating properties of the initial salivary pellicle-an AFM study. *Biofouling.* **19** (2003) 365–369.

126. Berg, C. H, Lindh, L. and Arnebrant, T. Intraoral lubrication of PRP-1, statherin and mucin as studied by AFM. *Biofouling*. **20** (2004) 63–165.

127. Levine, M. J., Aguire, A., Hatton, M. N. and Tabak, L. A. Artificial slivas: present and future. *J. Dent. Res.* **66** (1987) 693–698.

128. Hatton, M. N., Levine, M. J., Margarone, J. E. and Aguire, A. Lubrication and viscosity features of human saliva and commercially available saliva substitutes. *J. Oral. Maxillofac. Surg.* **45** (1987) 496–499.

129. Turrsi, C. P., Faraoni, J. J., Menezes, M. And Serra, M. C. Analysis of potential lubricants for in vitro wear testing. *Dent. Mater.* **22** (2002) 77–83.

130. Chrissterson, C. E., Lindh, L. and Arnebrant, T. Film-forming properties and viscosities of saliva substitutes and human whole saliva. *Eur. J. Oral. Sci.* **108** (2000) 418–425.

131. Moniaux, N., Andrianifahanana, M., Brand, R. E. and Batra, S. K. Multiple roles of mucins in pancreatic cancer, a lethal and challenging malignancy. *Brit. J. Cancer*. **91** (2004) 1633–1638.

132.   Wesseling, J., van der Valk, S. W. and Hilkens, J. A mechanism for inhibition of E cadherin mediated cell cell adhesion by the membrane - associated mucin episialin/MUC1. *Mol. Biol. Cell.* **7** (1996) 565–577.

133.   Komatsu, M., Tatum., L., Altman, N. H., Carraway, C. A. and Carraway, K. L. Potentiation of metastasis by cell surface sialomucin complex (rat Muc4), a multifunctional anti-adhesive protein. *Int. J. Cancer*. **87** (2000) 480–486.

134.   Bennick, A. *Crit. Rev. Oral Biol. Med*. Interaction of plant polyphenols with salivary proteins. **13** (2002) 184–196.

135.   Ozawa, T., Lilley, T. H. and Haslam, E. Polyphenol interactions: astringency and the loss of astringency in ripening fruit. *Phytochemistry*. **26** (1987) 2937–2942.

136.   Jobstl, E., O'Connell, J., Fairclough, J. P. A., Williamson, M. P., Molecular Model for Astringency Produced by Polyphenol/Protein Interactions. *Biomacromolecules.* **5** (2004) 942–949.

137.   Khanvilkar, K, Donovan, M. D. and Flanagan D. R. Drug transfer through mucus. *Adv. Drug. Del. Rev.* **48** (2001) 173–193.

138.   Donaldson, M.S. Nutrition and cancer: a review of the evidence for an anti-cancer diet. *Nutr. J.* **3** (2004) 1–21.

139.   Ahmad, N., Feyes, D. K., Meiminen, A. L., Agarwal, R. and Mukhtar, H. Green tea constituent epigallocatechingallate-3-gallate and induction of apoptosis and cell cycle arrest in human carcinoma cells. *J. Natl. Cancer Inst.* **89** (1997) 1881–1886.

140.   Yang, G. Y., Liao, J., Kim, K., Yurkow, E. J. and Yang C. S. Inhibition of tumor promoter-induced activator protein-1 activation and cell transformation by tea polyphenols, (-)-epigallocatechin gallate and the flavins. *Cancer Res.* **57** (1997) 4414–4419.

141.   Yang, C. S. and Wang, Z. Y. Tea and cancer. *J. Natl. Cancer Inst.* **85** (1997) 1038–1049.

142.   Kauffman, D. L. and Keller, P. The basic proline-rich proteins in human parotid saliva from a single subject. *J. Arch. Oral Biol.* **24** (1979) 249–256.

143.   Proctor, G.B. and Carpenter, G.H. The function of salivary proteins and the regulation of their secretion by salivary glands. *Biomed. Rev.* **9** (1998) 3–15.

144.   Charlton, A. J., Baxter, N. J., Khan, M. L., Moir, A. J. G., Haslam, E., Davies, A. P. and Williamson, M. P. Polyphenol/peptide binding and precipitation. *J. Agric. Food Chem.* **50** (2002) 1593–1601.

145.   Charlton, A. J., Haslam, E. and Williamson, M. P. J. Multiple conformations of the proline-rich protein/epigallocatechin gallate complex determined by time-averaged nuclear overhauser effects. *J. Am. Chem. Soc*. **124** (2002) 9899–9905.

146.   Murray, N. J., Williamson, M. P., Lilley, T. H. and Haslam, E. Study of the interaction between salivary praline-rich proteins and a polyphenol by ^{1}H-NMR spectroscopy. *Eur. J. Biochem*. **219** (1994) 923–935.

147.   Asquith, T. N., Uhlig, J., Mehansho, H., Putman, L., Carlson, D. M. and Butler L. Binding of condensed tannins to salivary proline-rich glycoproteins: the role of carbohydrate. *J. Agric. Food Chem*. **35** (1987) 331–334.

148.   Davies, A. N. The management of xerostomia: a review. *Eur. J. Cancer Care*. **6** (1997) 209–214.

149.   Coulomb, C. A. Théorie des machines simples, en ayant égard au frottement de leurs parties, et á la roideur des cordages. *Mém. Math. Phys.* **161** (1785).

150.   Morin, A. J. New friction experiments carried out at Metz in 1831-1833. *Proc. French. Roy. Acad. Sci.* **4** (1833) 1–128.

151.   Stribeck, R. Die wesentlichen eigenschaften der gleit und rollenlager. *Z. Ver. Dt. Ing.* **46** (1902) 1341–1348, 1432–1438 and **39** 1463–1470.

152.   Klein, J. Raviv, U. Perkin, S. Kampf, N. Chai, L. and Giasson, S. Fluidity of water and of hydrated ions confined between solid surfaces to molecularly thin films. *J. Phys. Cond. Matt.* **16** (2004) 5437–5448.

153.   Klein, J., Kumacheva, E., Mahalu, D., Perahia, D. and Fetters, L. Reduction of frictional forces between solid surfaces bearing polymer brushes. *Nature.* **370** (1994) 634–636.

154.   Grest, G. S. Normal and shear forces between polymer brushes. *Adv. Polym. Sci.* **138** (1999) 149–182.

155.   Kilbey, S. M. II., Schorr, P. A. and Tirrell, M. In Dynamics of small confining systems IV. Materials Research Society, Pittsburg, PA. (1999) 181–187.

156.   McCutchen, C. Cartilage is porolastic not viscoelastic. *J. Biomechanics.* **15** (1982) 325–327.

157.   Pritinder, K. and Li, A. Adhesive properties of human basal epidermal cells: An analysis of keratinocyte stem cells, transit amplifying cells and postmitotic differentiating cells. *J. Inv. Dermatology.* **114** (2000) 413–420.

158.   Folkman, J. and Moscona, A. Role of cell shape in growth control. *Nature.* 273 (1978) 345–349.

159.   Pennisi, E. How a growth control pathway takes a wrong turn to cancer. *Science*. **281** (1998) 1439–1441.

160.   Kurrat, R., Ramsden, J.J. and Presonil, J.E. Kinetic model for serum albumin adsorption: experimental verification. *J. Chem. Soc. Faraday. Trans.* **90** (1994) 587–590.

161.   Kurrat, R., Presonil, J. E. and Ramsden, J. J. Kinetics of human and bovine serum albumin adsorption at silica-titania surfaces. *J. Coll. Int. Sci.* **185** (1997) 1–8.

162.   Ramsden, J. J. Dynamics of protein adsorption at the solid/liquid interface. *Recent. Res. Dev. Phys. Chem.* **1** (1997) 133–142.

163.   Li, S-Y., Ramsden, J. J., Prenosil, J. E., and Heinzle, E. Measurement of adhesion and spreading kinetics of baby hamster kidney and hybridoma cells using an integrated optical method. *Biotechnol. Prog*. **10** 520–524 (1994).

164.   Ramsden, J. J. Optical method for measurement of number and shape of attached cells in real time. *Cytometry*. **19** (1995) 97–102.

165.   Griffith, L. G. and Lopina, S. Microdistribution of substratum PEO-tethered galactose. *Biomaterials*. **19** (1998) 979–986.

166.   Gryte, D. M., Ward, M. D. and Hu, W-S. Real-time measurement of anchorage-dependent cell adhesion using a quartz crystal microbalance. *Biotechnol. Prog.* **9** (1993) 105–108.

167.   Fredrikkson, C., Kihlmann, S., Rodahl, M. and Kasemo, B. The piezoelectric quartz crystal mass and dissipation sensor: a means of studying cell adhesion. *Langmuir.* **14** (1998) 248–251.

168.   Nimeri, G., Fredrikkson, C., Elwing, H., Liu, L., Rodahl, M. and Kasemo, B. Neutrophil interaction with protein –coated surfaces studied by an extended quartz crystal microbalance technique. *Coll. Surf. B: Biointerfaces.* **11** (1998) 255–264.

169.   Hug, T. S., Prenosil, J. E. and Morbidelli, M. Optical waveguide lightmode spectroscopy as a new method to study adhesion of anchorage-dependent cells as an indicator of metabolic state. *Biosens Bioelectron.* **16** (2000) 865–874.

170.   Tien, P. K. Integrated optics and new wave phenomena in optical waveguides. *Rev. Mod. Phys.* **49** (1977) 361–420.

171.   Tiefenthaler, K. and Lukosz, W. Sensitivity of grating couplers as integrated-optical chemical sensors. *J. Opt. Soc. Am. B.* **6** (1989) 209–220.

172.   de Feijter, J. A., Benjamins, J. and Veer, F. A. Ellipsometry as a tool to study the adsorption of synthetic and biopolymers at the air-water interface. *Biopolymers*. **17** (1978) 1759–1773.

173.   Lukosz, W. and Tiefenthaler, K. Sensitivity of integrated optical grating and prism couplers as (bio)chemical sensors. *Sensors Actuators*. **15** (1988) 273–284.

174.   Ball, V. and Ramsden, J. J. Bu   er dependence of refractive index incre-ments of protein solutions. *Biopolymers*. **46** (1998) 489–492.

175.   Horvath, R., Fricsovszky, G. and Papp, E. Application of OWLS to monitor lipid bilayer phase transition. *Biosens Bioelectronics.* **18** (2003) 415–428.

176.   Horvath, R., Voros, J., Graf, R., Fricsovszky, G., Textor, M., Lindvold, L. R., Spencer, N. D. and Papp, E. Effect of patterns and inhomogeneities on the surface of waveguides used for optical waveguide lightmode spectroscopy applications. *Appl Phys B – Lasers and optics*. **72** (2001) 441–447.

177.   Horvath, R., Pedersen, H. C., Skivesen, N., Selmeczi, D. and Larsen, N. B. Monitoring of living cell attachment and spreading using reverse symmetry waveguide sensing. *App. Phys. Lett.* **86** (2005) 071101.

178.   Minsky, M. U.S. patent 3013467

179.   Teixeira, S., Ferraz, M.P. and Monteiro, F.J. Biocompatability of highly macroporous ceramic scaffolds: cell adhesion and morphology studies. *J. Mater. Sci. Mater. Med.* **18** (2007) In press.

180.   Alvisi, G., Musiani, D., Jans, D. A. and Ripalta, A. An importin alpha/beta-recognised bipartite nuclear localisation signal mediates targeting of the human herpes simplex virus type 1 DNA polymerase catalytic subunit pUL30 to the nucleus. *Biochemistry*. **46** (2007) 9155–9163.

181.   Gerger, A., Koller, S., Kern, T., Massone, C., Steiger, K., Richtig, E., Kerl, H. And Smolle, J. Diagnostic applicability of in vivo confocal laser scanning micrscopy in melanolytic skin tumors. *J. Inv. Dermatol.* **124** (2006) 493–498.

182.   Ramsden, J. J. and Máte, M. Kinetics of monolayer particle deposition. *J. Chem. Soc. Faraday Trans.* **9**4 (1998) 783–788.

183.   Máte, M. and Ramsden, J. J. Addition of particles of alternating charge. *J. Chem. Soc. Faraday Trans.* **94** (1998) 2813–2816.

184.   Fernández, A. and Ramsden, J. J. On adsorption induced denaturation of folded proteins. *J. Biol. Phys. Chem.* **1** (2001) 81–84.

185. Ramsden, J. J. From kinetics to structure: High resolution molecular microscopy. In Proteins at solid-liquid interfaces. Springer – Verlag, Berlin, Heidelberg. (2006) 23–49.

186. Asakura, S. and Oosawa, J. On interaction of two bodies immersed in a solution of macromolecules. *J. Chem. Phys.* **22** (1954) 1255–1256.

187. van der Waals, J. D. Thermodynamische theorie der kapillaritat unter voraussetzung stetiger dichteanderung. *Z. Phys. Chem.* **13** (1894) 657–725.

188. Allain, C., Ausserré, D and Rondelez, F. Direct optical observation of depletion layers in polymer solutions. *Phys. Rev. Lett*. **49** (1982) 1694–1697.

189. Ausserré, D., Hervet, H and Rondelez, F. Concentration profile of polymer solutions near a solid wall. *Phys. Rev. Lett.* **54** (1985) 1948–1951.

190. Palmer, R.G., Stein, D. L., Abrahams, E. and Anderson, P.W. Models of hierarchically constrained dynamics for glassy relaxation. *Phys. Rev. Lett.* **53** (1984) 958–961.

191. Nemes, Cs., Rozlosnik, N. and Ramsden, J. J. Direct measurement of the viscoelasticity of adsorbed protein layers using atomic force microscopy. *Phys. Rev. E*. **60** (1999) 1166–1169.

192. Clerc, D. and Lukosz, W. Real-time analysis of avidin adsorption with an integrated-optical output grating coupler: adsorption kinetics and optical anisotropy of adsorbed monomolecular layers. *Biosens. Bioelectron.* **12** (1997) 185–194.

193. Horvath, R. and Ramsden, J. J. Quasi-isotropic analysis of anisotropic thin films on optical waveguides. *Langmuir.* **23** (2007) 9330–9334.

194. Born, M. and Wolf, E. Principles of optics, 7th ed: Cambridge University Press: New York. (1999).

195. Hiebl, M. and Maksymiw, R. Anomalous temperature dependence of the thermal expansion of proteins. *Biopolymers.* **31** (1991) 161–167.

196. Wiggins, P. M. Enzyme reactions and two state water. *J. Biol. Phys. Chem.* **2** (2002) 25–37.

197. Mentré, P. Interfacial water: a modulator of biological activity. *J. Biol. Phys. Chem.* **4** (2004) 115–123.

198. Bossard, F., Tsitsilianis, C., Yannopoulos, S. N., Petekidis, G. and S ka, V. A novel thermo-thickening phenomenon exhibited by a triblock polyampholyte in aqueous salt free solutions. *Macromolecules.* **38** (2005) 2883–2888.

199.   Norde, W. and Lyklema, J. The adsorption of human plasma albumin and bovine pancreas ribonuclease at negatively charged polystyrene surfaces. *J. Coll. Int. Sci.* **66** (1970) 295–302.

200.   McColl, J., Yakubov, G. E. and Ramsden, J. J. Complex desorption of mucin from silica. *Langmuir*. **23** (2007) 7096–7100.

201.   Averbukh, I. Sh., Blumenfeld, L. A., Kovarsky, V. A., and Perelman, N. F. A model of the mechanism of enzyme action in terms of protein conformational relaxation. *Biochim. Biophys. Acta.* **873** (1986) 290–296.

202.   Biggs, S. and Grieser, F. Atomic-force microscopy imaging of thin-films formed by hydrophobing reagents. *J. Coll. Int. Sci.* **165** (1994) 425–430.

203.   Raviv, U. and Klein, J. Healing of adsorbed polymer layers in a narrow gap following removal by shear. *Polym. Adv. Technol.* **13** (2002) 1032–1038.

204.   Raviv, U., Frey, J., Sak, R., Laurat, P., Tadmor, R., and Klein, J. Properties and interactions of physigrafted end-functionalized poly(ethylene glycol) layers. *Langmuir.* **18** (2002) 7482–7495.

205.   Raviv, U., Giasson, S., Kampf, N., Gohy, J.F., Jerome, R., and Klein, J. Lubrication by charged polymers. *Nature.* **425** (2003) 163–165.

206.   Kampf, N., Raviv, U., and Klein, J. Normal and shear forces between adsorbed and gelled layers of chitosan, a naturally occurring cationic polyelectrolyte. *Macromolecules.* **37** (2004) 1134–1142.

207.   Zhu, Y.X. and Granick, S. Biolubrication: Hyaluronic acid and the influence on its interfacial viscosity of an antiinflammatory drug. *Macromolecules.* **36** (2003) 973–976.

208.   Zhu, Y.X. and Granick, S. Superlubricity: A paradox about confined fluids resolved. *Phys. Rev. Lett.* **93** (2004).

209.   Tadmor, R., Chen, N. H., and Israelachvili, J. N. Thin film rheology and lubricity of hyaluronic acid solutions at a normal physiological concentration. *J. Biomed. Mater. Res.* **61** (2002) 514–523.

210.   Tadmor, R., Hernandez-Zapata, E., Chen, N. H., Pincus, P., and Israelachvili, J. N. Debye length and double-layer forces in polyelectrolyte solutions. *Macromolecules.* **35** (2002) 2380–2388.

211.   Tadmor, R., Chen, N. H., and Israelachvili, J. N. Thin film rheology and lubricity of hyaluronan solutions. *Biophysical. J.* **82** (2002) 163A–164A.

212.   Benz, M., Chen, N. H., and Israelachvili, J. Lubrication and wear properties of grafted polyelectrolytes, hyaluronan and hylan, measured in the surface forces apparatus. *J. Biomed. Mater. Res. A.* **71** (2004) 6–15.

213. Zappone, B., Ruths, M., Greene, G. W., Jay, G. D., and Israelachvili, J. N. Adsorption, lubrication, and wear of lubricin on model surfaces: Polymer brush-like behavior of a glycoprotein. *Biophysical. J.* **92** (2007) 1693–1708.

214. Luck, G., Liao, H., Murray N. J., Grimmer, H.R., Warminski, E., Williamson, M. P., Lilley, T. H. and Haslam E. Polyphenols, astringency and proline-rich proteins. *Phytochem.* **37** (1994) 357–371.

215. Haslam, E. and Lilley, T. H. natural astringency in food stuffs – a molecular interpretation. *Crit. Rev. Food. Sci. Nutr.* **27** (1998) 1.

216. Su, Y-L., Leung, L-K., Huang, Y. and Chen, Z-Y. Stability of tea theaflavins and catechins. *Food. Chem.* **83** (2003) 189–195.

217. El Hag, M. E., El Tinay, A. H., and Yousif, N. E. Effect of fermentation and dehulling on starch, total polyphenol, phytic acid content and in vitro protein digestibility of pearl millet. *Food. Chem.* **77** (2002) 193–196.

218. Griffith, L. G. Emerging design principles in biomaterials and scaffolds for tissue engineering. *Ann. N.Y. Acad. Sci.* **961** (2002) 83–95.

219. Gabriel, M. O., Grünheid, T. and Zentner A. Glycosylation pattern and cell attachment-inhibiting property of human salivary mucins. *J. Periodontol.* **76** (2005) 1175–1181.

220. Shi, L., Ardehali, R., Caldwell, K. D. and Valint, P. Mucin coating on polymeric material surfaces to suppress bacterial adhesion. *Coll. Surf. B: Biointerfaces.* **17** (2000) 229–239.

221. Gekas, J., Hindié, M., Faucheux, N., Lanvin, O., Maziére, C., Fuéntes, V., Gouilleux-Gruart, V., David, B., Maziére, J-C., Lassoued, K. and Nagel, M-D. The inhibition of cell spreading on a cellulose substrate (cuprophan) induces an apoptotic process via a mitochondria-dependent pathway. *FEBS Lett.* **563** (2004) 103–107.

222. Faucheux, N., Warocquier-Clérout, R., Duval, J. L., Haye, B., Nagel, M. D. cAMP levels in cells attached toAN69 and cuprophan: cAMP dependence of cell aggregation and the influence of serum. *Biomaterials.* **20** (1999) 159– 165.

223. Wittmer, C. R., Phelps, J. A., Saltzman, W. M., Van Tassel, P. R. Fibronectin terminated multilayer films: Protein adsorption and cell attachment studies. *Biomaterials.* **28** (2007) 851–860.

224. Shimizu, M., Weinstein, I. B. Modulation of signal transduction by tea catechins and related phytochemicals. *Mutation Res.* **591** (2005) 147–160.

225. Bate-Smith E C. Astringency in foods. *Food.* **23** (1954) 124–135.

226.   Lyo, T., Maki, Y., Sasaki, N. and Nakata, M. Anisotropic viscoelastic properties of cortical bone. *J. Biomechanics.* **37** (2004) 1433–1437.

227.   Alves, N. M., Gomez Ribelles, J. L., Gomez Tejedor, J. A., Mano, J. F. Viscoelastic behaviour of poly (methyl methacrylate) networks with different cross-linking degrees. *Macromolecules*. **37** (2004) 3735–3744.

228.   Beningo, K. A., Dembo, M., Kaverina, I., Small, V. and Wang, Y-L. Nascent focal adhesions are responsible for the generation of strong propulsive forces in migrating fibroblasts. *J. Cell. Biol.* **153** (2001) 881–887.

229.   Engler, A., Bacakova, L., Newman, C., Hategan, A., Griffin, M. and Discher, D. Substrate compliance versus ligand density in cell on gel responses. *Biophys. J.* **86** (2004) 617–628.

230.   Revel, J-P. and Hay, E. D. An autoradiographic and electron microscope study of collagen synthesis in differentiating cartilage. *Z. Zellforsch.* **61** (1963) 110–114.

231.   Lohne, J.A. and Harriot, 1560–1621. The Tyco Brahe of optics. *Centaurus*. **6** (1959) 113–121.

232.   Goos, F. and Hanchen, H. *Ann. Phys.* 6 (1947) 333.

233. Freshney, R. I. Culture of animal cells 5th ed. Wiley-Liss, New Jersey. (2005).

234. Bongaerts, J. H. H. Rossetti, K. Stokes, J. R. The lubricating properties of human whole saliva. *Tribology lett.* **27** (2007) 277–287.

235. Lin, L-C., Hung, L-C. And Tsai, T-H. Determination of (-)-epigallocatechin gallate in rat blood by microdialysis coupled with liquid chromatography. *J. Chromatogr. A*. **1032** (2004) 125–128.